การปรับค่าปริมาณรังสีและคุณภาพของภาพที่เหมาะสมในการถ่ายภาพรังสีช่องท้อง ด้วยเครื่องเอกซเรย์เคลื่อนที่ระบบดิจิทัล

นายสิรัณยาพงศ์ สุวรรณโอภาส

จุฬาลงกรณ์มหาวิทยาลัย
CHULALONGKORN UNIVERSITY

บทคัดย่อและแฟ้มข้อมูลฉบับเต็มของวิทยานิพนธ์ตั้งแต่ปีการศึกษา 2554 ที่ให้บริการในคลังปัญญาจุฬาฯ (CUIR)
เป็นแฟ้มข้อมูลของนิสิตเจ้าของวิทยานิพนธ์ ที่ส่งผ่านทางบัณฑิตวิทยาลัย
The abstract and full text of theses from the academic year 2011 in Chulalongkorn University Intellectual Repository (CUIR)
are the thesis authors' files submitted through the University Graduate School.

วิทยานิพนธ์นี้เป็นส่วนหนึ่งของการศึกษาตามหลักสูตรปริญญาวิทยาศาสตรมหาบัณฑิต
สาขาวิชาฉายาเวชศาสตร์ ภาควิชารังสีวิทยา
คณะแพทยศาสตร์ จุฬาลงกรณ์มหาวิทยาลัย
ปีการศึกษา 2559

ลิขสิทธิ์ของจุฬาลงกรณ์มหาวิทยาลัย

OPTIMIZATION OF RADIATION DOSE AND IMAGE QUALITY IN ABDOMINAL RADIOGRAPHY USING DIGITAL MOBILE X-RAY SYSTEM

Mr. Siranyapong Suwan-o-pas

จุฬาลงกรณ์มหาวิทยาลัย
CHULALONGKORN UNIVERSITY

A Thesis Submitted in Partial Fulfillment of the Requirements
for the Degree of Master of Science Program in Medical Imaging
Department of Radiology
Faculty of Medicine
Chulalongkorn University
Academic Year 2016
Copyright of Chulalongkorn University

Thesis Title	OPTIMIZATION OF RADIATION DOSE AND IMAGE QUALITY IN ABDOMINAL RADIOGRAPHY USING DIGITAL MOBILE X-RAY SYSTEM
By	Mr. Siranyapong Suwan-o-pas
Field of Study	Medical Imaging
Thesis Advisor	Kitiwat Khamwan, Ph.D.

Accepted by the Faculty of Medicine, Chulalongkorn University in Partial Fulfillment of the Requirements for the Master's Degree

....Dean of the Faculty of Medicine
(Professor Suttipong Wacharasindhu, M.D.)

THESIS COMMITTEE

....Chairman
(Associate Professor Anchali Krisanachinda, Ph.D.)

....Thesis Advisor
(Kitiwat Khamwan, Ph.D.)

....Examiner
(Associate Professor Kosuke Matsubara, Ph.D.)

....External Examiner
(Professor Franco Milano, Ph.D.)

จุฬาลงกรณ์มหาวิทยาลัย
CHULALONGKORN UNIVERSITY

สิรัณยาพงศ์ สุวรรณโอภาส : การปรับค่าปริมาณรังสีและคุณภาพของภาพที่เหมาะสมในการถ่ายภาพรังสีช่องท้องด้วยเครื่องเอกซเรย์เคลื่อนที่ระบบดิจิทัล (OPTIMIZATION OF RADIATION DOSE AND IMAGE QUALITY IN ABDOMINAL RADIOGRAPHY USING DIGITAL MOBILE X-RAY SYSTEM) อ.ที่ปรึกษาวิทยานิพนธ์หลัก: อ. ดร.กิติวัฒน์ คำวัน, 131 หน้า.

การถ่ายภาพเอกซเรย์ช่องท้องโดยเครื่องเอกซเรย์แบบเคลื่อนที่โดยปกติจะให้บริการเฉพาะผู้ป่วยในหอพักซึ่งไม่สามารถเคลื่อนย้ายเพื่อมารับบริการที่แผนกรังสีวิทยาได้ การตั้งค่าพารามิเตอร์นั้นต้องอาศัยประสบการณ์ของนักรังสีการแพทย์เพื่อให้ได้คุณภาพของภาพที่ดีและปริมาณรังสีที่เหมาะสมแก่ผู้ป่วย ดังนั้นวัตถุประสงค์ของงานวิจัยนี้เพื่อหาพารามิเตอร์ที่เหมาะสมสำหรับการถ่ายภาพเอกซเรย์ช่องท้องด้วยเครื่องเอกซเรย์เคลื่อนที่ระบบดิจิทัลในหุ่นจำลองที่มีขนาดความหนาของช่องท้อง 21 ซม. และเพิ่มความหนาของช่องท้องเป็น 25 และ 29 ซม. ด้วยอุปกรณ์เพิ่มความหนาเพื่อจำลองผู้ป่วยที่มีขนาดลำตัวหนาขึ้น ทำการทดสอบตั้งค่าพารามิเตอร์ต่างๆ โดยที่ค่าเควีพีเริ่มต้นที่ 70 ถึง 90 (เพิ่มขึ้นครั้งละ 5 เควีพี) และค่าเอ็มเอเอสเริ่มต้น 3.2, 6.3, 12.5, และ 25.0 ส่วนค่าพารามิเตอร์ที่ใช้ในทางคลินิกที่ความหนาของช่องท้อง 21, 25, และ 29 ซม ค่าพารามิเตอร์คือ 75 เควีพี 32 เอ็มเอเอส, 80 เควีพี 32 เอ็มเอเอส, และ 85 เควีพี 32 เอ็มเอเอสตามลำดับ โดยระยะห่างจากหลอดเอกซเรย์ถึงตัวรับภาพคือ 100 ซม. ประเมินค่าปริมาณรังสีดูดกลืนที่ผิวของหุ่นจำลองที่ได้รับและประเมินคุณภาพของภาพเอกซเรย์ในเชิงคุณภาพจากองค์ประกอบของภาพรังสีช่องท้องตามมาตรฐานของทบวงการพลังงานปรมาณูระหว่างประเทศ (5-7 คะแนน) และระดับของสัญญาณรบกวน (1 หรือ 2 คะแนน) โดยผู้ประเมินผล 3 ท่าน ประเมินคุณภาพของภาพถ่ายรังสีช่องท้องในเชิงปริมาณของภาพในรูปแบบของอัตราส่วนสัญญาณต่อสัญญาณรบกวน (เอสเอ็นอาร์) ใน 3 ตำแหน่ง ได้แก่ ตับ (ตำแหน่งที่ 1), กระดูกสันหลังส่วนบั้นเอวระดับที่ 4 บริเวณ Transvers process (ตำแหน่งที่ 2), และ กระดูกสะโพก (ตำแหน่งที่ 3) และประเมินอัตราส่วนความคมชัดบนภาพต่อสัญญาณรบกวน (ซีเอ็นอาร์) ใน 3 บริเวณ ได้แก่ บริเวณตับ (บริเวณที่ 1), บริเวณไตข้างซ้ายกับกระดูกสันหลังส่วนบั้นเอวระดับที่ 4 บริเวณ Transvers process (บริเวณที่ 2), และบริเวณไตข้างขวากับกระดูกสะโพก (บริเวณที่ 3) จากนั้นทำการบันทึกค่าดัชนีชี้วัดปริมาณรังสี

ผลการศึกษาพบว่าค่าพารามิเตอร์ที่เหมาะสมสำหรับการถ่ายภาพรังสีช่องท้องโดยเครื่องเอกซเรย์เคลื่อนที่ระบบดิจิทัลในหุ่นจำลองที่มีขนาดความหนาของช่องท้อง 21 ซม. ที่ระยะห่างจากหลอดเอกซเรย์ถึงตัวรับภาพคือ 100 ซม. คือ 80 เควีพี และ 6.3 เอ็มเอเอส โดยให้ค่าดัชนีชี้วัดปริมาณรังสีเท่ากับ 381 ในส่วนของคะแนนเฉลี่ยจากการประเมินคุณภาพของภาพจากผู้ประเมิน 3 ท่านและระดับของสัญญาณรบกวนมีค่าเท่ากับ 5.67 และ 1 คะแนน ตามลำดับ ค่าเฉลี่ยของอัตราส่วนสัญญาณต่อสัญญาณรบกวน (เอสเอ็นอาร์) ใน 3 ตำแหน่งมีค่าเท่ากับ 39.56, 61.55, และ 18.24 ตามลำดับ ค่าเฉลี่ยการประเมินอัตราส่วนความคมชัดบนภาพต่อสัญญาณรบกวน (ซีเอ็นอาร์) ใน 3 บริเวณคือ 5.97, 7.27, และ 1.50 ตามลำดับ

ค่าพารามิเตอร์ที่เหมาะสมสำหรับสำหรับการถ่ายภาพรังสีช่องท้องที่มีขนาดความหนาของช่องท้อง 25 ซม. คือ 85 เควีพี 6.3 เอ็มเอเอส ค่าดัชนีชี้วัดปริมาณรังสีคือ 395 ในส่วนของคะแนนเฉลี่ยการประเมินคุณภาพของภาพจากจำนวนองค์ประกอบของภาพรังสีช่องท้องและระดับของสัญญาณรบกวนคือ 5.17 และ 2 คะแนน ตามลำดับ ค่าเฉลี่ยการประเมินคุณภาพเชิงปริมาณของภาพรังสีช่องท้องในรูปแบบของอัตราส่วนสัญญาณต่อสัญญาณรบกวน (เอสเอ็นอาร์) ใน 3 ตำแหน่งคือ 43.67, 75.08, และ19.53 ตามลำดับ ค่าเฉลี่ยการประเมินอัตราส่วนความคมชัดบนภาพต่อสัญญาณรบกวน (ซีเอ็นอาร์) ใน 3 บริเวณคือ 6.42, 7.54, และ 1.75 ตามลำดับ

ค่าพารามิเตอร์ที่เหมาะสมสำหรับช่องท้องขนาด 29 ซม. คือ 85 เควีพี 12.5 ค่าเอ็มเอเอส โดยให้ค่าดัชนีชี้วัดปริมาณรังสีเท่ากับ 409 ในส่วนของคะแนนเฉลี่ยคุณภาพของภาพและระดับของสัญญาณรบกวนคือ 5.33 และ 1 คะแนน ตามลำดับ ค่าเฉลี่ยการประเมินคุณภาพเชิงปริมาณของภาพรังสีช่องท้องในรูปแบบของอัตราส่วนสัญญาณต่อสัญญาณรบกวน (เอสเอ็นอาร์) ใน 3 ตำแหน่งมีค่าเท่ากับ 35.47, 67.70, และ 19.43 ตามลำดับ ค่าเฉลี่ยการประเมินอัตราส่วนความคมชัดบนภาพต่อสัญญาณรบกวน (ซีเอ็นอาร์) ใน 3 บริเวณคือ 6.16, 5.59, และ 1.69 ตามลำดับ

ในปัจจุบันในประเทศไทยยังไม่มีค่าปริมาณรังสีอ้างอิงในการถ่ายภาพรังสีช่องสำหรับประชากรไทย ในงานวิจัยนี้การเปรียบเทียบปริมาณรังสีดูดกลืนที่ผิวของหุ่นจำลองของค่าพารามิเตอร์ที่เหมาะสมกับค่าพารามิเตอร์ที่ใช้ในทางคลินิก พบว่าการใช้ค่าพารามิเตอร์ที่เหมาะสมสำหรับสำหรับการถ่ายภาพรังสีช่องท้องที่ความหนา 21, 25, และ 29 ซม. ปริมาณรังสีที่ผิวของหุ่นจำลองลดลงร้อยละ 77, 78, และ 61 ตามลำดับ โดยยังสามารถรักษาคุณภาพของภาพเพื่อการวินิจฉัยไว้ และค่าพารามิเตอร์ที่เหมาะสมจากงานวิจัยนี้ควรนำไปทดสอบจริงในทางคลินิกสำหรับในผู้ป่วยต่อไป

ภาควิชา รังสีวิทยา	ลายมือชื่อนิสิต ....
สาขาวิชา ฉายาเวชศาสตร์	ลายมือชื่อ อ.ที่ปรึกษาหลัก ....
ปีการศึกษา 2559	

5874079030 : MAJOR MEDICAL IMAGING
KEYWORDS: DIGITAL MOBILE X-RAY SYSTEM / ABDOMINAL RADIOGRAPHY / ENTRANCE SURFACE AIR KERMA / EXPOSURE INDEX / OPTIMIZATION

SIRANYAPONG SUWAN-O-PAS: OPTIMIZATION OF RADIATION DOSE AND IMAGE QUALITY IN ABDOMINAL RADIOGRAPHY USING DIGITAL MOBILE X-RAY SYSTEM. ADVISOR: KITIWAT KHAMWAN, Ph.D., 131 pp.

The abdominal radiography using digital mobile x-ray system is commonly requested for the immobilized patient. The selection of the exposure parameters needs the experience of the operator for radiation dose and image quality. The purpose of this study was to optimize the radiation dose and image quality for abdominal radiography using digital mobile x-ray system in phantom at King Chulalongkorn Memorial Hospital. Digital mobile x-ray system model OptimaXR220amx and the Kyoto Kagaku phantom model PBU-60 with 21 cm of abdominal thickness were used. The buildup layer was enclosed on the phantom to simulate a larger body type of 25 and 29 cm thickness of abdomen. The setting for experimental exposure parameters, kVp range was 70-90 (in 5 kVp increments) and mAs was 3.2, 6.3, 12.5, and 25. The setting for routine clinical exposure parameters of 21, 25, and 29 cm thickness of abdomen were 75 kVp 32 mAs, 80 kVp 32 mAs, and 85 kVp 32 mAs, respectively. The setting source to image receptor distance (SID) was 100 cm. The experimental and routine clinical exposure parameters were performed and compared in terms of radiation dose and image quality evaluation. The determination of image quality score based on IAEA protocol (5 from 7 points) and qualitative noise (1 to 2 points) were scored by three observers. The quantitative analysis was evaluated in terms of signal-to-noise ratio (SNR) by 3 regions at liver (1st ROI), transverse process in 4th lumbar spine (2nd ROI), and pelvis (3rd ROI) and contrast-to-noise ratio (CNR) was evaluated on 3 areas at liver area (1st area), left kidney and transverse process in 4th lumbar spine (2nd area), and right kidney and pelvis (3rd area) on the image. The exposure index was also recorded.

The optimal parameter for 21 cm thickness of abdomen at 100 cm SID was 80 kVp, 6.3 mAs with the exposure index of 381. The image quality scoring and qualitative noise from 3 observers were 5.67 and 1, respectively. The average SNR in 1st, 2nd, and 3rd ROIs were 39.56, 61.55, and 18.24, respectively and the average of CNR in 1st, 2nd, and 3rd areas were 5.97, 7.27, and 1.50, respectively.

For 25 cm thickness, the optimal parameter was 85 kVp, 6.3 mAs with the exposure index of 395. The image quality scoring and qualitative noise were 5.17 and 2, respectively. The average SNR 1st, 2nd, and 3rd ROIs were 43.67, 75.08, and 19.53, respectively and the average of CNR 1st, 2nd, and 3rd areas were 6.42, 7.54, and 1.75, respectively.

For 29 cm thickness, the optimal parameter was 85 kVp, 12.5 mAs with exposure index 409. The image quality scoring and qualitative noise were 5.33 and 1, respectively. The average SNR in 1st, 2nd, and 3rd ROIs were 35.47, 67.70, and 19.43, respectively and the average of CNR in 1st, 2nd, and 3rd areas were 6.16, 5.59, and 1.69, respectively.

Currently, there is no dose reference level of abdominal radiography for Thai population. The comparison between the routine clinical and optimal parameters, the entrance surface air kerma (ESAK) in the optimal parameter of 21, 25, and 29 cm thicknesses of abdomen were lower than 77%, 78%, and 61% to the routine clinical parameter. However, the optimal parameters in this study can maintain the image quality for acceptable diagnosis in various abdominal thicknesses. The optimal parameters from this study should be applied to the patient for the routine clinical parameter in the future.

Department:	Radiology	Student's Signature	....
Field of Study:	Medical Imaging	Advisor's Signature	....
Academic Year:	2016		

ACKNOWLEDGEMENTS

I would like to deeply grateful and appreciation to Mr. Kitiwat Khamwan, Ph.D., Department of Radiology, Faculty of Medicine, Chulalongkorn University, my advisor for his invaluable suggestion, helpful, constructive comments, patience, motivation and polishing of the thesis writing to improve English expression.

I would like to express my deeply thankfulness to Miss Petcharleeya Suwanpradit, M.Sc., Department of Radiology, King Chulalongkorn Memorial Hospital, my co-advisor for her encouragement, kind guidance, sharing useful experience, constructive direction, support in equipment and English language proof in this research.

I would like to greatly grateful to Associate Professor Anchali Krisanachinda, Ph.D., Department of Radiology, Faculty of Medicine, Chulalongkorn University, Chairman of thesis defense for her kind suggestion, invaluable advice, and constructive comments.

I would like to deeply thank Professor Franco Milano, Ph.D., University of Florence, Italy and Associate Professor Kosuke Matsubara, Ph.D., Kanazawa University, Japan, the external examiners of thesis defense for their invaluable suggestion and constructive comments in this research.

I would like to deeply thank Associate Professor Sivalee Suriyapee, M.Eng., and Mr. Taweap Sanghangthum, Ph.D., Division of Radiation Oncology, Department of Radiology, Faculty of Medicine, Chulalongkorn University, for their invaluable guidance and constructive comments.

I would like extremely grateful for all teachers, lecturers, and staffs at Master of Science Program in Medical Imaging, Faculty of Medicine, Chulalongkorn University, for teaching, suggestion, and supports.

I would like extremely grateful all radiological technologists of Division of Diagnostic Radiology, Department of Radiology, King Chulalongkorn Memorial Hospital for their kind helpful, contributing and providing the digital mobile x-ray system through this research.

Finally, I must express my very profound gratitude to my parents for providing me with unfailing support and continuous encouragement throughout my years of study and through the process of researching and writing this thesis. This accomplishment would not have been possible without them.

CONTENTS

Page

Page

Page

Page

Page

จุฬาลงกรณ์มหาวิทยาลัย
CHULALONGKORN UNIVERSITY

LIST OF TABLES

Table **Page**

Table **Page**

จุฬาลงกรณ์มหาวิทยาลัย
Chulalongkorn University

LIST OF FIGURES

Figure		Page

Figure **Page**

LIST OF ABBREVIATIONS

AAPM	American Association of Physicists in Medicine
AEC	Automatic Exposure Control
ALARA	As Low As Reasonably Achievable
AP	Anterio-Posterior
BSF	Backscatter Factor
CNR	Contrast-to-Noise Ratio
CR	Computed Radiography
DQE	Detective quantum efficiency
DR	Digital Radiography
DRL	Dose Reference Level
EI	Exposure Index
EI_T	Target Exposure Index
ER	Emergency department
ESAK	Entrance Surface Air Kerma
IAEA	International Atomic Energy Agency
IEC	International Electrotechnical Commission
KCARE	King's Center for the Assessment of Radiological Equipment
K_i	Incident air kerma
kVp	Kilo Voltage Peak
mAs	MiliAmpere-Second
mGy	Miligray
MTF	Modulation Transfer Function
NPS	Noise Power Spectrum
PACS	Picture Archiving and Communication System
QA	Quality Assurance
QC	Quality Control
ROI	Region of interest
SCD	Source to Chamber Distance
SDD	Source to Detector Distance
SID	Source to Image receptor Distance
SNR	Signal-to-Noise Ratio
TFT	Thin-Film Transistor

CHAPTER I

INTRODUCTION

1.1 Background and rationale

Digital radiography (DR) is a form of x-ray imaging where digital sensors replace the screen-film system to provide several advantages such as time efficiency through bypassing chemical processing, the ability to digitally transfer and enhance images and also less radiation can be used to produce an image of similar contrast to conventional radiography (CR) [1].

At the present, there are two digital technologies currently used in department of diagnostic radiology for general x-ray, i.e. computed tomography (CR) and digital radiography (DR). CR is used to replace film-screen system by a storage phosphor plate as the image receptor. The latent image on the exposed plate is scanned by a laser beam and converted to digital data to produce the image. DR involves collecting image data in digital format, without laser scanning to extract the latent image. Flat-panel thin-film transistor (TFT) detectors are exposed by x-ray directly and display images in nearly real time [2] offered the higher image quality with better detective quantum efficiency (DQE) and straight transfer to picture archiving and communication system (PACS). The important thing is that the DR system can decrease the radiation dose substantially compared to CR and screen-film system (SFS). Consequently, the exposure chart of CR or SFS should not be applied to DR system.

Digital technology provides better image quality since its dynamic range and digital image processing compensates for incorrect techniques even if the dose is higher than necessary. The range of radiation dose that digital image receptors can detect has allowed wider values to be processed digitally to display a diagnostic quality image in comparison to screen film system. This concept is illustrated as in figure 1.1. The digital image has original raw data that should be kept intact. Post-processing can change the original raw data and the set point that establishes the levels of gray scale assigned to the pixels. A change in the raw data can loss information in the PACS system and affects the viewing capabilities [3].

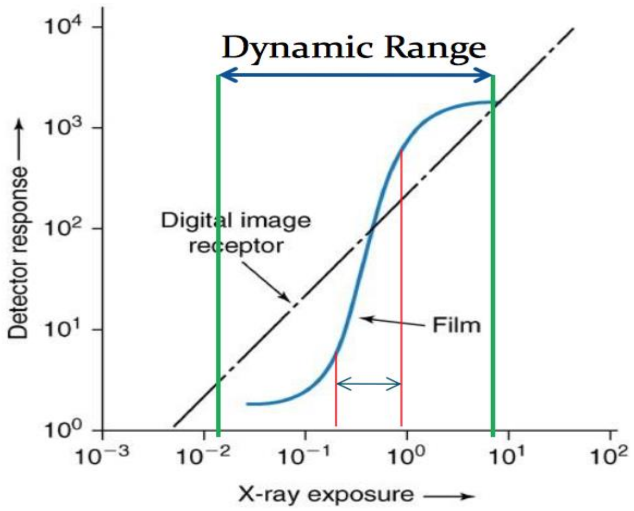

Figure 1.1 The dynamic range of screen-film combinations with digital detectors [4].

The radiation dose in DR is less compared to other modality that using ionizing radiation for clinical examinations such as fluoroscopy or computed tomography (CT) and still decrease when image processing could enhance the image quality of the x-ray image without missing lesion for diagnosis. However, the principle of radiation protection is still important point for decreasing the scattered radiation and associated risk to stuff and public people around. The proper x-ray room design is the first priority before establishing the x-ray machine in the radiology department.

The technology of digital radiography also has been transferred to mobile X-ray system. The advantages are expressed in the many aspects of user. For physicians, they can preview the clinical image and do planning to patient especially in Intensive care unit (ICU) or Emergency department (ER) without moving patient to the x-ray room. For radiological technologists, they can check the image quality of x-ray image as well as send to PACS immediately.

According to the efficiency of digital mobile x-ray system is increased, the chest x-ray portable is not only one part of requesting for immobilized patients, but also another organ such as abdomen, hip, pelvis or even the skull. Most patient wards are not well designed for radiation protection. The optimal parameter setting is based on the thickness and condition of the patient following the “As Low As Reasonably Achievable” (ARALA) principle in order to decrease the radiation dose while maintaining the image quality.

Recently, Piyatas Seangdao et al. [3] investigated the optimal parameter in chest radiography using digital mobile X-ray system and recommended to study in other organs. The abdominal radiography using mobile x-ray system is commonly requested for immobilized patients. In 2015, a number of requests for abdominal radiography using x-ray mobile system at In-Patient Department (IPD), King Chulalongkorn Memorial Hospital (KCMH) were approximately 300 patients and the requests from physicians are still increasing. There is no automatic exposure control (AEC) mode for most of digital mobile x-ray systems. Therefore, the selection of the exposure parameters needs the experience of the operator for justification. The appropriate parameters could reduce scattered radiation to patient, staff and public. However, some of radiographers still used exposure parameters as according to the CR system including the abdominal radiographic images. Currently, there is no standardized parameter technique for abdominal radiography using mobile x-ray system at KCMH. So, the optimal parameters should be established.

1.2 Research objectives

1.2.1. To optimize the radiation dose and image quality for abdominal radiography in phantom using digital mobile x-ray system at King Chulalongkorn Memorial Hospital (KCMH).

1.2.2. To optimize the parameters using digital mobile x-ray system for abdominal radiography in various thicknesses.

1.3 Significance of this study

The finding of this study is to obtain the optimal parameters for abdominal radiography using digital mobile x-ray system in various thicknesses in phantom.

1.4 Definitions

Back Scatter Factor (BSF): The ratio of a radiation quantity measure by dosimeter at the phantom/material surface expose directly from the radiation source and the radiation quantity measure at the same position in air.

Detective Quantum Efficiency (DQE): The efficiency of the x-ray detector converts x-ray energy into the image signal.

Dynamic range: The range of the image receptor that respond to the x-ray energy to generate the digital data.

Entrance Surface Air KERMA (ESAK): The absorb dose in air at the center point of the X-ray beam at the surface of patient including back scatter factor.

Optimization: The balancing between the approximate image quality of the clinical image of the patient and the proper radiation dose.

CHAPTER II

REVIEW OF RELATED LITERATURE

2.1 Theory

2.1.1 Introduction

The abdominal radiography is the image using ionizing radiation to produce pictures of the inside of the abdominal cavity. It is used to evaluate the stomach, liver, intestines and spleen and may be used to help diagnose unexplained pain, nausea or vomiting and also performed to help diagnose conditions such as kidney and bladder stones and gallstones, intestinal blockages, perforation of the stomach or intestine, ingestion of foreign objects and abdominal aortic aneurysm [5].

The bedside abdominal radiography is necessary for in-patient department (IPD) because moving of the patients to the x-ray room may affect the condition of the patients especially in intensive care unit (ICU) or emergency room (ER).

2.1.2 Digital radiography (DR)

The digital radiography system using direct capture of x-rays for digital images was introduced with DR using of a charge-coupled device in 1990. The technology evolved and improved over the next decade and by 2001, flat-panel thin-film transistor (TFT) detectors could expose and display images in near real time [6].

Flat-panel systems, also known as large area x-ray detectors, integrate an x-ray sensitive layer and an electronic readable system based on TFT arrays. Detectors using a scintillator layer and a light-sensitive TFT photodiode are called indirect conversion TFT detectors. Those using an x-ray sensitive photoconductor layer and a TFT charge collector are called direct conversion TFT detectors [7]. The structure of a DR flat-panel system is shown in figure 2.1.

This electronic readable system allows an active readout process, also called active matrix readout, in opposition to the storage-phosphor systems where no active readout elements are integrated within the detector. The entire readout process is very fast, allowing further developments in digital real-time x-ray detectors [7].

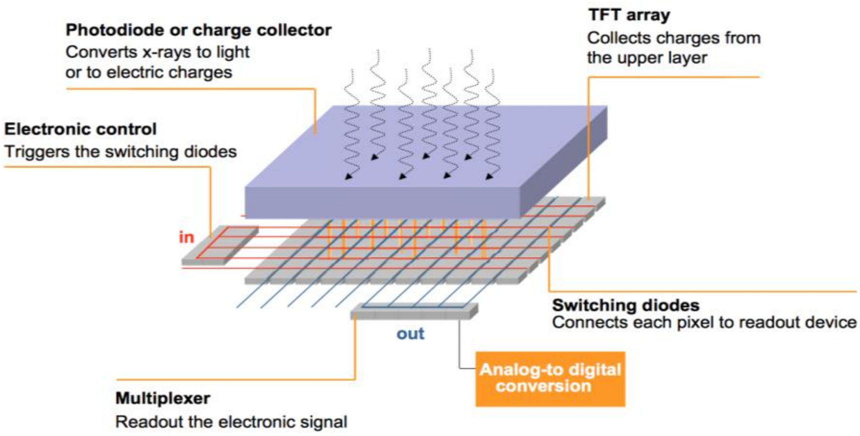

Figure 2.1 Flat-panel structure [8].

TFT arrays (figure. 2.2) are typically deposited onto a glass substrate in multiple layers, with readout electronics at the lowest level, and charge collector arrays at higher levels. Depending on the type of detector being manufactured, charge collection electrodes or light sensing elements are deposited at the top layer of this ‘‘electronic sandwich” [8].

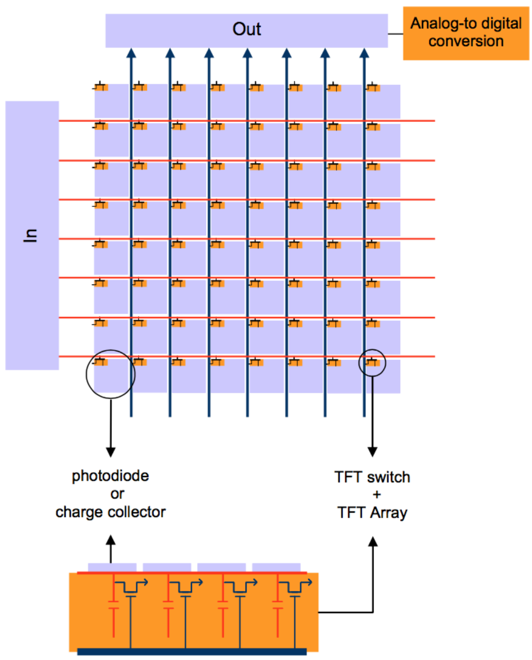

Figure 2.2 TFT array [8].

The advantages of this design include compact size and immediate access to digital images. The performance of DR systems greatly exceeds the performance of CR systems, which have efficiencies of 20-35%, and of screen-film systems for chest radiography, which have nominal efficiencies of 25% [8].

Wireless DR flat-panel systems have become commercially available by 2009. Wireless DR systems are nonintegrated detectors that could be used to obtain radiographs in a similar way to CR. With wireless DR detector, it is mandatory to use a wireless LAN for communications between the DR detector unit and the workstation console. This way each performed radiograph is transferred at almost real time from the cassette DR to the workstation. The DR cassette includes a built-in battery to power supply and this allows the detector's necessary autonomy to obtain several radiographs and to transfer the obtained radiographs to the system for further viewing [8].

2.1.2.1 Direct-conversion flat panel detector

Large area direct conversion systems use amorphous selenium (a-Se) as the semiconductor material because of its x-ray absorption properties and extremely high intrinsic spatial resolution. Before the flat-panel is exposed to x-rays an electric field is applied across the selenium layer. Then the x-ray exposure generates electrons and holes within the a-Se layer: the absorbed x-ray photons are transformed into electric charges and drawn directly to the charge-collecting electrodes due to the electric field. Those charges proportional to the incident x-ray beam are generated and migrate vertically to the both surfaces of the selenium layer, without much lateral diffusion. At the bottom of the a-Se layer, charges are drawn to the TFT charge collector, where they are stored until readout. The charge collected at each storage capacitor is amplified and quantified to a digital code value for the corresponding pixel. During the readout, the charge of the capacitors of every row is conducted by the transistors to the amplifiers [8].

2.1.2.2 Indirect-conversion flat panel detector

Large area indirect conversion systems use cesium iodide (CsI) or gadolinium oxisulphide (Gd_2O_2S) as an x-ray detector. The scintillators and phosphors used in indirect conversion detectors can be either structured or unstructured (figure 2.3). Unstructured scintillators scatter a large amount of light and this reduces spatial resolution. Structured scintillators consist of phosphor material in a needlelike structure (the needles being perpendicular to the screen surface). This increases the number of x-ray photon interactions and reduces the lateral scattering of light photons. When the scintillator layer is exposed to x-rays the beam is absorbed and converted into fluorescent light. At a second stage that light is converted into an electric charge by means of an a-Si photodiode array. Indirect conversion detectors are constructed by adding an a-Si photodiode circuitry and a scintillator as the top layers of the TFT sandwich. These layers replace the x-ray semiconductor layer used in a direct conversion device. The active area of the detector is divided into an integrated array of image elements e the pixel e and each element contains a photo-diode and a TFT switch available for the readout process [8].

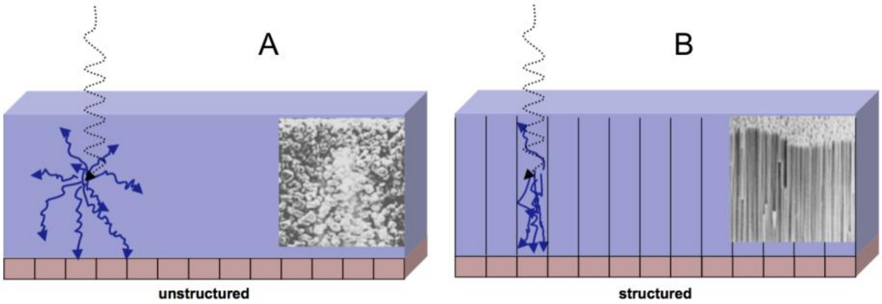

Figure 2.3 Unstructured (A) and structured scintillator (B) [8].

2.1.3 Image post processing

Digital imaging offers post processing capabilities that are not possible with film-screen radiography. The digital image has raw data that should be kept intact. Image post processing can change the raw data and the set point that establishes the levels of gray scale assigned to the pixels. A change in the raw data can cause loss of information and thereby affect the viewing capabilities in the PACS where it will be accessed by the radiologist or referring physician for diagnosis. Thus, the adjustment of window level or width should be set only necessary [6]. The post processing image can enhance the image quality even the image was poor by high or low radiation dose setting. It can reduce noise, remove artifact and adjust the contrast or brightness of the x-ray image as in figure 2.4.

Figure 2.4 Digitally processing on image appearance: raw data without any processing (A), Contrast enhancement (B), Contrast reduction (C), and Edge enhancement (D) [2, 3].

2.1.4 The factors affecting image quality in diagnostic radiology

Several factors account for the image quality in medical image especially in digital radiography.

2.1.4.1 Pixel size, Matrix, and Detector size

Digital images consist of picture elements, or pixels. The two-dimensional collection of pixels in the image is called the matrix, which is usually expressed as length (in pixels) by width (in pixels). Maximum achievable spatial resolution (Nyquist frequency, given in cycles per millimeter) is defined by pixel size and spacing. The smaller the pixel size, the higher the maximum achievable spatial resolution. The overall detector size determines if the detector is suitable for all clinical applications. Larger detector areas are needed for chest imaging than for imaging of the extremities. In cassette-based systems, different sizes are available [2].

2.1.4.2 Dynamic range

Dynamic range is a measure of the signal response of a detector that is exposed to x-rays. In conventional screen-film combinations, the dynamic range gradation curve is S-shaped within a narrow exposure range for optimal film blackening. Thus, the film has a low tolerance for an exposure that is higher or lower than required, resulting in failed exposures or insufficient image quality. For digital detectors, dynamic range is the range of x-ray exposure over which a meaningful image can be obtained. Digital detectors have a wider and linear dynamic range, which, in clinical practice, virtually eliminates the risk of a failed exposure. Another positive effect of a wide dynamic range is that differences between specific tissue absorptions (example; bone vs soft tissue) can be displayed in one image without the need for additional images. On the other hand, because detector function improves as radiation exposure increases, special care has to be taken not to overexpose the patient by applying more radiation than is needed for a diagnostically sufficient image [2] as in figure 2.3.

2.1.4.3 Detective quantum efficiency

Detective quantum efficiency (DQE) is one of the fundamental physical variables related to image quality in radiography and refers to the efficiency of a detector in converting incident x-ray energy into an image signal. DQE is calculated by comparing the signal-to-noise ratio at the detector output with that at the detector input as a function of spatial frequency. DQE is dependent on radiation exposure, spatial frequency, MTF, and detector material. The quality (voltage and current) of the radiation applied is also an important influence on DQE [2].

High DQE values indicate that less radiation is needed to achieve identical image quality; increasing the DQE and leaving radiation exposure constant will improve image quality [9].

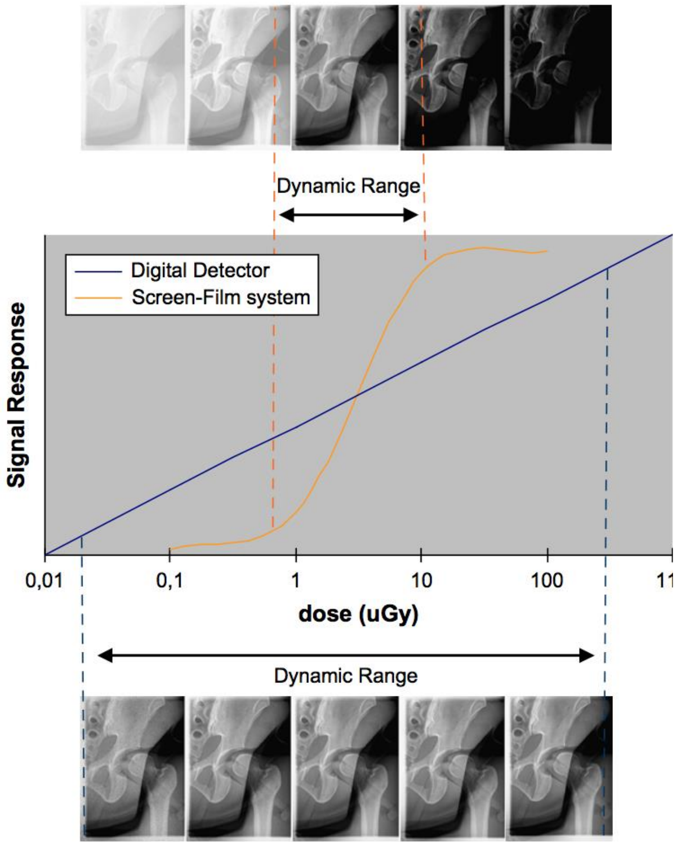

Figure 2.5 The curve of dynamic range between screen-film system and digital detector with qualitative indication of the images [9].

2.1.4.4 Spatial resolution

In digital detectors, spatial resolution is defined and limited by the minimum pixel size. Increasing the radiation applied to the detector will not improve the maximum spatial resolution. On the other hand, scatter of x-ray quanta and light photons within the detector influences spatial resolution. Therefore, the intrinsic spatial resolution for selenium-based direct conversion detectors is higher than that for indirect conversion detectors. Structured scintillators offer advantages over unstructured scintillators [2].

According to the Nyquist theorem, given a pixel size a, the maximum achievable spatial resolution is a/2. At a pixel size of 200 m, the maximum detectable spatial frequency will be 2.5 cycles/mm. The diagnostic range for general radiography is 0 – 3 cycles/mm. For digital mammography, the demanded diagnostic spatial resolution is substantially higher (5 cycles/mm), indicating the need for specially designed dedicated detectors with smaller pixel sizes and higher resolutions [2]. The sharpness of the imaging system is characterized in terms of Modulation Transfer Function (MTF).

2.1.4.5 Contrast

Contrast is defined as a measure of the relative brightness difference between two locations in an image. The contrast of an imaging system is described by the characteristic response curve of the system. This curve has a typical S-shape for a SF system but in digital systems the characteristic curve is generally linear. SF systems have a characteristic curve that is in relation with the logarithm of incident intensity, while digital systems measure their characteristic response directly with respect to exposure (figure 2.5). There is an obvious risk that the patient exposure can be unnecessarily high since a digital detector does not set the limit as film does with respect to film blackening and thus the risk of over or underexposure could be present [8]. The concept of contrast was illustrated in figure 2.6.

The perception of the contrast will depend on the transmitted x-ray incident through the attenuating materials. Thus, the relationship of the contrast between transmitted x-ray beam X_1 and X_2 are follow this equation:

$$\textbf{Contrast} = \log_{10} X_1/X_2$$
$$\textbf{Contrast} = 0.43(\mu_1 X_1 - \mu_2 X_2)$$

As the increasing of the incident x-ray beam energy, leading to increase the scattered radiation cause Compton effect. As the result, the contrast on the x-ray image will be decrease.

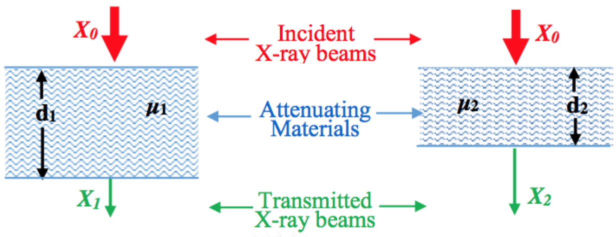

Figure 2.6 A schematic diagram shown the concept of the contrast [3].

2.1.4.6 Noise

Noise arises from a number of sources such as quantum and electronic noise that produces random variations of signal that can obscure useful information in a diagnostic image. Random noise means fluctuations of the signal over an image, as result of a uniform exposure, and can be characterized by the standard deviation of the signal variations over the image of a uniform object. Noise is a major limiting factor in object detection because it remains constant in a given system unless dose is increased. The noise in images is recognized as an important factor in determining image quality. Image noise may be characterized by the noise power spectrum (NPS) [9].

2.1.5 Objective image quality measurement

2.1.5.1 Modulation transfer function (MTF)

MTF is the capacity of the detector to transfer the modulation of the input signal at a given spatial frequency to its output. At radiography, objects having different sizes and opacity are displayed with different gray-scale values in an image. MTF has to do with the display of contrast and object size. More specifically, MTF is responsible for converting contrast values of different-sized objects (object contrast) into contrast intensity levels in the image (image contrast). For general imaging, the relevant details are in a range between 0 and 2 cycles/mm, which demands high MTF values [2].

2.1.5.2 Signal-to-noise ratio (SNR)

The SNR represents the relationship between contrast and noise in an image for large scale objects. While signal sensitivity (contrast) and image noise properties are important by themselves, it is the ratio between them that carries the most significance and constitutes the most significant indicator of image quality. In digital X-ray systems, as noise decreases and SNR increases, object detection increases very rapidly [9].

2.1.5.3 Contrast-to-noise ratio (CNR)

The CNR is a quantization of a medical imaging modality system's ability to distinguish between structures and noise in an acquired image. CNR can be quantized follow this equation [10].

$$\mathbf{CNR = S_a - S_b \,/\, Noise}$$

where S_a and S_b are the average signal strength in tissue *a* and *b*, respectively.

Noise is measured as the standard deviation in a region of interest (ROI).

2.1.5.4 Noise power spectrum (NPS)

The NPS or Wiener spectra (WS) represent the noise power in an image as a function of spatial frequency. It represents the relationship between noise and spatial resolution. It may be thought of as the variance of image intensity (i.e., image noise) distributed among the various frequency components of the image or may be pictured as the variance of a given spatial frequency component in an ensemble of measurements of that spatial frequency [9].

2.1.6 The factors affecting the radiation dose

2.1.6.1 Average beam energy

Average beam energy primarily depends on the peak kilovoltage (kVp) selected and the amount of filtration in the beam. If all other variables are held constant, radiation dose will change as the square of the change in peak kilovoltage. The selection of higher peak kilovoltage increases the average energy of the x-rays and therefore beams penetrability. As the beam becomes more penetrating, more x-rays will reach the image receptor during the same period of time. In practice, this may allow for use of a lower tube current or a shorter exposure, thus reducing the dose to the patient [3].

2.1.6.2 Filtration

The use of filtration at least 2.5 mm of aluminum is necessary in X-ray units in diagnostic department. It removes the lower photon energies from the X-ray beam. This also have effect on both the quantity and quality of the X-ray beam. It is not only reducing the overall x-ray output but also decreasing the proportion of low energy photons to the patient.

2.1.6.3 Collimator

For every radiographic examination, the x-ray bram shold be limited only the area of clinical interest for reduced the radiation dose from unnecessary exposed. The small field of view also improves the contrast on the image.

2.1.6.4 Grids

จุฬาลงกรณ์มหาวิทยาลัย
Chulalongkorn University

Grids were introduced into radiography to reduce the amount of scattered radiation that reaches the image receptor, resulting in images with much improved contrast and increased patient dose. A grid also absorbs a portion of the primary x-rays that would have contributed to exposing the image receptor and the only way to achieve the degree of exposure required to produce the image is to increase the amount of radiation incident on the grid and therefore the patient. A grid removes a much larger fraction of scattered x-rays than primary x-ray, and the doses are typically increased from two to five times those encountered without the use of a grid. This proportion is commonly referred to as the Bucky factor and represents the ratio of the dose with a grid to the dose without a grid. The higher-quality images achieved with grid, however, may result in fewer retakes and more accurate diagnoses [3].

2.1.6.5 Thickness

As the thickness of the area being imaged increases, the amount of radiation incident on the patient increases because adequate x-ray penetration is needed to create an acceptable image. Technique charts that display suggested radiographic technique factors for various examinations and patient thicknesses placed near the operator's console may be helpful [3].

2.1.7 Exposure index (EI)

In traditional screen-film radiography, film optical density serves as an exposure indicator, and direct feedback is obtained by simple visual inspection of the processed film image (figure 2.7). CR and DR detectors have wide exposure latitude and with image post-processing, these systems produce consistent image gray scale even with underexposed and overexposed images (figure 2.8). With the capability of automatically adjusting the gray scale on digital radiographic images, the checks and balances provided to the technologist from the immediate feedback of film density are lost. Underexposed DR images use fewer absorbed x-rays, and can be recognized by increased image noise, but overexposed images can easily go unnoticed, resulting in unnecessary overexposure to the patient. Furthermore, underexposed images are likely to be criticized by radiologists for excessive image noise, whereas overexposed images will likely be of high quality; this may lead to a phenomenon known as "dose creep," whereby technologists tend to use unnecessarily high exposures. Dose creep is most likely to occur in examinations such as portable radiography in which automatic exposure control is not feasible and manual technique factors must be chosen [11].

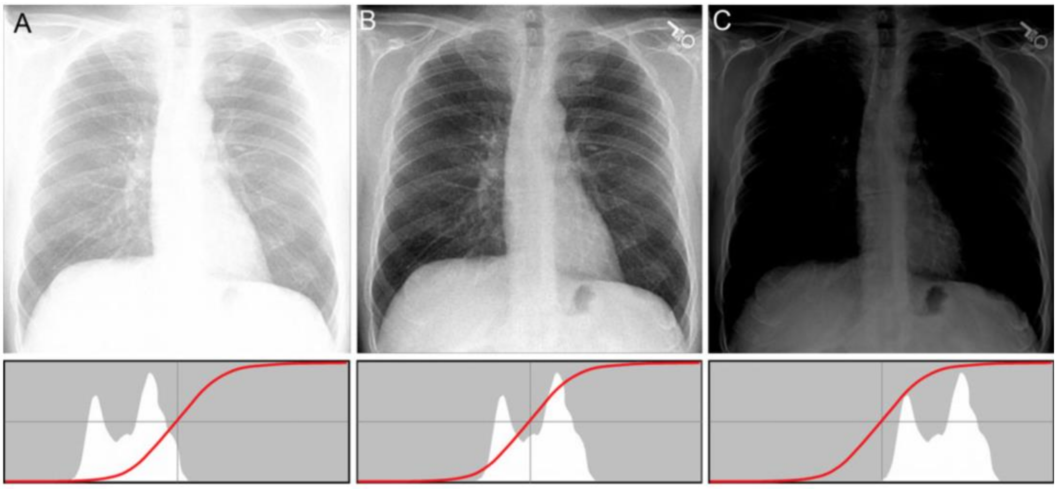

Figure 2.7 The responses of a screen-film detector with a fixed radiographic speed to (A) underexposure, (B) correct exposure and (C) overexposure. Underneath each image is a histogram representing the intensity of X-rays transmitted through the patient. The x-axis represents transmitted exposure intensity and the y-axis represents magnitude. The s-shape line is the characteristic curve that translates exposure intensity into optical density on the processed film. Note that this curve does not change position along the exposure axis [12].

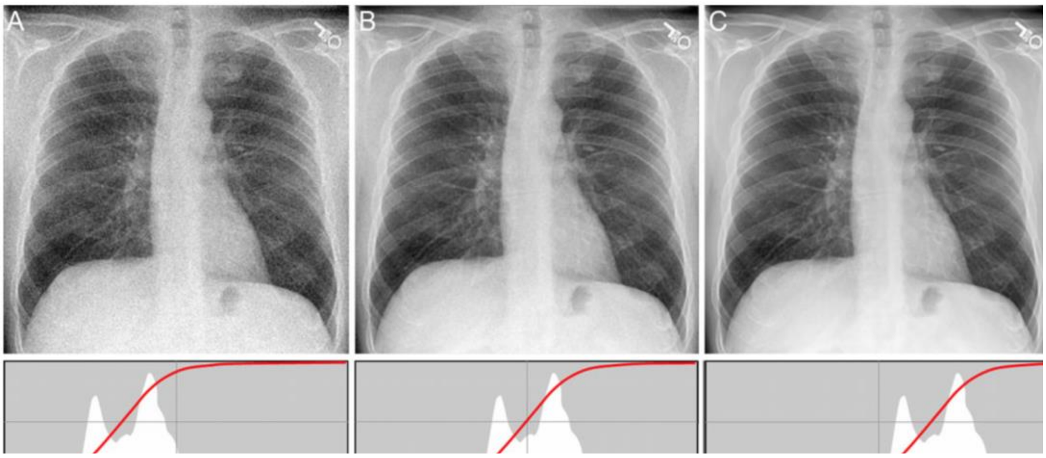

Figure 2.8 Response of a digital detector to exposure intensity variations. (A) Underexposure. (B) Correct exposure. (C) Overexposure. Underneath each image is a histogram representing the frequency distribution of digital values (directly related to intensity of x-rays transmitted through the patient, as in figure. 2.7). The x-axis represents digital value and the y-axis represents frequency. The s-shape line is the characteristic curve (a digital value of interest look-up-table, VOILUT) that translates raw digital value into a contrast and brightness optimized image ready for presentation. The VOILUT is adjusted to the histogram to achieve optimal rendering of the image content [12].

In most digital radiographic systems, image-processing algorithms are used to align measured histogram values (after exposure) with a predetermined look-up-table, to make image gray scale appear similar to screen-film images. The measured histogram distribution on each radiograph is used to determine the incident radiation exposure to the detector, and to provide an "exposure index" value. Anatomically relevant areas of the radiograph are segmented (parts of the image corresponding to no patient attenuation high values, and collimated regions—low values, are excluded), a histogram is generated from the relevant image area, and it is compared to an examination-specific (e.g. chest, forearm, head, etc.) histogram shape. The gray scale values of the raw image are then digitally transformed using a look-up-table (LUT) to provide desirable image contrast in the "for presentation" image [11].

The median value of the histogram is used in many systems to determine a proprietary exposure index (EI) value, which is dependent on each manufacturer's algorithm and detector calibration method. This exposure index indicates the amount of radiation reaching the detector and is not an indicator of dose to the patient. Unfortunately, widely different methods to calculate the EI value have evolved, as shown in table 2.1 [11].

An international standard for an exposure index for digital radiographic systems has been published by the International Electrotechnical Commission (IEC), IEC 62424-1. This standard describes "Exposure Indices" and "Deviation Indices," along with a method for placing these values in the DICOM header of each radiographic image. The manufacturer's responsibility is to calibrate the imaging detector according to a detector-specific procedure, to provide methods to segment pertinent anatomical information in the relevant image region, and to generate an EI from histogram data that is proportional to detector exposure [11].

Table 2.1 DR Exposure indicators, Units, and Calibration conditions [13].

Manufacturer	Indicator name	Symbol	Units	Exposure dependence	Calibration conditions
Fujifilm	S Value	S	Unitless	200/s X(mR)	1 mR at 80 kVp 3mm Al (Total) => S200[a]
GE	Uncompensated Detector Exposure	UDExp	μGy Air KERMA	UDExp $\propto$ X (μGy)	80 kVp, standard filtration, no grid
GE	Compensated Detector Exposure	CDExp	μGy Air KERMA	CDExp $\propto$ X (μGy)	kVp, grid, and additional filter compenssation
GE	Detector Exposure Index	DEI	Unitless	DEI $\approx$ 2.4X (mR)[a]	Not available
Philips	Exposure Index	EI	Unitless	100/S $\propto$ X (mR)	RQA5, 70 kV, +21mm Al, HVL=7.1mm Al
Siemens Medical Systems	Exposure Index	EXI	μGy Air KERMA	X(μGy)=EI/100	RQA5, 70 kV, +0.6mm Al, HVL=6.8mm Al

2.1.7.1 Target exposure index (EI_T)

EI_T is the target reference exposure obtained when the image receptor is exposure properly. The values may differ for each body part and projection (for example, chest, abdomen, and foot) and vary by the sensitivity of the detector in each examination room (depending on the factors such as filtration or sensitivity of detector plate) [14].

The EI_T should provide the exposure that produces a balance between image quality and noise level acceptable to the radiologist. Currently, little information exits about establishing EI_T value. A unique value may be needed for each detector type and each body part. However, similar body part (for example, Abdomen and pelvis, hands and feet) may use similar value of EI_T, provide the image processing by the vendor and kVp on the x-ray machine are similar [14].

2.1.7.2 Deviation index (DI)

Feedback to the user on whether an "appropriate" exposure has been achieved is given by the deviation index (DI), calculated as

$$\mathbf{DI = 10 \times (Log_{10}\ [EI/EI_T])}$$

The DI provides feedback to the operator with a value that is equal to 0 (zero) when the intended exposure to the detector is achieved (i.e., EI = EI_T), a positive number when an overexposure has occurred, and a negative number when an underexposure has occurred. A DI of +1 indicates an overexposure of about 26%; a value of -1 indicates an underexposure of 20% less than desired. The acceptable range of DI values is approximately from +1 to -1. When the DI is in the desired range, the radiographic system is considered to be working well and is able to deliver the EI_T values set up by the institution. Tracking DI values with respect to equipment and technologist can be useful in maintaining high image quality for radiography at an institution [11].

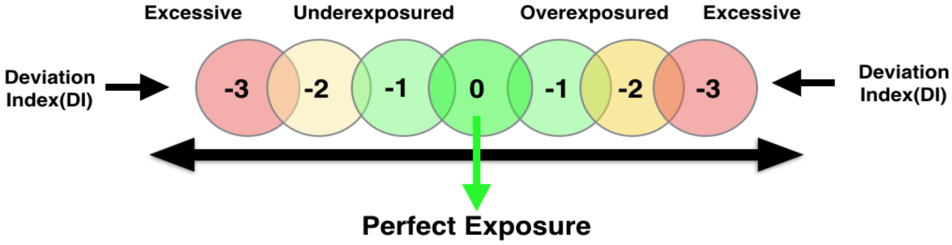

Figure 2.9 The feedback of the deviation index.

2.1.7.3 Limitation of exposure index

The EI is an indication of incident x-ray exposure at the image detector and not the radiation dose of the patient. There are various methods that manufacturers use to determine relevant image regions to analyze when generating EI values depending on the vendor. The wide exposure range afforded by digital imaging and issues such as poor collimation, patient positioning or a patient's unusual body habitus can cause EIs to be higher or lower than expected [6].

2.1.8 ALARA

With increasing awareness of the need for radiation protection, a paradigm shift can be observed from the principle of "image quality as good as possible" to "image quality as good as needed." The radiation dose to patients should be as low as reasonably achievable (ALARA) while still providing image quality adequate to enable an accurate diagnosis. ALARA does not necessarily mean the lowest radiation dose, nor, when implemented, does it result in the least desirable radiographic image. What, indeed, constitutes adequate image quality is still open for discussion for the various imaging task. There is a multitude of studies in the literature comparing the performance of one system with another "reference" system to define the amount of possible dose reduction that would still achieve an image quality equivalent to that provided by the acknowledged reference. Using this approach, it is possible to survey parameters, such as the detection of artificial lesions or the semi-quantitative assessment of subjective image impression, as a surrogate for image quality and relate these parameters to a reference of dose. To define, however, the minimum level of image quality needed to reliably make a certain type of diagnosis is much more difficult. Individually defining the minimal dose to reliably answer a specific diagnostic question in a prospective manner seems to be impossible, given the vast variety of patient-related and disease-related conditions and the workflow for radiographic examinations [15].

Reduction of patient dose according to the ALARA principle is not only a question of selecting the right detector, but also requires the optimization of the whole imaging chain and the selection of appropriate imaging parameters [15].

2.1.9 Observer performance methods based on visibility of anatomical structures

The methods used to evaluate the visibility of anatomic structures such as visual grading analysis (VGA) and image criteria (IC). In VGA analysis, the aim is to compare the visibility of defined structures in the image to be evaluated with the same structures in a reference image. This evaluation is often based on a 5-level grading scale for image comparison. In IC analysis, the aim is to decide if the image criterion based on a reference frame is present or not in the image giving a score for that purpose. The criteria can be used to highlight optimum radiographic technique in terms of image quality and patient dose [9].

2.2 Review of related literature

Sangdao P, et al. [3] (2014) investigated the radiation dose and image quality for digital mobile chest radiography**.** Lung phantom was firstly used to study the appropriate exposure parameters to optimize the radiation dose at surface of the phantom and image quality based on the Commission of European Communities (CEC). The exposure parameters obtained also further used for patients. The proper exposure parameter for chest radiography was 90 kVp and 0.63 mAs for the patient chest thickness equal to or less than 23 cm. 50 patients were exposed by optimal parameters, then the patient dose had been calculated and the image quality has been assessed by three observers. The average patient dose was 0.076 mGy and the average of patient chest thickness was 19.70 cm. 88% of the images showed the image criteria score equal to or more than 3. The acceptable score ranged from 3 to 6 were obtained. 70% and 30% of the images showed the qualitative noise scores of 2 and 3 with the acceptable score ranged from 2 to 3 respectively. The patient dose for routine chest study was 0.192 mGy. Therefore, the patient doses using optimal protocol was 60% less than routine study and also lower than the International Atomic Energy Agency (IAEA) dose reference level of 0.4 mGy recommended for chest radiography.

Masoud A, et al. [16] (2006) evaluated the radiation doses to patient during chest and abdomen CR examinations, and assessed the related level of optimization at five referral hospitals in Tanzania. The international code of practice for dosimetry in diagnostic radiology was applied to determine the entrance surface air kerma (ESAK) to patients. The level of optimization was assessed from low-contrast objects scores of phantom images at different exposures. The results showed that mean ESAK varied from 0.16 to 0.37 mGy for chest PA and from 2 to 6 mGy for abdomen AP. Assuming similar patient and phantom attenuations, the optimization performed at all facilities was consistent with phantom evaluations in terms of tube potential settings in use. However, all facilities seemed to operate at higher tube load values above 5 mAs for chest examination, which can lead to unnecessary patient doses. Inadequate initial training on CR technology explains in large proportion the inappropriate use of exposure parameters.

Aldrich JE, et al. [17] (2006) compared the patient x-ray exposures that arise from common medical imaging procedures when using screen-film radiography, computed radiography, and digital radiography. The study consist of measurement of the radiation exposures received by a reference group of patients for common radiographic procedures such as chest PA, chest LAT, abdomen AP, and pelvis AP using screen-film radiography, CR, or DR. 110 patients were measured the surface dose during chest, abdomen and pelvis radiography selected only on the basis of patient weight (70 ± 10 kg). For film-screen and CR, the surface doses were measured with TLDs and converted to ESAK. For DR, the dose was estimated from the DAP meter built into the collimator of the DR equipment and converted to ESAK. CR doses were the same as or higher than for film-screen, and the doses were lower for DR compared to film-screen. Subsequent clinical experience with the systems led to changes in the technique used for chest examinations both for CR and for DR. For CR, it was possible to change the algorithm and decrease the dose to one quarter of the initial value with acceptable image quality. For DR, it was decided to reduce noise by increasing the dose by a factor of two. No changes were made to abdomen or pelvic imaging techniques for either CR or DR. The final patient surface doses using CR were similar to published diagnostic reference doses; for DR, all patient doses were less than published reference levels.

Muhogora WE, et al. [18] (2008) presented patient doses in radiographic examinations in 12 countries in Asia, Africa, and Eastern Europe covering 45 hospitals which using screen film system in 2005. This study was to survey image quality and the entrance surface air kerma (ESAK) for patients in radiographic examinations and to perform comparisons with diagnostic reference levels. The rate of unsatisfactory images and image quality grade were noted, and causes for poor image quality were investigated. The entrance surface doses for adult patients were determined in terms of the entrance surface air kerma (ESAK) on the basis of x-ray tube output measurements and x-ray exposure parameters. The fraction of images rated as poor was as high as 53%. The image quality improved up to 16% in Africa, 13% in Asia, and 22% in Eastern Europe after implementation of a quality control (QC) program. Patient doses varied by a factor of up to 88, although the majority of doses were below diagnostic reference levels. The mean entrance surface air kerma values in mGy were 0.33 (chest, posteroanterior), 4.07 (lumbar spine, anteroposterior), 8.53 (lumbar spine, lateral), 3.64 (abdomen, anteroposterior), 3.68 (pelvis, anteroposterior), and 2.41 (skull, anteroposterior). Patient doses were found to be similar to doses in developed countries and patient dose reductions ranging from 1.4% to 85% were achieved. Poor image quality constitutes a major source of unnecessary radiation to patients in developing countries. Comparison with other surveys indicates that patient dose levels in these countries are not higher than those in developed countries.

Asada Y, et al. [19] (2016) were surveyed patient exposure from general radiography and mammography in Japan in 2014. Questionnaires were sent to 3000 facilities nationwide in Japan. Surveys asked questions on a total of 16 items related to general radiography, including the chest, abdomen, and breast. Output data from x-ray tubes measured in the Chubu area of Japan were used as the mean in these estimates. The index of patient exposure was adopted as the entrance skin dose (ESD) for general radiography and as the mean glandular dose (MGD) for mammography. The response rate for this survey was 21.9%. The mean entrance skin dose (ESD) were 0.48 (chest, posteroanterior), 3.35 (lumbar spine, anteroposterior), 8.86 (lumbar spine, lateral), 2.24 (abdomen, anteroposterior), 2.48 (pelvis, anteroposterior), 2.07 (skull, anteroposterior) and 1.66 (Mammography). The results showed that doses received through the use of flat-panel detector (FPD) devices were lower than those received through computed radiography devices. These results suggest that more widespread use of FPD devices could lead to decreases in the ESD and MGD, thereby reducing patient exposure.

From the literatures reviewed, the image quality using CR and DR are not significantly different in clinical images. However, the lower radiation dose using DR system is expected compared with the same radiographic examination using CR system because the efficiency of the physical properties in DR detector is better in terms of DQE, MTF, dynamic range and post image processing. Therefore, the radiation doses in patients are reduced. The aimed of this study is to optimize the radiation dose and image quality in abdominal radiography using digital mobile x-ray system based on human-liked phantom.

CHAPTER III

RESEARCH METHODOLOGY

3.1 Research design

This is an experimental study.

3.2 Research design model

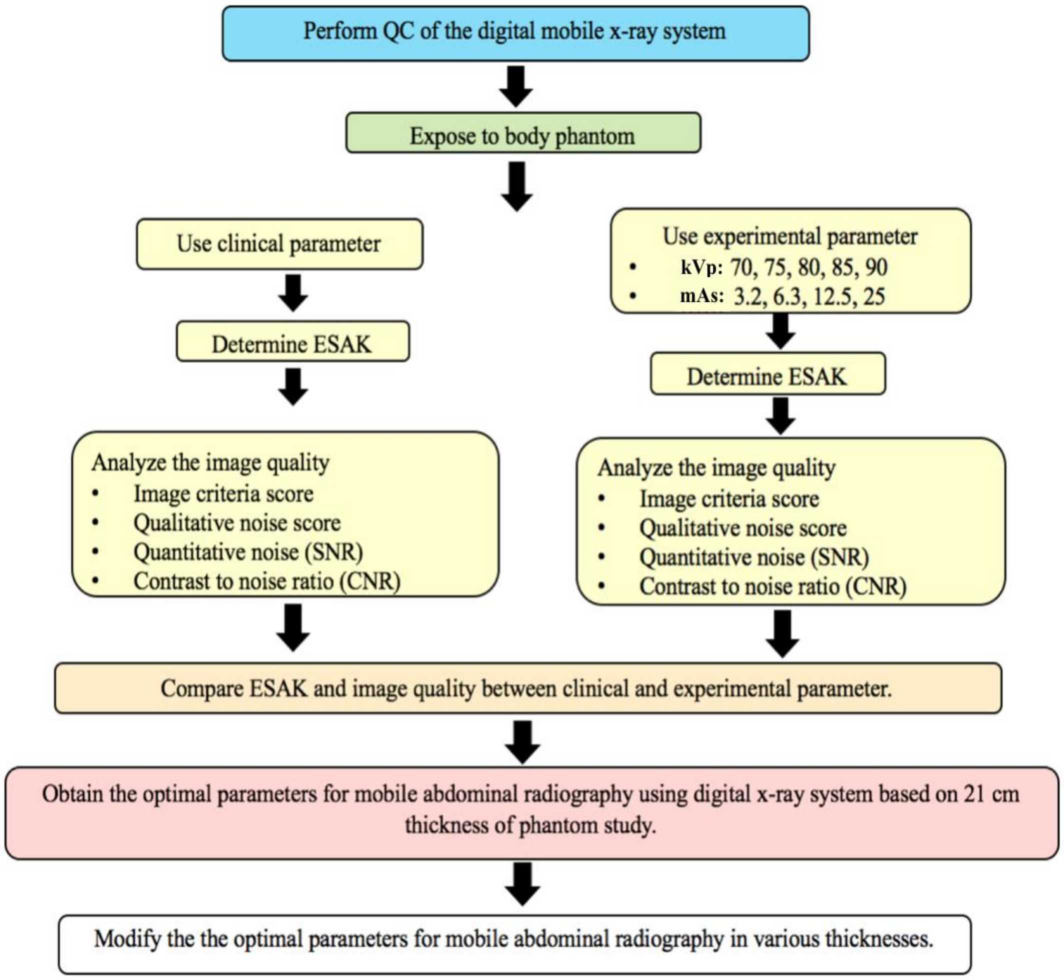

Figure 3.1 Research design model.

3.3 Conceptual framework

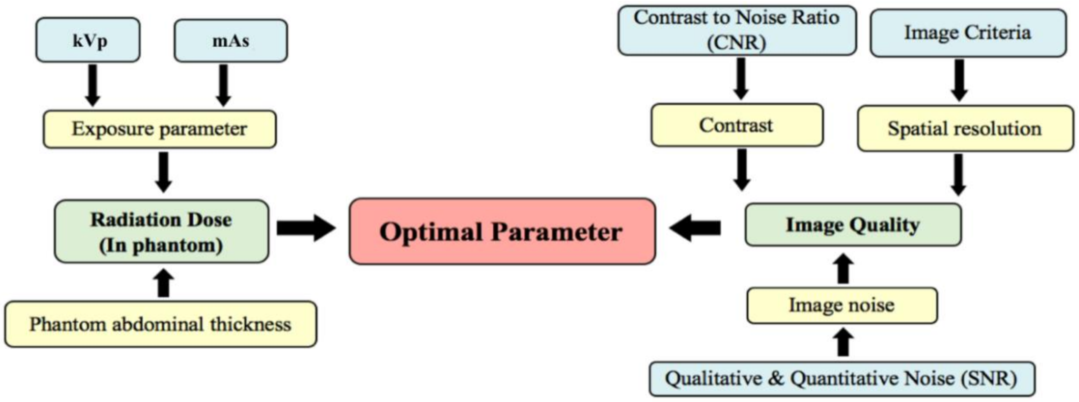

Figure 3.2 Conceptual framework.

3.4 Research question

What is the optimal exposure parameter for abdominal radiography using digital mobile x-ray system in phantom study?

3.5 Research objectives

3.5.1 To optimize the radiation dose and image quality for abdominal radiography in phantom using digital mobile x-ray system at King Chulalongkorn Memorial Hospital (KCMH).

3.5.2 To optimize the parameters using digital mobile x-ray system for abdominal radiography in various thicknesses.

3.6 Materials

3.6.1 Digital mobile x-ray system

In this study, digital mobile x-ray system manufactured by General Electric (GE), model Optima XR220amx at King Chulalongkorn Memorial Hospital was used as illustrated in figure 3.3. The kVp selection range was 50-125, in 1 kVp increments. The tube current-time selection range was 0.20-400.00 mAs. The mAs selections are not available at all kVp settings. The digital flat panel detector model Flatpad including anti-scatter grid was used as the image receptor. The physical characteristic of the receptor consists of single panel amorphous silicon detector (Indirect conversion detector) with a Cesium Iodide scintillator. The image area of detector is 40.4 x 40.4 cm^2. The weight of digital receptor is 4.3 kilograms. The grid ratio is 6:1.

Figure 3.3 Digital mobile x-ray system manufacturer General Electric (GE), model Optima XR220amx and digital receptor with grid.

3.6.2 Solid state dosimeter

The solid state dosimeter manufactured by Radcal Corporation model Accu-Gold with DDX6-W sensor was used to calibrate the radiation dose in digital mobile x-ray system in terms of beam quality, exposure consistency, kVp accuracy and mAs linearity. The properties of solid state dosimeter could measure dose, dose rate, pulse, pulse rate, dose/frame, kVp, time, HVL, total filtration and waveforms simultaneously. The advantage of this dosimeter is not influenced by temperature and pressure. The Accu-Gold dosimeter physical characteristic is shown as in figure 3.4.

Figure 3.4 The solid state dosimeter dosimeter; Radcal Corporation model ACCU-Gold.

Table 3.1 Specification of the solid state dose sensors model 10X6-6.

Chamber	**10X6-6**
Min dose rate	20 nGy/s
Max dose rate	205 mGy/s
Min dose	100 nGy
Max dose	559 Gy
Accuracy:	±5% using x-rays @ 80 kVp with 2,5 mm Al total filtration (IEC 61267 RQR-6)
Energy dependence:	±5% from 50 kVp to 120 kVp at 2.5 mm Al
Filtration dependence:	+10% to -5% from 2.5 mm Al to 23 mm Al
Size	35.6 mm x 20.0 mm x 11.8 mm

3.6.3 Luminance meter

The luminance meter manufactured by UNFORS Raysafe model Xi was used to calibrate the display monitor as shown in figure 3.5.

Figure 3.5 The luminance meter manufacturer UNFORS Raysafe model Xi.

3.6.4 Ionization chamber dosimeter

The ionization chamber dosimeter manufacturer Radcal Corporation model Accu-Gold with ion chamber dose sensors model 10X6-6 was used to measure the entrance surface air kerma (ESAK) and incident air kerma in anthropomorphic as in figure 3.6. The chamber sensitive volume is 38 mm^3.

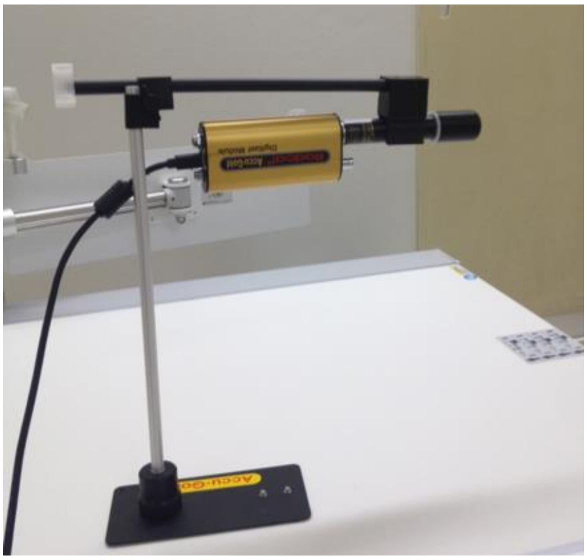

Figure 3.6 The ionization chamber dosimeter; Radcal Corporation model ACCU-Gold with ion chamber dose sensors model 10X6-6.

Table 3.2 Specification of the ion chamber dose sensors model 10X6-6.

Chamber	**10X6-6**
Min dose rate	20 nGy/s
Max dose rate	149 mGy/s
Min dose	100 nGy
Max dose	516 Gy
Cine specifications	1 nGy/f >10 mGy/f
Calibration accuracy	±4% using x-rays @ 60kVp and 2.8 mm Al HVL
Exposure rate Dependence	±5%, 0.4 mR/s to 80 R/s, up to 500 R/s for 50 us pulses
Energy dependence	±5%, 30 keV to 1.33 MeV (with build-up material)
Construction	Polycarbonate walls and electrode conductive graphite interior coating; 6 cm^3, active volume; 0.05 kg

จุฬาลงกรณ์มหาวิทยาลัย
CHULALONGKORN UNIVERSITY

3.6.5 The whole-body phantom

The whole-body phantom manufacturer Kyoto Kagaku model PBU-60 as in figure 3.7 is life-size human phantom with a life-size syntactic skeleton which is embedded in a radiological soft-tissue substitute. The abdominal part of the phantom, 21 cm thickness, embedded with liver, kidneys, spleen, pancreas, stomach (air), sigmoid colon and rectum was used for investigating the parameters in this study.

Figure 3.7 The whole-body phantom, KYOTOKAGAKU model PBU-60.

Table 3.3 Specification of the whole-body phantom, KYOTO KAGAKU model PBU-60.

KYOTOKAGAKU model PBU-60	
Original phantom materials	Radiology absorption and Hounsfield number approximate to human body.
Materials and features	
Soft tissue and organs	Urethane base resin (SZ-50)
Synthetic bones	Epoxy base resin
Joint attachments	Epoxy, urethane with carbon fiber
Screws	Poly carbonate
Phantom size	165 cm height
Phantom weight	50 kg
Internal organs: **Trunk**	Vertebrae, clavicles, ribs, sternum, scapula, coxal bones, femurs, lungs with pulmonary vessels (up to third bifurcations), trachea (up to fourth bifurcations), liver with portal and hepatic veins Pancreas, gallbladder, spleen, ureter, urinary bladder, prostate, rectum, sigmoid and colon
Hounsfield number (Approximation)	
Soft tissue	-70
Liver	70
Kidney	30

จุฬาลงกรณ์มหาวิทยาลัย
Chulalongkorn University

Table 3.3 Specification of the whole-body phantom, KYOTO KAGAKU model PBU-60 (Continuned).

KYOTOKAGAKU model PBU-60	
Density g/cm^3	
Soft tissue	1,061
Liver	1,089
Kidney	1,075

3.6.6 Buildup layer of multipurpose chest phantom N1 LUNGMAN

The buildup layer of multipurpose chest phantom N1 LUNGMAN was used to simulate a larger body type and x-ray absorption to obtain various thickness sizes of phantom. The buildup layer was enclosed on both anterior and posterior of the whole-body phantom. The thickness of abdominal part was then increased to 25 and 29 cm as in figure 3.8.

Figure 3.8 The whole-body phantom with buildup layer**.**

3.6.7 Medical grade high-resolution display monitors widescreen 3 mega pixels

The medical grade high resolution display monitor widescreen 3 mega pixels, Barco model Coronis Fusion as illustrated in figure 3.9 was used for displaying and evaluating the image quality and noise level of the abdominal x-ray images in various parameters.

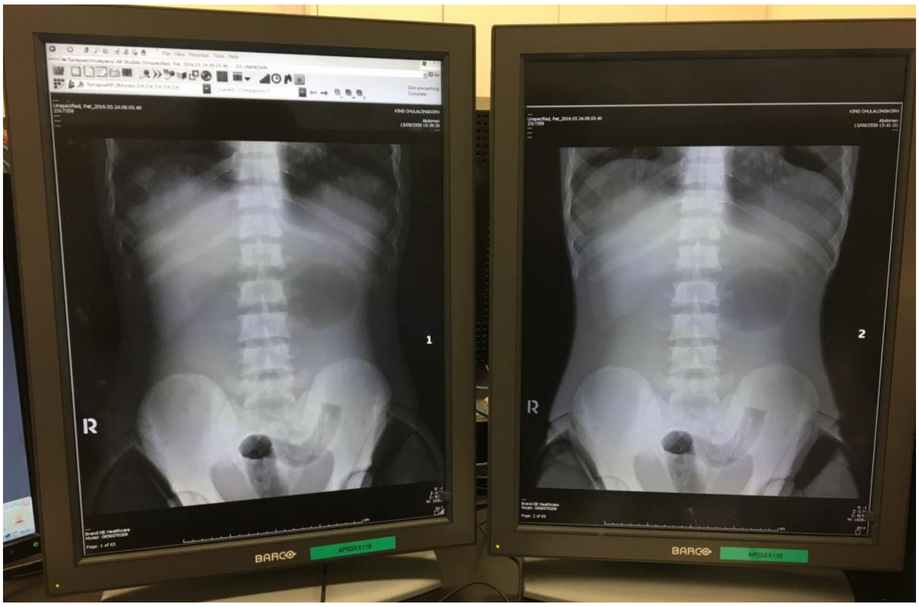

Figure 3.9 Display monitor widescreen 3 mega pixels, Barco model Coronis.

3.7 Methods

3.7.1 Perform the quality control of digital mobile x-ray system and digital image receptor

The quality control of digital mobile system was operated following the American Association of Physicists in Medicine (AAPM) report No.74 [20] including electromechanical component and radiation dose. The quality control of the digital image receptor following King's Center for the Assessment of Radiological Equipment (KCARE) [21] protocol was used protocol to assess the digital detector performance. The tests consist of dosimetry, linearity and system transfer properties, image retention, sensitivity index consistency, uniformity, scaling error, blurring and stitching artifacts, limiting spatial resolution, and threshold contrast detail detectability. The example of quality control of the digital mobile system and digital image receptor were shown in figure 3.10.

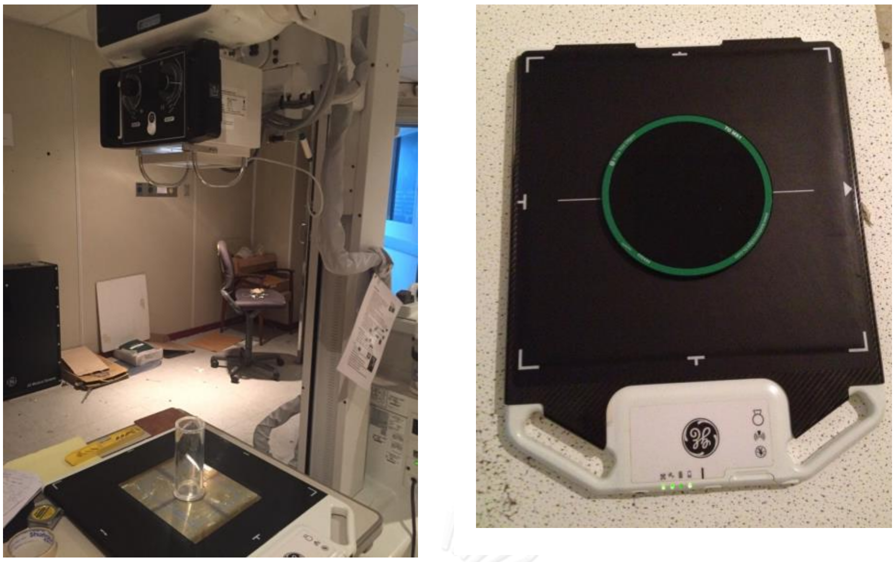

A B

Figure 3.10 (A) Set up of the cross hair centering in the quality control of x-ray tube.
(B) Set up of blurring and stitching artifacts in the quality control digital image receptor.

3.7.2 Perform the quality control of display monitor

The quality control of display monitor was operated following the AAPM Task Group 18 [22]. The TG18-QC test image consists of general image quality and artifacts, geometric distortion, luminance and resolution as in shown figure 3.11.

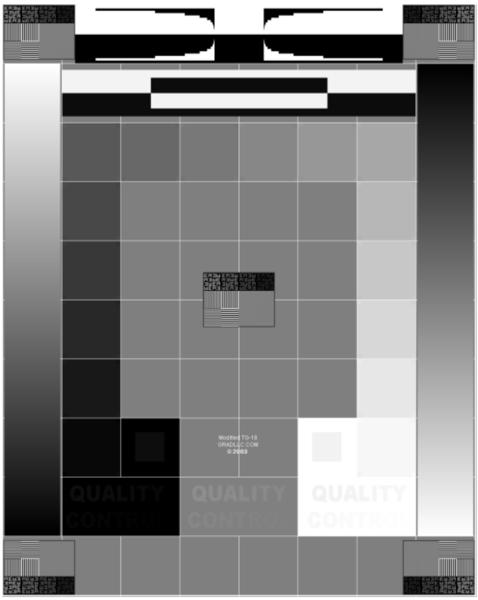

Figure 3.11 TG18-QC (Test image)

วิทยาลัย
UNIVERSITY

3.7.3 Determine the backscatter factors (BSF)

The backscatter factor from the whole-body phantom was determined for varying exposure parameters of tube voltage ranged from 70-90 kVp, and the various thicknesses of the abdomen consist of 21, 25, and 29 cm as below.

3.7.3.1 For 21 cm thickness of abdomen in phantom, the x-ray tube of digital mobile x-ray unit and ionization chamber dosimeter were set up in air by positioning 100 cm of source to detector distance (SDD), 79 cm of source to chamber distance (SCD) which is closed to the surface of the phantom, and 41×41 cm^2 of field size as illustrated in figure 3.12.

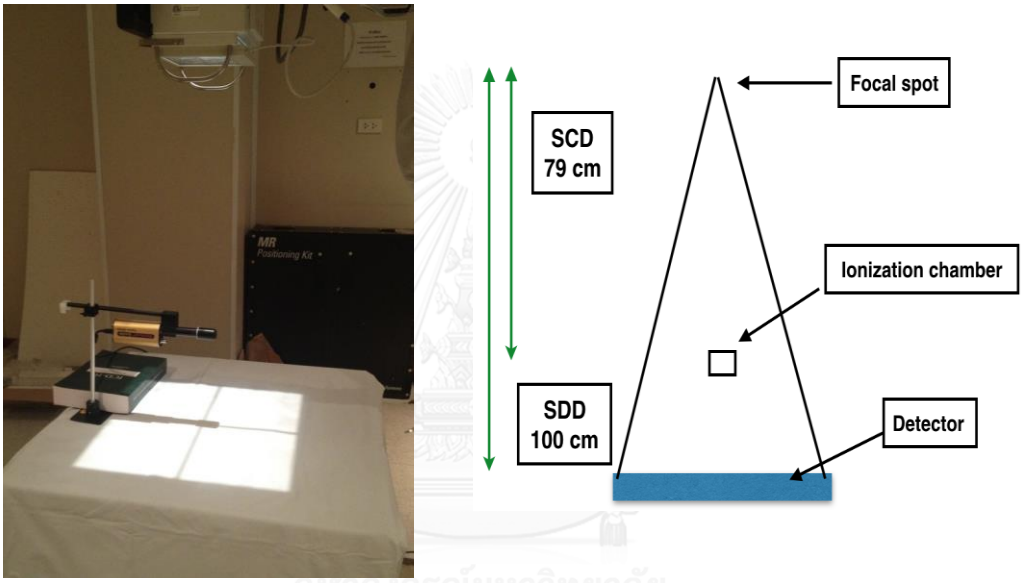

Figure 3.12 Set up positioning for incident air kerma (K_i) measurement for 21 cm thickness of abdomen in phantom.

จุฬาลงกรณ์มหาวิทยาลัย
CHULALONGKORN UNIVERSITY

3.7.3.2 Varied the experimental parameters as follows: kVp at 70, 75, 80, 85, and 90, and mAs at 3.2, 6.3, 12.5, and 25.0 including the routine clinical parameter for abdominal radiography of 21 cm thickness at 75 kVp and 32 mAs. The ionization chamber was then exposed to determine the incident air kerma (K_i).

3.7.3.3 Set the whole-body phantom under the ionization chamber and exposed with same parameters as in 3.7.3.2 to measure the entrance surface air kerma (ESAK) with the same field size (41×41 cm^2) as in figure 3.13.

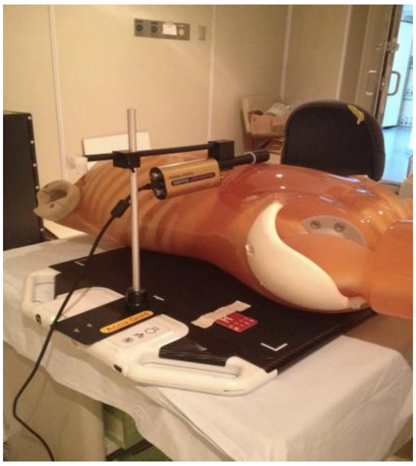

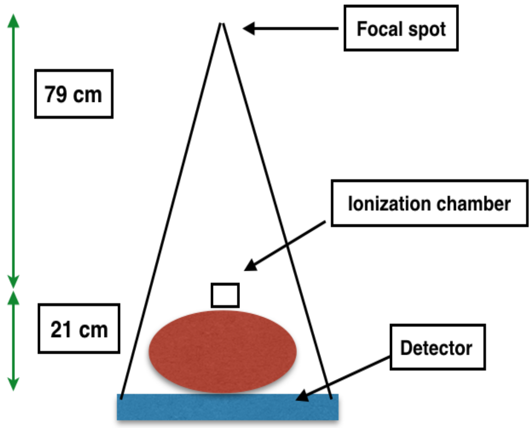

Figure 3.13 Set up for entrance surface air kerma (K_e) measurement for 21 cm thickness of abdomen in phantom.

3.7.3.4 Calculate the backscatter factor for the 21 cm thickness of abdomen in whole-body phantom by the following equation

$$\mathbf{BSF} = \frac{\textbf{Entrance surface air kerma (ESAK)}}{\textbf{Incident air kerma (Ki)}} \quad \text{......... Equation 3.1}$$

3.7.3.5 For 25 cm thickness, the build up layer was enclosed on the phantom and set the x-ray tube of digital mobile x-ray unit and ionization chamber dosimeter in air by positioning 100 cm of SDD, 75 cm of SCD which is closed to the surface of the phantom and 41×41 cm^2 of field size as illustrated figure 3.14.

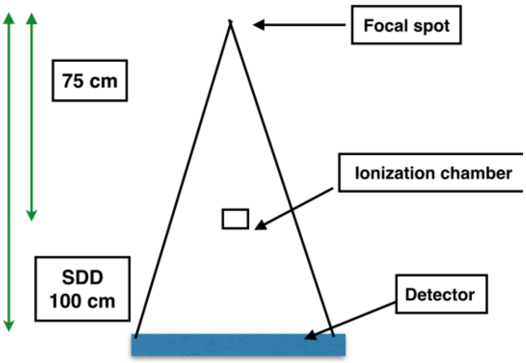

Figure 3.14 Set up positioning for incident air kerma (K_i) measurement for 25 cm thickness of abdomen in phantom.

3.7.3.6 Varied the experimental parameters as follows: kVp at 70, 75, 80, 85, and 90, and mAs at 3.2, 6.3, 12.5, and 25.0 including the routine clinical parameter for abdominal radiography of 25 cm thickness at 80 kVp and 32 mAs. The ionization chamber was then exposed to determine incident air kerma (K_i).

3.7.3.7 Set the whole-body phantom, 25 cm thickness under the ionization chamber and exposed with same parameters as in 3.7.3.6 to measure the entrance surface air kerma (ESAK) with the same field size (41×41 cm^2) as shown in figure 3.15.

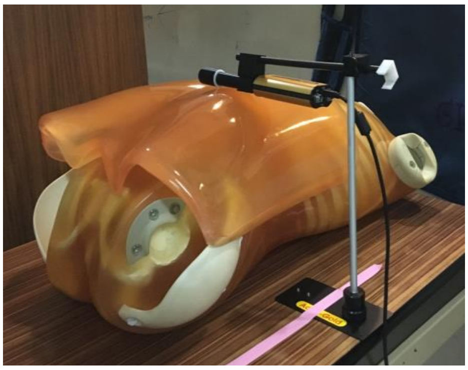

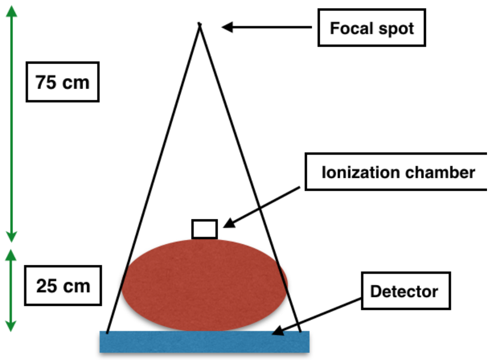

Figure 3.15 Set up for entrance surface air kerma (K_e) measurement for 25 cm thickness of abdomen in phantom.

3.7.3.8 Calculate the backscatter factor for the 25 cm thickness of abdomen in whole-body phantom by using equation 3.1.

3.7.3.9 For 29 cm thickness, the buildup layer was enclosed on the phantom and set the x-ray tube of digital mobile x-ray unit and ionization chamber dosimeter was set up in air by positioning 100 cm of SDD, 71 cm of SCD which is closed to the surface of the phantom, and 41×41 cm^2 of field size as illustrated figure 3.16.

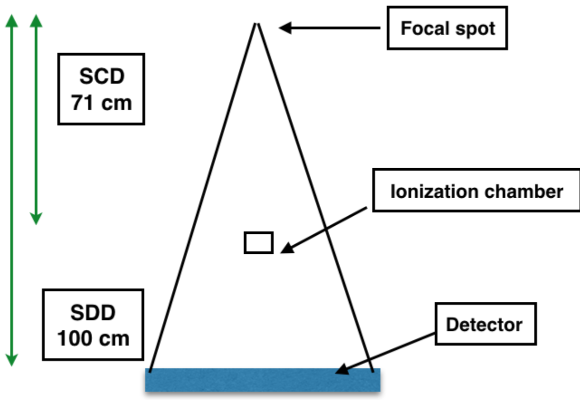

Figure 3.16 Set up positioning for incident air kerma (K_i) measurement for 29 cm thickness of abdomen in phantom.

3.7.3.10 Varied the experimental parameter as follows: kVp at 70, 75, 80, 85, and 90 and mAs at 3.2, 6.3, 12.5, and 25.0 including the routine clinical parameter setting for abdominal radiography of 29 cm thickness at 85 kVp and 32 mAs. The ionization chamber was then exposed to determine incident air kerma (K_i).

3.7.3.11 Set the whole-body phantom, 29 cm thickness under the ionization chamber and exposed with same parameters as in 3.7.3.10 to measure the entrance surface air kerma (ESAK) with the same field size (41×41 cm^2) as illustrated in figure 3.17.

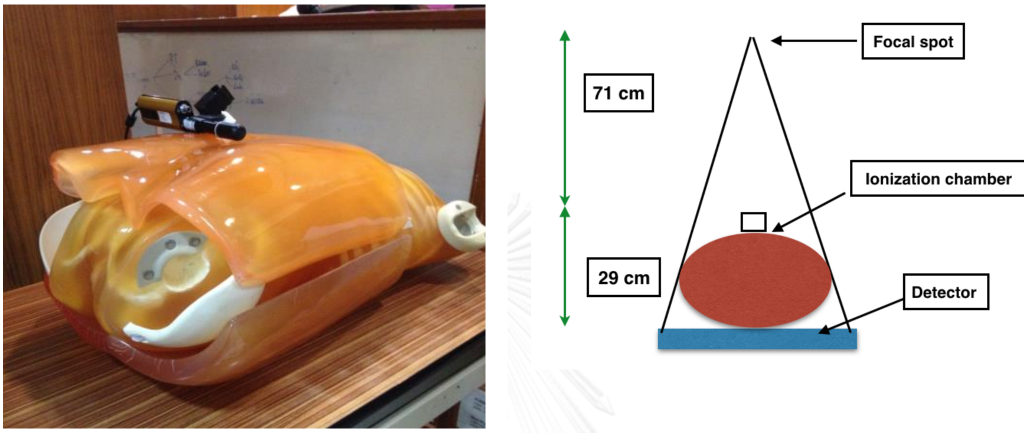

Figure 3.17 Set up for entrance surface air kerma (K_e) measurement for 29 cm thickness of abdomen in phantom.

3.7.3.12 Calculate the backscatter factor for the 29 cm thickness of abdomen in whole-body phantom by the following equation in 3.1.

3.7.4 Calculate the ESAK in the phantom in each thickness

The ESAK for 21, 25 and 29 cm thickness of whole-body phantom was calculated for various exposed experimental parameters of 70-90 kVp and 3.2-25.0 mAs. These also included the routine clinical parameters of 75, 80, 85 kVp and 32 mAs for portable abdominal radiography at SID 100 cm. The ESAK can be calculated by equation 3.2 and 3.3:

$$\mathbf{K_i = Y(d) \times P}\boldsymbol{It} \times (\frac{\mathbf{d}}{\mathbf{d\ FTD-tp}})^2 \text{ .... Equation 3.2}$$

$$\mathbf{K_e = K_i \times BSF} \text{ .... Equation 3.3}$$

Where:

	K_i	=	Incident air kerma (mGy)
	Y(d)	=	X-ray tube output (mGy/mAs)
	P_{it}	=	Tube loading (mAs)
	d	=	Focus to chamber distance (cm)

d_{FTD} = Focus to table top distance (cm)
t_p = Phantom thickness (cm)
K_e = Entrance Surface Air Kerma (mGy)
BSF = Back Scatter Factor

3.7.5 Image quality evaluations

For the 21 cm thickness of whole-body phantom, the experimental and routine clinical parameters were set as in 3.7.3.2. For the 25 cm thickness of whole-body phantom, the experimental and routine clinical parameters were set as in 3.7.3.6. And 29 cm thickness of whole-body phantom, the experimental and routine clinical parameters was set as in 3.7.3.10.

3.7.5.1 Evaluate the image quality and qualitative noise on phantom images.

The image quality of the abdominal radiographs in each protocol was then evaluated by randomized blinded method by at least two years' experience of three observers. The qualitative image quality score was analyzed based on the International Atomic Energy Agency (IAEA) as shown in table 3.4 and the qualitative noise score was evaluated based on the whole images noise as shown in table 3.5.

Table 3.3 Score image criteria based on the IAEA.

Item	Image criteria	Score
1	Sharp visualization of ribs.	
2	Visualization of lower margin of liver, spleen and kidneys.	
3	Visualization of spleen.	
4	Visualization of kidneys.	
5	Sharp visualization of stomach and bowel loop.	
6	Visualization of ribs and transverse processes of lumbar vertebrae.	
7	Markers indicating either upright or supine position.	

* Rate image score: 0,0.5, and 1 where 0 = not fulfilled, 0.5 = partly fulfilled, 1 = fulfilled

The acceptable of image quality score; total score ≥ 5 from 7 points.

Table 3.4 Rate of qualitative noise score.

Qualitative noise	**Score**
Rate of qualitative noise score**:** 0 = free of noise, 1 = scarce noise, 2 = significant noise, 3 = obvious noise	

*__Score 1 or 2 is acceptable of image noise criteria__.

3.7.5.2 Quantitative image analysis

The quantitative image analysis was evaluated in terms of signal-to-noise ratio (SNR) and contrast-to-noise ratio (CNR).

3.7.5.2.1 Signal-to-noise ratio (SNR)

The SNR was evaluated by placing 3 regions of interests (ROIs) on the image 3 times for each position (figure 3.14) by using raw data image following this equation:

$$\mathbf{SNR} = \frac{\mathbf{Pixel\ value\ in\ ROI}}{\mathbf{SD\ in\ ROI}}$$

The size of 1st, 2nd, and 3rd ROIs was 200 mm^2, 35 mm^2, and 318 mm^2, respectively.

1st ROI represents middle of the liver area.

2nd ROI represents left side of transverse process in 4th lumbar spine.

3rd ROI represents right side of flat bone in pelvis.

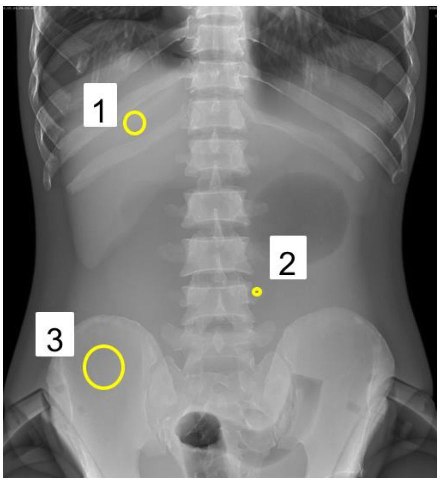

Figure 3.18 ROIs on the radiographic image.

3.7.5.2.2 Contrast-to-noise ratio (CNR)

The CNR was used to evaluate the contrast between two adjacent areas on the raw data image following this equation:

$$\mathbf{CNR} = \frac{(\bar{X}_S - \bar{X}_{Bg})}{\sigma_{Bg}}$$

Where $\bar{x}_s$ represents mean pixel value of ROI in the interested organs.
$\bar{x}_{Bg}$ represents mean pixel value of ROI in the background.
σ_{BG} represents the standard deviation in the background.

3 ROIs were added on the image as the background to measure mean pixel value and SD in the background (figure 3.19). The size of 4^{th}, 5^{th}, and 6^{th} ROIs were 200 mm^2, 35 mm^2, and 318 mm^2, respectively.

4^{th} ROI represents Lower lobe of liver.

5^{th} ROI represents Left kidney.

6^{th} ROI represents Right kidney.

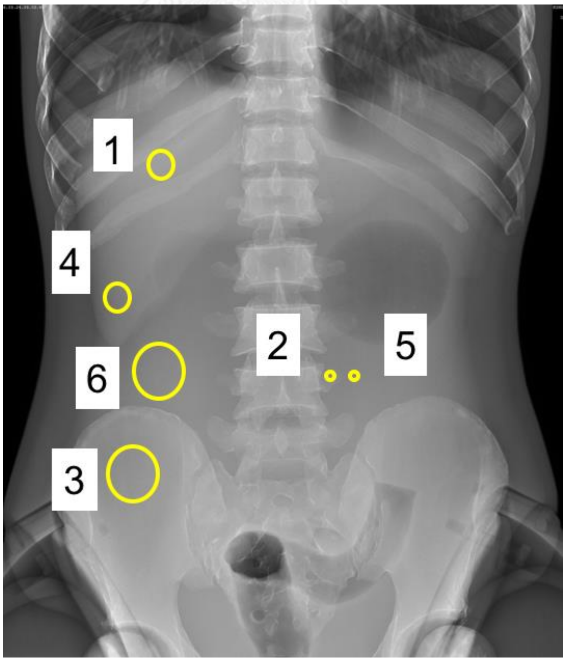

Figure 3.19 ROIs on the radiographic image for evaluating CNR.

3.7.6 Optimal parameter consideration

The optimal parameters in 21, 25, and 29 cm abdominal thickness were justified using the information of entrance surface air kerma (ESAK), exposure index (EI), image criteria score from 3 observers, and qualitative and quantitative image analysis. Ideally, the lowest radiation dose while obtaining acceptable images quality will be selected.

The ranking for obtaining the optimal parameter

3.7.6.1 The image quality score was greater or equal 5 points and the qualitative noise score were between 1 and 2.

3.7.6.2 The ESAK of abdomen was not exceed to 1.86 mGy [17].

3.5.6.3 The EI was closed to the target exposure at 336.

3.7.7 Obtain the parameters optimization for abdomen radiography using digital mobile x-ray system based on phantom study.

3.7.8 Determine the optimal parameter in various abdominal thicknesses using digital mobile x-ray system.

3.8 Outcome measurement

3.8.1 ESAK for each protocol.

3.8.2 The detector EI.

3.8.3 The image quality scored by three observers on
- Image criteria score
- Qualitative noise score

3.8.4 SNR and CNR.

3.8.5 The optimized parameter in various abdominal thicknesses using digital mobile x-ray system.

3.9 Statistical analysis

3.9.1 Descriptive statistics: mean, minimum and maximum of the radiation dose, image criteria, SNR and CNR were calculated. Mode or median of qualitative noise were determined by using Microsoft office excel.

3.9.2 Intra-class correlation coefficient (ICC) was used to evaluate the inter-rater reliability of 3 observers in terms of image criteria by using SPSS statistic version 22.

3.10 Sample size determination

As this research was performed in the phantom which is based on the experimental study, the variation of phantom can be disregarded. Statistical variation for sample size can be negligible. However, each protocol should be performed three time in order to reduce the uncertainty and variation from the exposure. As a result, the sample sizes of 189 experiments were obtained.

3.11 Data presentation format

The scatter plot and graphs were presented the correlation between radiation dose, image quality scoring, qualitative noise scoring and quantitative noise analysis.

3.12 Expected benefit

The optimization protocol for abdominal radiography in digital mobile x-ray system will be obtained in human-like phantom. The optimal protocol could be applied in abdomen AP supine projection which patient thickness had various thicknesses and maintained with low radiation dose and accepted image quality for clinical practices.

3.13 Limitation

This study was only performed in the anthropomorphic whole-body phantom, KYOTO KAGAKU model PBU-60. Only 21 cm body phantom thickness is available to study the optimal parameter. Otherwise, the build-up layer was used instead to represent the larger size thickness of the phantom.

3.14 Ethical consideration

This research is an experimental study. The research proposal has been submitted and already approved by the Institutions Review Board (IRB) of Faculty of Medicine, Chulalongkorn University, on 8 June 2016. The approved document (IRB No.243/59) is shown in appendix D.

CHAPTER IV

RESULTS

4.1 Quality control of radiographic equipment

4.1.1 Digital mobile x-ray system

The quality control of the digital mobile x-ray system was operated following the AAPM report No. 74 [20]. The tests consist of electromechanical component and radiation dose. The results of quality control were within the acceptable limits of the AAPM protocol. The summaries and details of the quality control are illustrated in appendix A.

4.1.2 Digital image receptor

The quality control of the digital image receptor was operated following the KCARE protocol [21]. The tests consist of dosimetry, linearity and system transfer properties, image retention, sensitivity index consistency, uniformity, scaling error, blurring and stitching artifacts, limiting spatial resolution, and threshold contrast detail detectability**.** The results of quality control were within the acceptable limits of the KCARE protocol. The reports of quality control of digital image receptor are illustrated in appendix B.

4.1.3 Display monitors

The quality control of display monitors was operated following the AAPM Task Group 18 [22]. The tests consist of general image quality and artifacts, geometric distortion, luminance and resolution. The reports are illustrated in appendix C.

4.2 Radiation dose and image quality evaluation of the anthropomorhine whole-body phantom

4.2.1 21 cm thickness of abdomen

4.2.1.1 Radiation dose

4.2.1.1.1 The backscatter factors (BSF)

The BSF were investigated by setting the experimental parameters at 70, 75, 80, 85, and 90 kVp and 3.2, 6.3, 12.5, and 25.0 mAs including the routine clinical parameter setting for abdominal radiography in 21 cm thickness at 75 kVp and 32 mAs. The results of BSF are shown as in table 4.1.

Table 4.1 The results of BSF in 21 cm thickness of abdomen phantom.

Parameter		Dosimeter reading (mGy)		BSF	Average±SD
kVp	mAs	ESAK (K_e)	Incident air kerma (K_i)		
70	3.2	0.232	0.169	1.373	1.380±0.005
	6.3	0.459	0.332	1.383	
	12.5	0.901	0.652	1.381	
	25.0	1.804	1.304	1.383	
75	3.2	0.272	0.196	1.391	1.394±0.002
	6.3	0.540	0.388	1.393	
	12.5	1.059	0.758	1.396	
	25.0	2.119	1.519	1.395	
	32.0	2.714	2.714	1.395	
80	3.2	0.318	0.226	1.404	1.406±0.002
	6.3	0.629	0.447	1.408	
	12.5	1.227	0.873	1.406	
	25.0	2.455	1.746	1.406	
85	3.2	0.366	0.259	1.415	1.417±0.002
	6.3	0.722	0.509	1.419	
	12.5	1.406	0.991	1.418	
	25.0	2.814	1.987	1.416	
90	3.2	0.415	0.291	1.429	1.427±0.002
	6.3	0.820	0.573	1.430	
	12.5	1.591	1.116	1.426	
	25.0	3.189	2.238	1.425	

4.2.1.1.2 The entrance surface air kerma (ESAK)

The ESAK of the whole-body phantom in 21 cm thickness of abdomen was calculated for experimental parameters for tube voltage at 70, 75, 80, 85, and 90 kVp, and tube current-time at 3.2, 6.3, 12.5, and 25.0 mAs including the routine clinical parameter at 75 kVp and 32 mAs by using tube output from quality control of digital mobile x-ray system as mentioned previously. The example for ESAK calculation is illustrated as in appendix F. The range of ESAK corresponding to 21 exposure parameters was between 0.234 and 3.218 mGy as shown in table 4.2.

Table 4.2 The calculated ESAK of 21 cm thickness in abdomen.

kVp	mAs	Calculated ESAK (mGy)
70	3.2	0.234
	6.3	0.461
	12.5	0.915
	25.0	1.830
75	3.2	0.275
	6.3	0.541
	12.5	1.074
	25.0	2.147
	32.0*	2.748
80	3.2	0.318
	6.3	0.626
	12.5	1.242
	25.0	2.443
85	3.2	0.364
	6.3	0.716
	12.5	1.420
	25.0	2.841
90	3.2	0.412
	6.3	0.811
	12.5	1.609
	25.0	3.218

*Routine clinical parameter

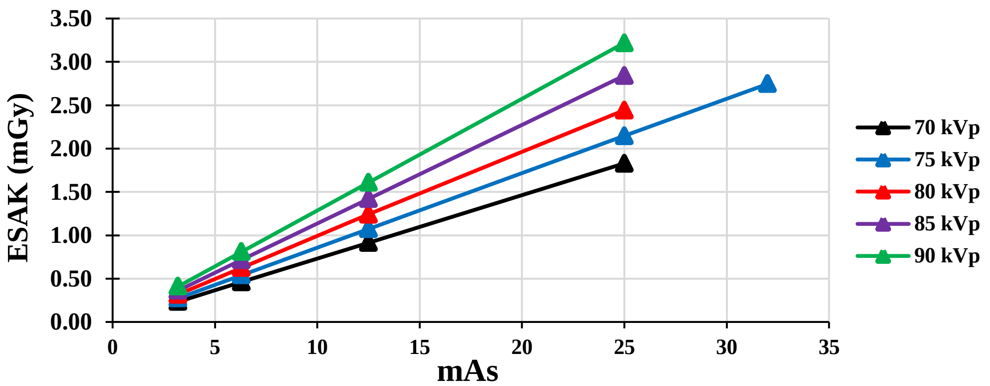

Figure 4.1 Relation between calculated ESAK and the exposure parameters in 21 cm thickness.

4.2.1.1.3 The exposure index (EI)

The EI of the whole-body phantom in 21 cm thickness of abdomen was recorded for each parameter as shown in table 4.3. The target EI for abdominal radiography approximately of 336 has been recommended by manufacturer (GE).

Table 4.3 The results of EI and ESAK in each parameter in 21 cm thickness.

kVp	mAs	Calculated ESAK	EI
70	3.2	0.234	91.81
	6.3	0.461	185.78
	12.5	0.915	363.34
	25.0	1.830	706.76
75	3.2	0.275	133.82
	6.3	0.541	272.83
	12.5	1.074	520.54
	25.0	2.147	1,009.04
	32.0*	2.748	1,262.38
80	3.2	0.318	188.82
	6.3	0.626	381.53
	12.5	1.242	717.59
	25.0	2.443	1,370.65
85	3.2	0.364	252.91
	6.3	0.716	509.72
	12.5	1.420	949.28
	25.0	2.841	1,788.56
90	3.2	0.412	329.56
	6.3	0.811	650.90
	12.5	1.609	1,206.08
	25.0	3.218	2,252.80

*Routine clinical parameter

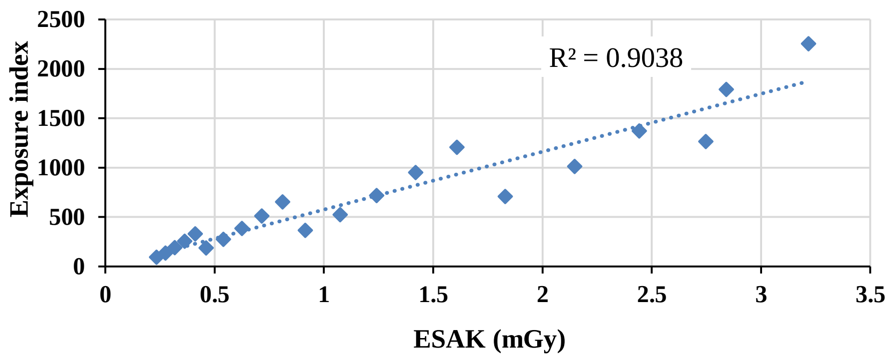

Figure 4.2 Relation between calculated ESAK and the EI in 21 cm thickness of abdomen with R^2 = 0.9038.

For the abdomen thickness of 21 cm, there were 3 parameters that the EI closed to the target EI as shown in table 4.4.

Table 4.4 The parameters and EI in 21 cm thickness in abdomen.

kVp	mAs	EI
70	12.5	363.34
80	6.3	381.53
90	3.2	329.56

4.2.1.2 Image quality evaluation

4.2.1.2.1 Image quality and qualitative noise analysis

The results of the image quality and qualitative noise analysis evaluated by three observers are shown in table 4.5.

Table 4.5 The image quality and qualitative score by three observers.

kVp	mAs	1st Observer		2nd Observer		3rd Observer	
		Image quality	Qualitative noise	Image quality	Qualitative noise	Image quality	Qualitative noise
70	3.2	4.0	2	4.5	2	5.5	2
	6.3	4.5	1	4.5	1	6.0	1
	12.5	6.5	1	6.5	1	6.0	0
	25.0	6.0	1	6.0	1	6.0	1
75	3.2	4.5	2	4.5	2	5.0	2
	6.3	4.5	1	5.5	2	5.0	0
	12.5	5.5	1	6.0	1	5.5	0
	25.0	6.5	1	7.0	1	6.0	1
	32.0*	7.0	1	7.0	1	6.0	1
80	3.2	4.5	2	5.5	2	5.5	1
	6.3	5.5	1	5.5	1	6.0	1
	12.5	6.0	1	6.0	2	6.0	1
	25.0	5.5	1	7.0	1	6.0	0
85	3.2	4.5	1	4.5	2	5.0	0
	6.3	5.5	1	5.5	1	6.0	1
	12.5	6.0	1	6.0	1	6.0	1
	25.0	4.5	1	6.0	1	6.0	1

*Routine clinical parameter

จุฬาลงกรณ์มหาวิทยาลัย
Chulalongkorn University

Table 4.5 The image quality and qualitative score by three observers (Continued).

kVp	mAs	1st Observer		2nd Observer		3rd Observer	
		Image quality	Qualitative noise	Image quality	Qualitative noise	Image quality	Qualitative noise
90	3.2	4.5	1	4.5	1	5.5	1
	6.3	5.5	1	5.5	1	5.5	0
	12.5	6.5	1	7.0	1	6.0	1
	25.0	4.0	1	6.0	1	6.0	1

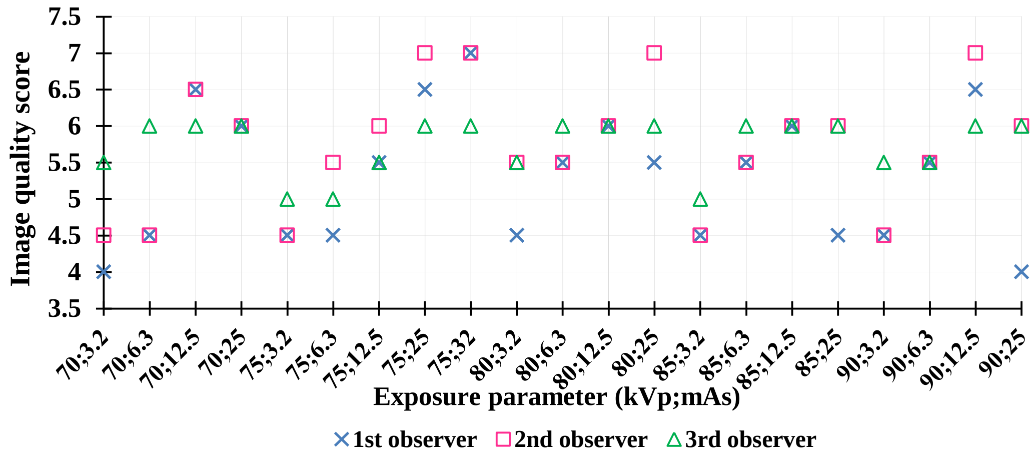

Figure 4.3 Scatter plots of image criteria score and exposure parameters by three observers.

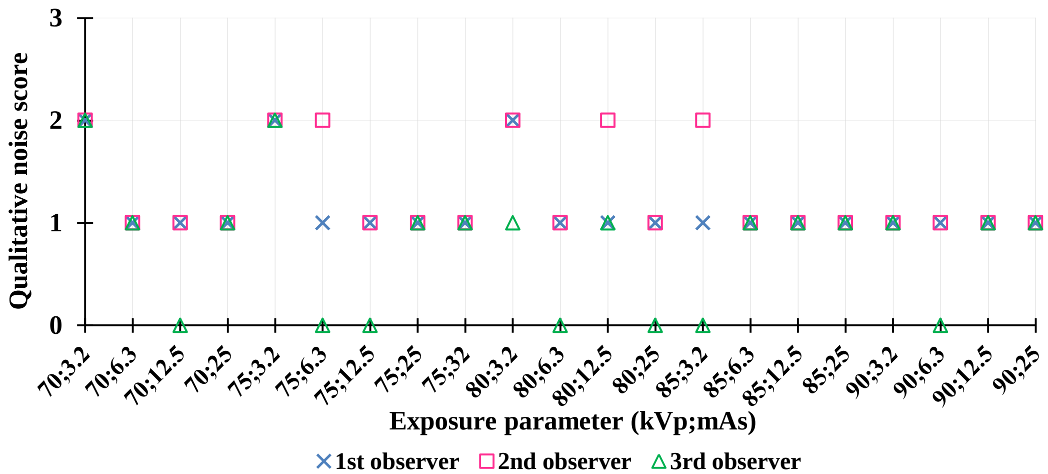

Figure 4.4 Scatter plots of qualitative noise score and exposure parameters by three observers.

The results of image quality score and the qualitative noise scored by three observers are shown as in figure 4.3 and figure 4.4, respectively. It was found that the range of the image criteria and qualitative noise score were 4 to 7 and 0 to 2, respectively. The classification of qualitative noise score was shown as in figure 4.5.

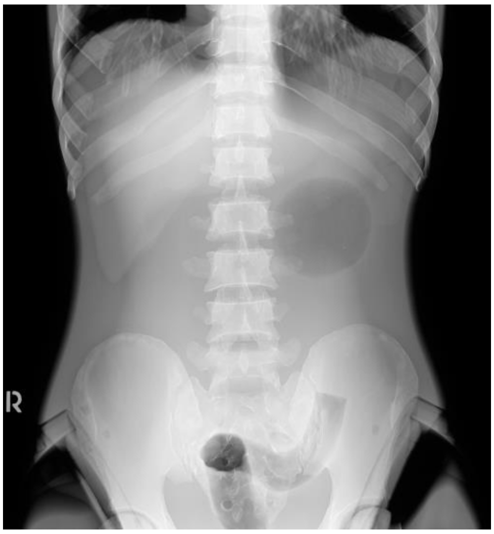

A. Score = 0 (Free of noise)

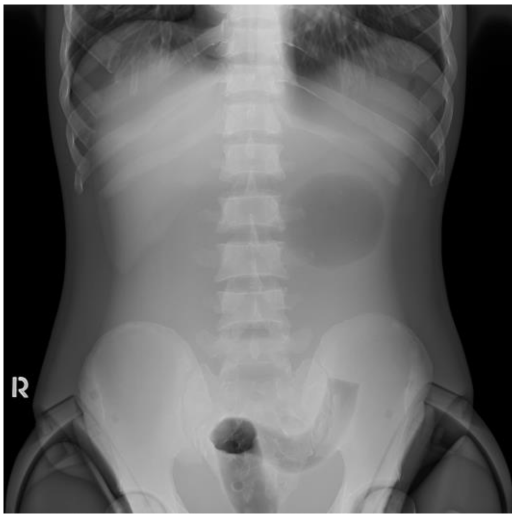

B. Score = 1 (Scarce noise)

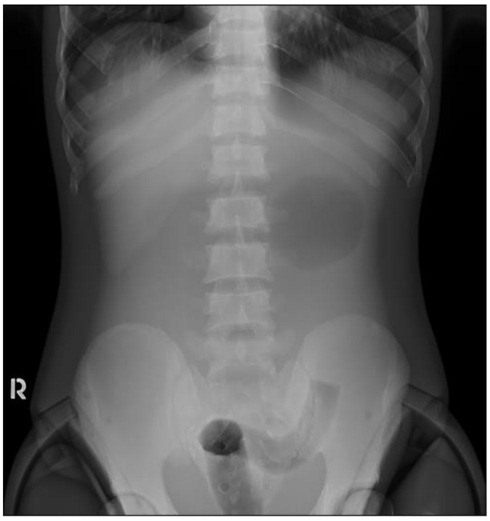

C. Score = 2 (Significant noise)

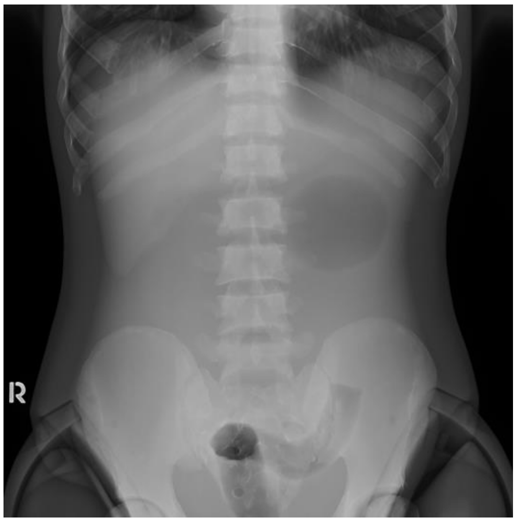

D. Score = 3 (Obvious noise)

Figure 4.5 Rate of qualitative noise scoring.

The average inter-class correlation coefficient for inter rater reliability of image quality scoring between three observers was 0.765. The strength of agreement was good. Therefore, the average of image quality score in each parameter of three observers was used for identifying the image quality score. For qualitative noise score by three observers, mode or median was used to identify the quality noise score as shown in table 4.7.

Table 4.6 The inter-item correlation matrix between observers in terms of image quality scoring phantom in 21 cm thickness of abdomen.

Observers	Inter-item correlation value
1st observer and 2nd observer	0.762
1st observer and 3rd observer	0.540
2nd observer and 3rd observer	0.619

*The average inter-class correlation coefficients for inter rater reliability values and inter-item correlation value were calculated by using SPSS Version 22.0.

Table 4.7 The average image quality and qualitative noise score by three observers in 21 cm thickness in abdomen.

Parameters		EI	ESAK (mGy)	Scoring	
kVp	mAs			Image quality	Qualitative noise
70	3.2	91.81	0.234	4.67	2
	6.3	185.78	0.461	5.00	1
	12.5	363.34	0.915	6.33	1
	25.0	706.76	1.830	6.00	1
75	3.2	133.82	0.275	4.67	2
	6.3	272.83	0.541	5.00	1
	12.5	520.54	1.074	5.67	1
	25.0	1,009.04	2.147	6.50	1
	32.0*	1,262.38	2.748	6.67	1
80	3.2	188.82	0.318	5.17	2
	6.3	381.53	0.626	5.67	1
	12.5	717.59	1.242	6.00	1
	25.0	1,370.65	2.443	6.17	1
85	3.2	252.91	0.364	4.67	1
	6.3	509.72	0.716	5.67	1
	12.5	949.28	1.420	6.00	1
	25.0	1,788.56	2.841	5.50	1

*Routine clinical parameter

Table 4.7 The average image quality and qualitative noise score by three observers in 21 cm thickness in abdomen (Continued).

Parameters		EI	ESAK	Scoring	
kVp	**mAs**		**(mGy)**	**Image quality**	**Qualitative noise**
90	3.2	329.56	0.412	4.83	1
	6.3	650.90	0.811	5.50	1
	12.5	1,206.08	1.609	6.50	1
	25.0	2,252.80	3.218	5.33	1

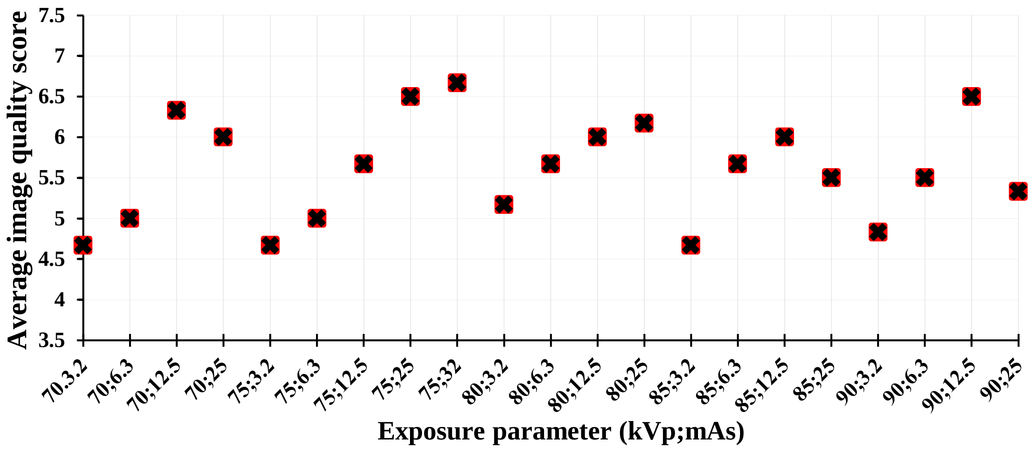

Figure 4.6 Scatter plots of average image quality score by three observers.

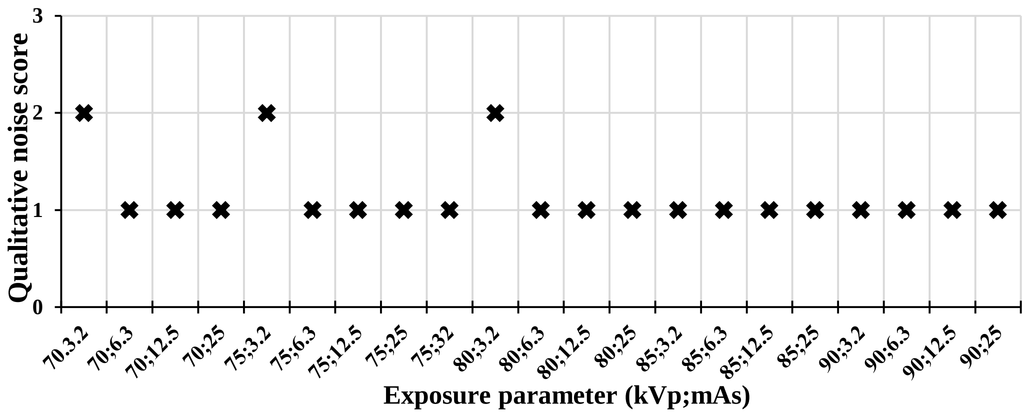

Figure 4.7 Scatter plots of qualitative noise score by three observers.

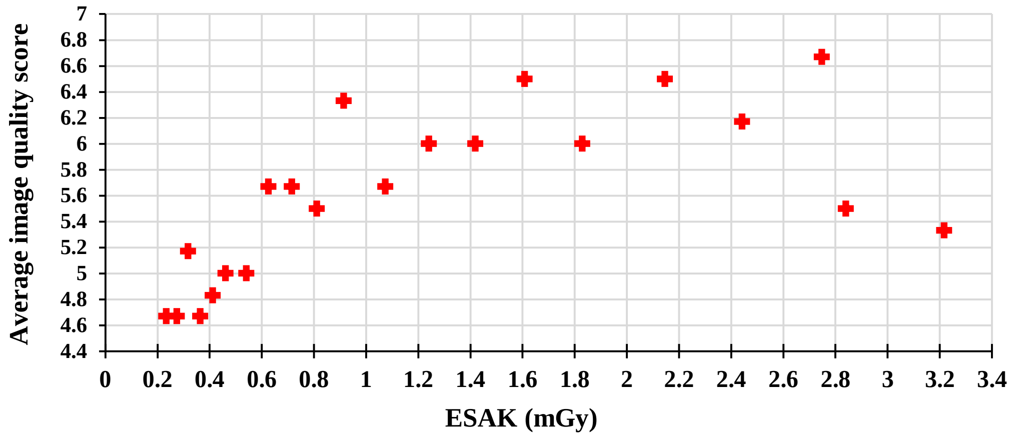

Figure 4.8 Scatter plots of the ESAK and the average image quality score by three observers in each parameter.

The image quality evaluation using digital mobile abdominal radiography in this study, the observers were recommended the level of acceptance for diagnosis as followings:

- Image quality scoring ≥ 5
- Qualitative noise must be 1 and 2

4.2.1.2.2 Quantitative image analysis

4.2.1.2.2.1 Signal-to-noise ratio (SNR)

The results of the average SNR in the 21 abdominal radiographic images are illustrated in table 4.8.

Table 4.8 The average of SNR in each parameter in the 21 cm thickness in abdominal images.

kVp	mAs	Average signal-to-noise ratio (SNR)		
		1st ROI Liver	2nd ROI 4th Lumbar	3rd ROI Flat bone
70	3.2	26.52	37.00	15.43
	6.3	36.56	49.62	15.86
	12.5	40.02	54.76	16.20
	25.0	41.41	60.81	16.58

Table 4.8 The average of SNR in each parameter in the 21 cm thickness in abdominal images (Continued).

kVp	mAs	Average signal-to-noise ratio (SNR)		
		1st ROI Liver	**2nd ROI 4th Lumbar**	**3rd ROI Flat bone**
75	3.2	29.75	47.33	16.82
	6.3	38.51	55.30	17.11
	12.5	42.48	59.42	17.66
	25.0	43.07	66.52	17.76
	32.0*	45.66	74.59	17.85
80	3.2	36.89	50.53	18.05
	6.3	39.56	61.55	18.24
	12.5	43.87	62.34	18.35
	25.0	45.09	72.36	18.69
85	3.2	37.61	62.29	19.35
	6.3	45.06	72.77	19.73
	12.5	45.36	75.56	19.93
	25.0	46.68	78.36	20.19
90	3.2	43.59	69.30	20.66
	6.3	46.32	73.22	20.86
	12.5	47.31	83.86	20.99
	25.0	47.71	98.98	21.20

*Routine clinical parameter

The range of average SNR in 1st, 2nd, and 3rd ROIs were 26.5 - 47.71, 37.00 - 98.98, and 15.43-21.20, respectively.

จุฬาลงกรณ์มหาวิทยาลัย
Chulalongkorn University

4.2.1.2.2.2 Contrast-to-noise ratio (CNR)

The results of the average of CNR in the 21 abdominal radiographic images are illustrated in table 4.9.

Table 4.9 The average of CNR in each parameter in the 21 cm thickness in abdominal images.

kVp	mAs	Average contrast-to-noise ratio (CNR)		
		1st Area Liver Area	2nd Area 4th Lumbar and Left kidney	3rd Area Flat bone and Right kidney
70	3.2	5.46	4.94	0.74
	6.3	5.62	6.59	1.09
	12.5	5.67	7.66	1.40
	25.0	6.00	8.61	1.46
75	3.2	5.51	4.99	0.77
	6.3	5.64	7.01	1.18
	12.5	6.00	8.32	1.65
	25.0	6.04	8.78	1.72
	32.0*	6.16	9.44	1.83
80	3.2	5.92	5.32	0.96
	6.3	5.97	7.27	1.50
	12.5	6.18	8.66	1.75
	25.0	6.28	9.06	1.86
85	3.2	6.17	5.46	0.99
	6.3	6.44	7.44	1.63
	12.5	6.59	8.75	1.80
	25.0	6.74	9.28	1.93
90	3.2	6.35	5.51	1.26
	6.3	6.48	7.50	1.81
	12.5	6.82	8.88	2.03
	25.0	7.02	9.32	2.16

*Routine clinical parameter

The range of average CNR in 1st, 2nd, and 3rd areas was 5.46-7.02, 4.99-9.32, and 0.74-2.16, respectively.

จุฬาลงกรณ์มหาวิทยาลัย
Chulalongkorn University

4.2.1.3 The optimal parameter for the whole-body phantom in 21 cm thickness of abdomen

The optimal parameters from image quality with score ≥ 5 points, qualitative noise score between 1 and 2, and EI closed to target EI at 336 are shown as in table 4.10, and the quantitative analysis in terms of SNR and CNR are shown in table 4.11 and table 4.12.

Consequencely, the optimal parameter of 80 kVp, 6.3 mAs was obtained. The ESAK was 0.626 mGy with EI at 381.53. The score of the average image quality and the qualitative noise were 5.67 and 1 respectively. For the quantitative image analysis, the average SNR of the 1st, 2nd, and 3rd ROIs were 39.56, 61.55, and 18.54, respectively and the average CNR of 1st, 2nd, and 3rd areas were 5.97, 7.27, and 1.50, respectively.

Table 4.10 The ESAK, EI, and qualitative image analysis of the optimal and other parameters in whole-body phantom in 21 cm thickness of abdomen.

Parameters		ESAK (mGy)	EI	Scoring	
kVp	**mAs**			**Average image quality**	**Qualitative noise**
80	6.3	0.626	381.53	5.67	1
85	6.3	0.716	509.72	5.67	1
90	6.3	0.811	650.90	5.50	1

Table 4.11 The average SNR of the optimal and other parameters in whole-body phantom in 21 cm thickness of abdomen.

Parameters		Average signal-to-noise ratio (SNR)		
kVp	**mAs**	**1st ROI Liver**	**2nd ROI 4th Lumbar**	**3rd ROI Flat bone**
80	6.3	39.56	61.55	18.24
85	6.3	45.06	72.77	19.73
90	6.3	46.32	73.22	20.86

Table 4.12 The average CNR of the optimal and other parameters in whole-body phantom in 21 cm thickness of abdomen.

Parameters		Average contrast-to-noise ratio (CNR)		
kVp	**mAs**	**1st Area Liver Area**	**2nd Area 4th Lumbar and Left kidney**	**3rd Area Flat bone and Right kidney**
80	6.3	5.97	7.27	1.50
85	6.3	6.44	7.44	1.63
90	6.3	6.48	7.50	1.81

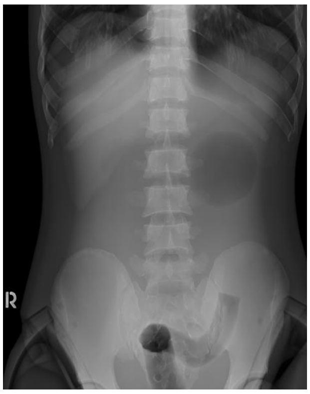

A. 80 kVp 6.3 mAs
ESAK = 0.626 mGy
Image criteria = 5.67
Qualitative noise = 1

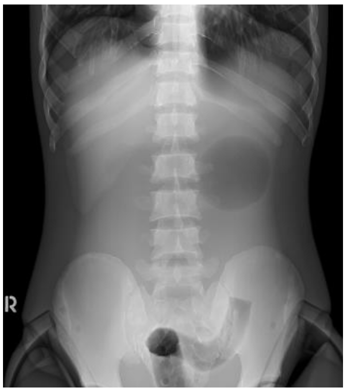

B. 85 kVp 6.3 mAs
ESAK = 0.716 mGy
Image criteria = 5.67
Qualitative noise = 1

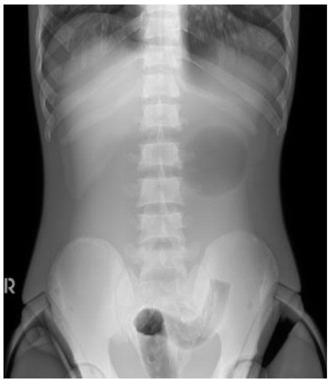

C. 80 kVp 12.5 mAs
ESAK = 0.915 mGy
Image criteria = 6
Qualitative noise = 1

Figure 4.9 Example of phantom's radiographs from different exposure parameters for 21 cm thickness.

4.2.1.4 The comparison between routine clinical and optimal parameter for the whole-body phantom in 21 cm thickness of abdomen

The radiation dose and image quality using the routine clinical and optimal parameter in terms of entrance surface air kerma (ESAK), exposure index, image quality score, qualitative and quantitative analysis are shown in table 4.13.

Table 4.13 The comparison between the routine clinical and optimal parameter in 21 cm thickness in abdomen.

	Routine clinical parameter	**Optimal parameter**
ESAK	2.748 mGy	0.626 mGy
EI	1,262.28	381.53
Qualitative analysis		
Image quality score	6.67	5.67
Qualitative noise score	1	1
Quantitative analysis Average SNR		
- 1st ROI	45.66	39.56
- 2nd ROI	74.59	61.55
- 3rd ROI	17.59	18.24

จุฬาลงกรณ์มหาวิทยาลัย
Chulalongkorn University

Table 4.13 The comparison between the routine clinical and optimal parameter in 21 cm thickness in abdomen.

	Routine clinical parameter	**Optimal parameter**
Average CNR		
- 1st area	6.16	5.97
- 2nd area	9.44	7.27
- 3rd area	1.83	1.50

By using the optimal parameter, the reduction of ESAK and EI were decreased by 77% and 70% from the routine clinical parameter, respectively. For qualitative analysis, the image quality score was 15% lower than the routine clinical parameter while the quantitative image analysis score was slightly different. For the quantitative analysis, the average SNR of 1st and 2nd ROIs were decreased by 13% and 17% and 3rd ROI was increased 2% from the routine clinical parameter. The average CNR of 1st, 2nd, and 3rd areas were decreased 3%, 23%, and 18% from the routine clinical parameter, respectively as shown in figure 4.10.

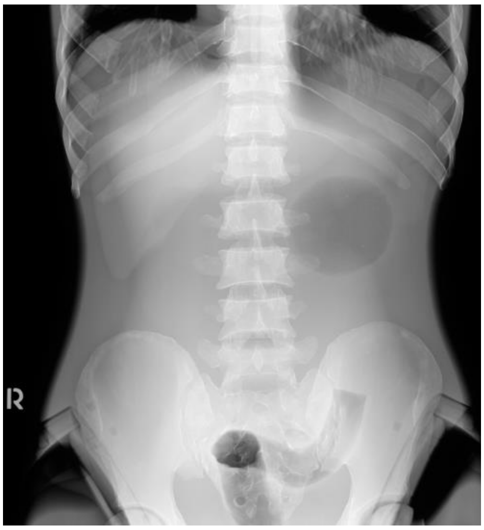

A. Routine clinical parameter
75 kVp 32 mAs
ESAK = 2.748 mGy

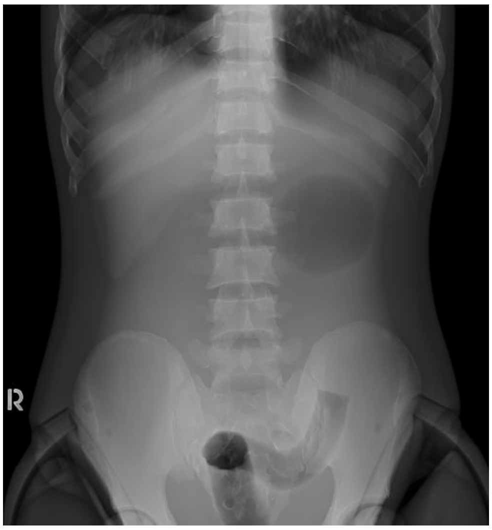

B. Optimal parameter
80 kVp 6.3 mAs
ESAK = 0.626 mGy

Figure 4.10 Abdominal radiography using routine clinical and optimal parameter in 21 cm thickness in abdomen.

4.2.2 25 cm thickness of abdomen

4.2.2.1 Radiation dose

4.2.2.1.1 The backscatter factors (BSF)

The BSF were investigated by setting the experimental parameters at 70, 75, 80, 85, and 90 kVp and 3.2, 6.3, 12.5, and 25.0 mAs including the routine clinical parameter setting for abdominal radiography in 25 cm thickness at 80 kVp and 32 mAs. The results of BSF are shown as in table 4.14

Table 4.14 The results of BSF in 25 cm thickness of abdomen phantom.

Parameter		Dosimeter reading (mGy)		BSF	Average±SD
kVp	**mAs**	**ESAK (K_e)**	**Incident air kerma (K_i)**		
70	3.2	0.265	0.195	1.357	1.362±0.003
	6.3	0.526	0.386	1.363	
	12.5	1.031	0.758	1.361	
	25.0	2.067	1.514	1.365	
75	3.2	0.311	0.227	1.367	1.373±0.004
	6.3	0.618	0.450	1.375	
	12.5	1.211	0.880	1.376	
	25.0	2.422	1.764	1.373	
80	3.2	0.363	0.261	1.391	1.385±0.004
	6.3	0.719	0.520	1.383	
	12.5	1.400	1.013	1.382	
	25.0	2.805	2.026	1.385	
	32.0	3.590	2.597	1.382	
85	3.2	0.418	0.300	1.393	1.393±0.003
	6.3	0.823	0.591	1.394	
	12.5	1.599	1.152	1.388	
	25.0	3.208	2.308	1.390	
90	3.2	0.473	0.338	1.397	1.397±0.001
	6.3	0.914	0.653	1.399	
	12.5	1.813	1.298	1.397	
	25.0	3.630	2.600	1.396	

4.2.2.1.2 The entrance surface air kerma (ESAK)

The ESAK of the whole-body phantom in 25 cm thickness of abdomen was calculated for experimental parameters for tube voltage at 70, 75, 80, 85, and 90 kVp, and tube current-time at 3.2, 6.3, 12.5, and 25.0 mAs including the routine clinical parameter at 80 kVp and 32 mAs by using tube output from quality control of digital mobile x-ray system. The method for ESAK calculation is illustrated as in appendix F. The results of ESAK corresponding to 21 exposure parameters were between 0.256 to 3.496 mGy as shown in table 4.15.

Table 4.15 The calculated ESAK of 25 cm thickness in abdomen.

kVp	mAs	Calculated ESAK (mGy)
70	3.2	0.256
	6.3	0.505
	12.5	1.001
	25.0	2.002
75	3.2	0.300
	6.3	0.591
	12.5	1.173
	25.0	2.346
80	3.2	0.347
	6.3	0.684
	12.5	1.357
	25.0	2.715
	32.0*	3.475
85	3.2	0.397
	6.3	0.781
	12.5	1.549
	25.0	3.099
90	3.2	0.447
	6.3	0.881
	12.5	1.748
	25.0	3.496

*Routine clinical parameter

จุฬาลงกรณ์มหาวิทยาลัย
CHULALONGKORN UNIVERSITY

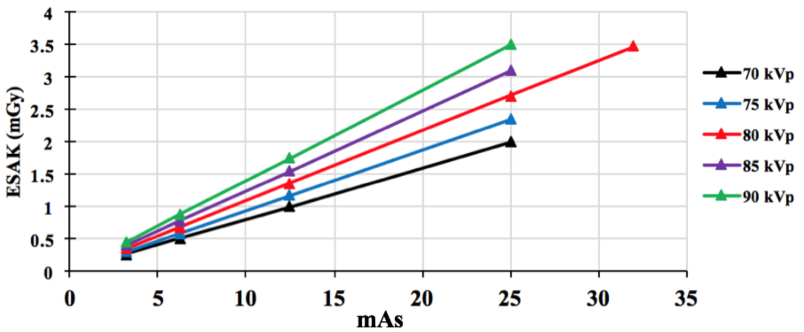

Figure 4.11 Relation between calculated ESAK and the exposure parameters in 25 cm thickness.

4.2.2.1.3. The exposure index (EI)

The EI of the whole-body phantom in 25 cm thickness of abdomen was recorded for each parameter as shown in table 4.16.

Table 4.16 The results of EI and ESAK in each parameter in 25 cm thickness.

kVp	mAs	Calculated ESAK (mGy)	EI
70	3.2	0.256	68.86
	6.3	0.505	141.18
	12.5	1.001	271.53
	25.0	2.002	495.05
75	3.2	0.300	101.77
	6.3	0.591	208.30
	12.5	1.173	336.92
	25.0	2.346	677.31
80	3.2	0.347	143.34
	6.3	0.684	293.62
	12.5	1.357	489.36
	25.0	2.715	914.63
	32.0*	3.475	1,128.13
85	3.2	0.397	194.45
	6.3	0.781	395.39
	12.5	1.549	657.39
	25.0	3.099	1,194.39
90	3.2	0.447	255.94
	6.3	0.881	450.39
	12.5	1.748	835.38
	25.0	3.496	1,528.28

*Routine clinical parameter

จุฬาลงกรณ์มหาวิทยาลัย
CHULALONGKORN UNIVERSITY

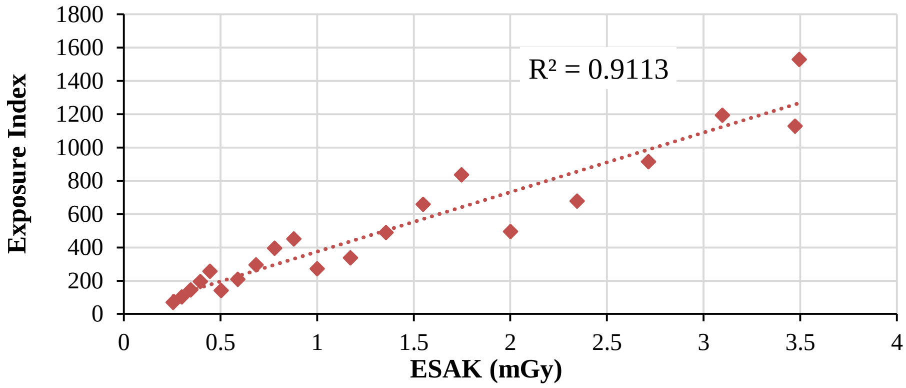

Figure 4.12 Relation between calculated ESAK and the EI in 25 cm thickness in abdomen with R^2 = 0.9113.

For the abdomen thickness of 25 cm, there were 2 parameters that the EI closed to the target EI as shown in table 4.17.

Table 4.17 The parameters and EI in 25 cm thickness of abdomen.

kVp	mAs	Target EI	EI
75	12.5	336	336.92
85	6.3	336	395.39

4.2.2.2 Image quality evaluation

4.2.2.2.1 Image quality and qualitative noise analysis

The results of the image quality and qualitative noise analysis evaluated by three observers are shown in table 4.18

Table 4.18 The image quality and qualitative scoring by three observers.

kVp	mAs	1st Observer		2nd Observer		3rd Observer	
		Image quality	Qualitative noise	Image quality	Qualitative noise	Image quality	Qualitative noise
70	3.2	4.5	2	4.5	2	4.5	3
	6.3	5.0	2	4.5	2	5.5	2
	12.5	5.0	1	6.0	1	6.0	1
	25.0	6.0	0	6.5	1	6.0	1
75	3.2	4.0	2	4.5	2	4.5	2
	6.3	3.5	1	6.0	1	5.0	1
	12.5	5.5	1	5.5	2	6.0	1
	25.0	6.5	0	6.5	1	6.5	1

Table 4.18 The image quality and qualitative scoring by three observers (Continued).

kVp	mAs	1st Observer Image quality	1st Observer Qualitative noise	2nd Observer Image quality	2nd Observer Qualitative noise	3rd Observer Image quality	3rd Observer Qualitative noise
80	3.2	4.5	2	4.0	2	3.5	3
	6.3	5.0	1	5.5	2	4.5	2
	12.5	5.5	1	5.5	2	6.0	1
	25.0	6.0	1	6.0	1	6.0	1
	32.0*	6.5	0	7.0	1	6.0	1
85	3.2	4.0	2	4.5	2	4.0	2
	6.3	5.0	1	5.0	2	5.5	2
	12.5	5.5	1	6.0	2	6.0	1
	25.0	5.5	0	6.5	1	6.0	1
90	3.2	4.5	2	4.0	2	4.0	2
	6.3	5.0	1	5.0	2	6.0	1
	12.5	5.5	1	5.5	2	6.0	1
	25.0	5.0	1	6.0	1	6.5	0

*Routine clinical parameter

The image quality score and qualitative noise score are shown in figure 4.13 and figure 4.14.

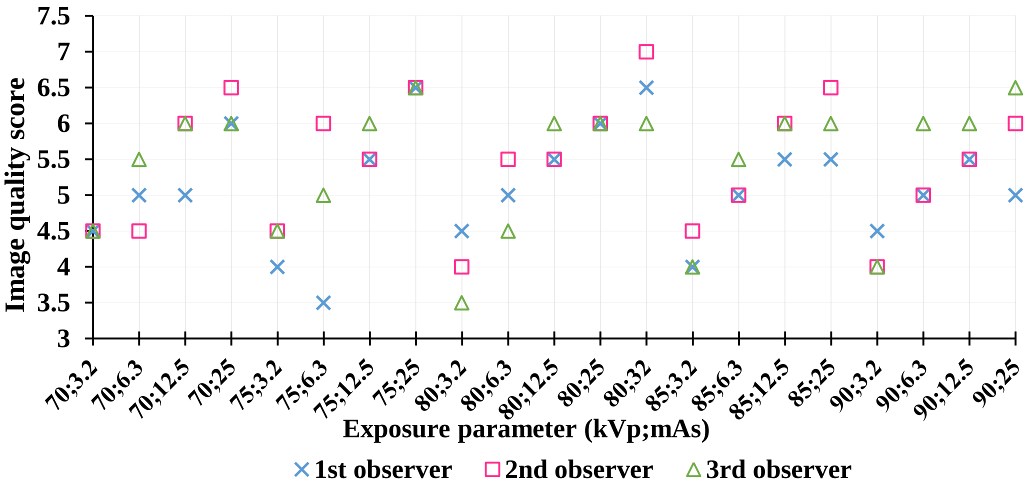

Figure 4.13 Scatter plot of image criteria score and exposure parameters by three observers.

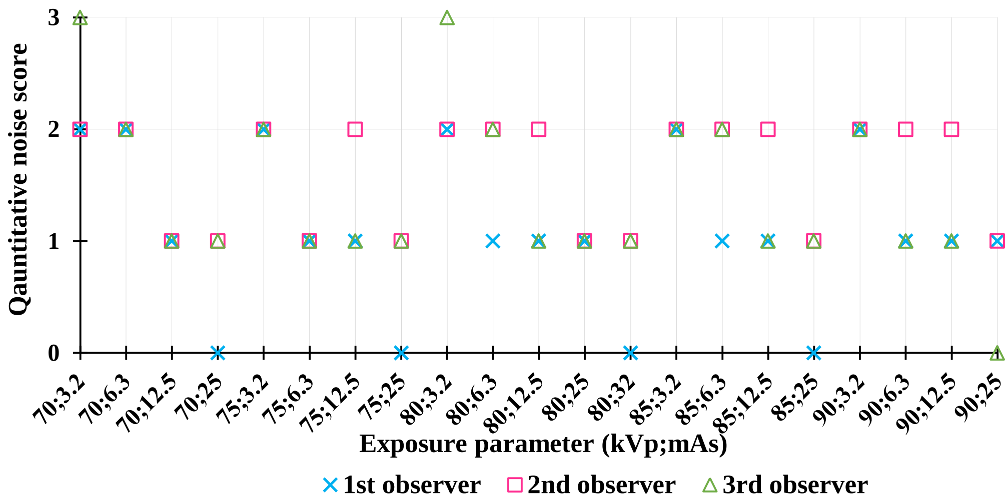

Figure 4.14 Scatter plots of qualitative noise score and exposure parameters three observers.

The range of the image criteria and qualitative noise score were 3.5 to 7 and 0 to 3, respectively.

The average inter-class correlation coefficient for inter rater reliability of image quality scoring between three observers was 0.872. The strength of agreement was excellent. Therefore, the average of image quality score in each parameter of three observers was used for identifying the image quality score. For qualitative noise score by three observers, mode or median was used to identify the quality noise score as shown in table 4.20.

Table 4.19 The inter-item correlation matrix between observers in term of image quality scoring in 25 cm thickness in abdomen.

Observers	Inter-item correlation value
1st observer and 2nd observer	0.675
1st observer and 3rd observer	0.720
2nd observer and 3rd observer	0.773

*The average inter-class correlation coefficients for inter rater reliability values and inter-item correlation value were calculated by using SPSS Version 22.0.

Table 4.20 The average image quality score and qualitative noise score by three observers in 25 cm thickness of abdomen in 25 cm thickness in abdomen.

Parameters		EI	ESAK	Scoring	
kVp	mAs		(mGy)	Image quality	Qualitative noise
70	3.2	68.86	0.256	4.50	2
	6.3	141.18	0.505	5.00	2
	12.5	271.53	1.001	5.67	1
	25.0	495.05	2.002	6.17	1
75	3.2	101.77	0.300	4.33	2
	6.3	208.30	0.591	4.83	1
	12.5	336.92	1.173	5.67	1
	25.0	677.31	2.346	6.5	1
80	3.2	143.34	0.347	4.00	2
	6.3	293.62	0.684	5.00	2
	12.5	489.36	1.357	5.67	1
	25.0	914.63	2.715	6.00	1
	32.0*	1128.13	3.475	6.50	1
85	3.2	194.45	0.397	4.17	2
	6.3	395.39	0.781	5.17	2
	12.5	657.39	1.549	5.83	1
	25.0	1194.39	3.099	6.00	1
90	3.2	255.94	0.447	4.17	2
	6.3	450.39	0.881	5.33	1
	12.5	835.38	1.748	5.67	1
	25.0	1528.28	3.496	5.83	1

*Routine clinical parameter

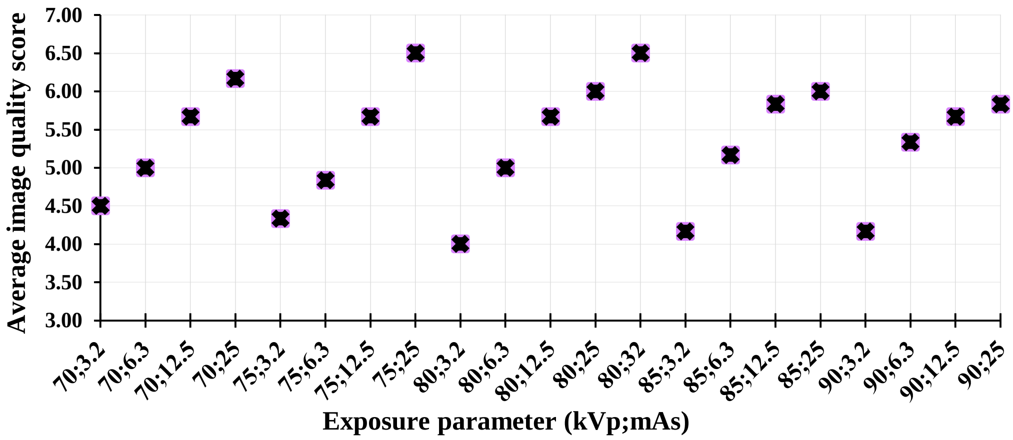

Figure 4.15 Scatter plots of mean image quality score by three observers.

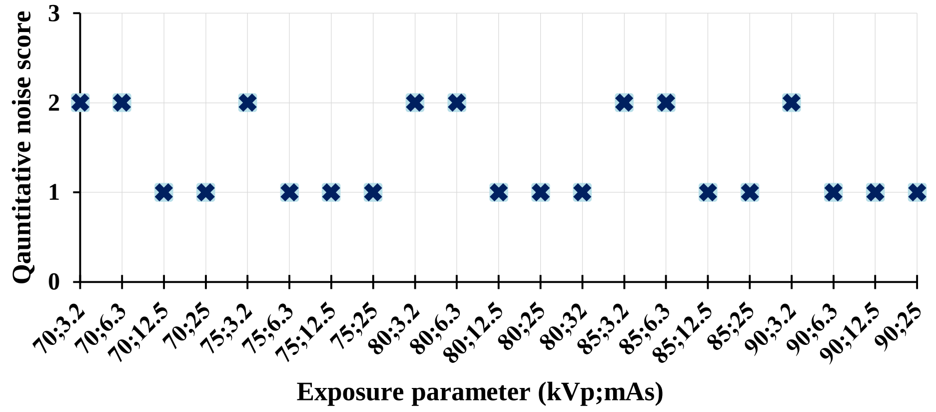

Figure 4.16 Scatter plots of qualitative noise score by three observers.

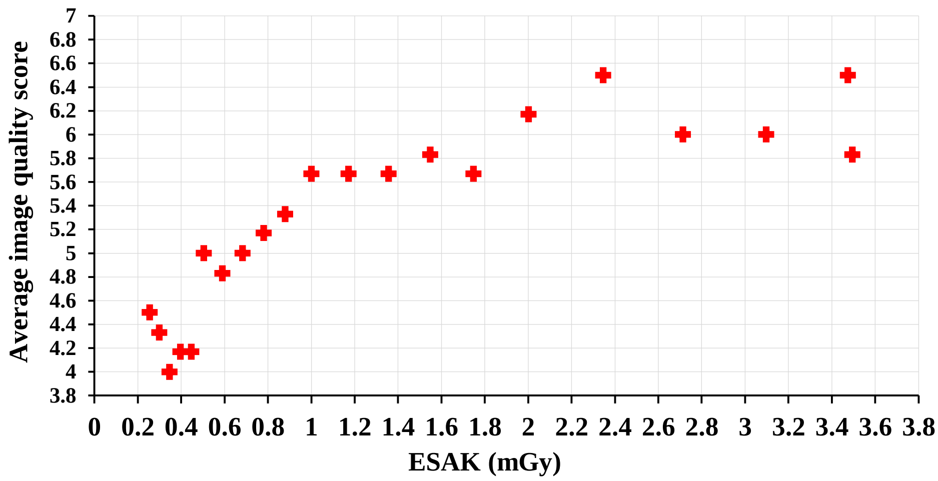

Figure 4.17 Scatter plots of the ESAK and the average image quality score by three observers in each parameter.

4.2.2.2.2 Quantitative image analysis

4.2.2.2.2.1 Signal-to-noise ratio (SNR)

The results of the average SNR in the 21 abdominal radiographic images are illustrated in table 4.21.

Table 4.21 The average of SNR in each parameter in the 25 cm thickness in abdominal images.

kVp	mAs	Average signal-to-noise ratio (SNR)		
		1st ROI Liver	2nd ROI 4th Lumbar	3rd ROI Flat bone
70	3.2	24.74	30.89	13.81
	6.3	30.94	47.27	14.77
	12.5	36.41	53.27	15.17
	25.0	41.21	59.14	16.24
75	3.2	28.23	39.28	16.34
	6.3	34.86	54.29	16.82
	12.5	39.73	58.45	17.40
	25.0	42.05	65.82	17.54
80	3.2	34.10	48.28	17.97
	6.3	37.15	59.25	18.19
	12.5	43.24	60.87	18.21
	25.0	44.34	71.65	18.45
	32.0*	45.07	85.02	18.99
85	3.2	35.73	54.56	19.26
	6.3	40.65	70.55	19.45
	12.5	43.67	75.08	19.53
	25.0	44.93	76.84	19.88
90	3.2	38.38	61.12	20.08
	6.3	43.05	72.37	20.46
	12.5	45.60	81.52	20.52
	25.0	45.95	96.81	20.84

*Routine clinical parameter

The range of average SNR in 1st, 2nd, and 3rd ROIs were 24.74 - 45.95, 30.89 - 96.81, and 13.81-20.84, respectively.

4.2.2.2.2.2 Contrast-to-noise ratio (CNR)

The results of the average of CNR in the 21 abdominal radiographic images are illustrated in table 4.22.

Table 4.22 The average CNR in each parameter in the 25 cm thickness in abdominal images.

kVp	mAs	Average contrast to noise ratio (CNR)		
		1st Area Liver Area	2nd Area 4th Lumbar and Left kidney	3rd Area Flat bone and Right kidney
70	3.2	5.37	2.97	0.62
	6.3	5.41	4.00	0.90
	12.5	5.64	6.39	1.30
	25.0	5.72	7.30	1.41
75	3.2	5.46	3.12	0.65
	6.3	5.61	4.46	1.11
	12.5	5.73	6.98	1.57
	25.0	5.80	7.47	1.64
80	3.2	5.72	3.17	0.82
	6.3	5.82	4.56	1.40
	12.5	6.03	7.11	1.68
	25.0	6.12	7.56	1.80
	32.0*	6.34	7.84	2.06
85	3.2	6.07	3.19	0.94
	6.3	6.20	4.73	1.58
	12.5	6.42	7.54	1.75
	25.0	6.68	7.90	1.84
90	3.2	6.22	3.23	1.16
	6.3	6.37	4.85	1.77
	12.5	6.52	7.65	1.99
	25.0	6.84	8.16	2.01

*Routine clinical parameter

The range of average CNR in 1st, 2nd, and 3rd areas was 5.37-6.84, 2.97-8.16, and 0.62-2.01, respectively.

จุฬาลงกรณ์มหาวิทยาลัย
Chulalongkorn University

4.2.2.3 The optimal parameter for the whole-body phantom in 25 cm thickness of abdomen

The optimal parameters from image quality with score ≥ 5 points, qualitative noise score between 1 and 2, and EI closed to target EI at 336 are shown in table 4.23. The quantitative analysis in terms of SNR and CNR are shown in table 4.24 and table 4.25.

Consequencely, the optimal parameter was 85 kVp, 6.3 mAs and the ESAK was 0.781, with EI at 395.1. The score on the image quality and the qualitative noise were 5.17 and 2 respectively. For the quantitative image analysis, the average SNR of the 1st, 2nd, and 3rd ROIs were 40.65, 70.55, and 19.45, respectively and the average CNR of the 1st, 2nd, and 3rd area were 6.20, 4.73, and 1.58, respectively.

Table 4.23 The ESAK, EI, and qualitative image analysis of the optimal and other parameters in whole-body phantom in 25 cm thickness of abdomen.

Parameters		**ESAK (mGy)**	**EI**	**Scoring**	
kVp	**mAs**			**Image quality**	**Qualitative noise**
85	6.3	0.781	395.39	5.17	2
90	6.3	0.881	450.39	5.33	1
75	12.5	1.173	336.92	5.67	1

Table 4.24 The average SNR of the optimal and other parameters in whole-body phantom in 25 cm thickness of abdomen.

Parameters		**Average signal-to-noise ratio (SNR)**		
kVp	**mAs**	**1st ROI Liver**	**2nd ROI 4th Lumbar**	**3rd ROI Flat bone**
85	6.3	40.65	70.55	19.45
90	6.3	43.05	72.37	20.46
75	12.5	39.73	58.45	17.40

Table 4.25 The average CNR of the optimal and other parameters in whole-body phantom in 25 cm thickness of abdomen.

Parameters		**Average contrast-to-noise ratio (CNR)**		
kVp	**mAs**	**1st Area Liver Area**	**2nd Area 4th Lumbar and Left kidney**	**3rd Area Flat bone and Right kidney**
85	6.3	6.20	4.73	1.58
90	6.3	6.37	4.85	1.77
75	12.5	5.73	6.98	1.57

A. 85 kVp 6.3 mAs
ESAK = 0.781 mGy
Image criteria = 5.17
Qualitative noise = 2

B. 90 kVp 6.3 mAs
ESAK =0.881 mGy
Image criteria = 5.33
Qualitative noise = 1

C. 75 kVp 12.5 mAs
ESAK =1.173 mGy
Image criteria = 5.67
Qualitative noise = 1

Figure 4.18 Example of phantom's radiographs from different exposure parameters for 25 cm thickness.

4.2.2.4 The comparison between routine clinical and optimal parameter for the whole-body phantom in 25 cm thickness of abdomen

The radiation dose and image quality using clinical and optimal parameter in terms of ESAK, EI, image quality score, qualitative and quantitative image analysis are shown in table 4.26.

Table 4.26 The comparison between the routine clinical and optimal parameter in 25 cm thickness of abdomen.

	Routine clinical parameter	**Optimal parameter**
ESAK	3.475 mGy	0.781 mGy
EI	1,128.13	395.39
Qualitative analysis		
Image quality score	6.17	5.17
Qualitative noise score	1	2
Quantitative analysis		
Average SNR		
-1st ROI	45.07	40.65
-2nd ROI	85.02	70.55
-3rd ROI	18.99	19.45

Table 4.26 The comparison between the routine clinical and optimal parameter in 25 cm thickness of abdomen (Continued).

	Routine clinical parameter	**Optimal parameter**
Average CNR		
-1st area	6.34	6.20
-2nd area	7.84	4.73
-3rd area	2.06	1.58

By using the optimal parameter, the reduction of ESAK and EI were lower 78% and 65% from the routine clinical parameter respectively. The image quality score was 20% lower than the routine clinical parameter. For the quantitative image analysis, the average SNR of 1st and 2nd ROIs were decreased by 10% and 17% and 3rd ROIs was increased 2% from the routine clinical parameter. The average CNR of the 1st, 2nd, and 3rd areas were decreased by 2%, 40%, and 23% from the routine clinical parameter respectively as shown in figure 4.19.

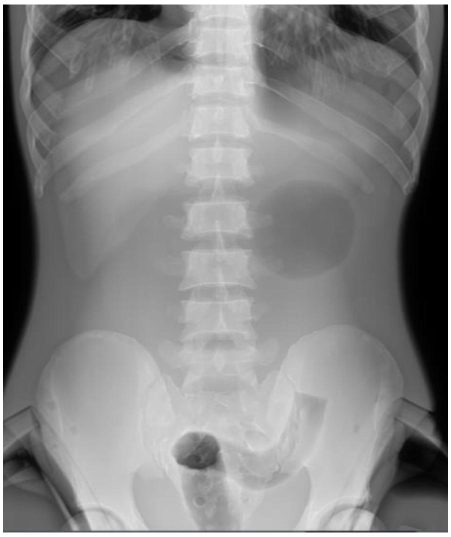

A. Clinical parameter
80 kVp 32 mAs
ESAK = 3.475 mGy

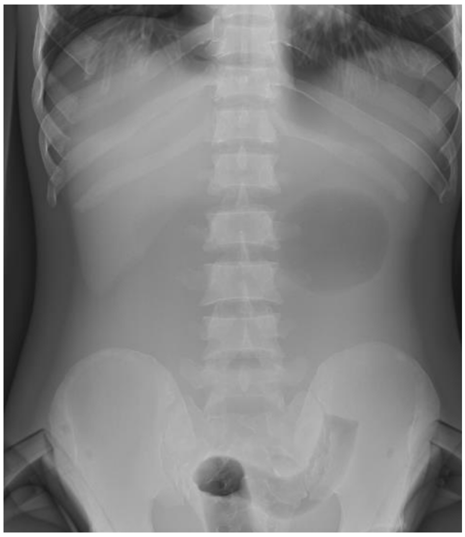

B. Optimal parameter
85 kVp 6.3 mAs
ESAK = 0.781 mGy

Figure 4.19 Abdominal radiography using routine clinical and optimal parameter in 25 cm thickness of abdomen.

4.2.3 29 cm thickness of abdomen

4.2.3.1 Radiation dose

4.2.3.1.1 The backscatter factors (BSF)

The BSF for the abdomen thickness of 29 cm were investigated by setting the experimental parameters at 70, 75, 80, 85, and 90 kVp and 3.2, 6.3, 12.5, and 25.0 mAs including the routine clinical parameter setting for abdominal radiography in 29 cm thickness at 85 kVp and 32 mAs. The results of BSF are shown as in table 4.27.

Table 4.27 The results of BSF in 29 cm thickness of abdomen phantom.

Parameter		Dosimeter reading (mGy)		BSF	Average±SD
kVp	mAs	EASK (K_e)	Incident air kerma (K_i)		
70	3.2	0.291	0.224	1.299	1.294±0.003
	6.3	0.575	0.445	1.292	
	12.5	1.126	0.870	1.294	
	25.0	2.250	1.741	1.292	
75	3.2	0.340	0.261	1.303	1.302±0.001
	6.3	0.675	0.518	1.302	
	12.5	1.318	1.013	1.301	
	25.0	2.638	2.024	1.303	
80	3.2	0.396	0.300	1.318	1.314±0.003
	6.3	0.783	0.596	1.314	
	12.5	1.524	1.162	1.312	
	25.0	3.053	2.328	1.311	
85	3.2	0.455	0.344	1.322	1.320±0.001
	6.3	0.897	0.680	1.320	
	12.5	1.744	1.322	1.319	
	25.0	3.494	2.647	1.320	
	32.0	4.472	3.389	1.320	
90	3.2	0.515	0.387	1.329	1.328±0.003
	6.3	1.017	0.766	1.328	
	12.5	1.972	1.487	1.326	
	25.0	3.949	2.977	1.327	

4.2.3.1.2 The entrance surface air kerma (ESAK)

The ESAK of the whole-body phantom with 29 cm thickness in abdomen was calculated for experimental parameters of kVp at 70, 75, 80, 85, and 90, mAs at 3.2, 6.3, 12.5, and 25.0 including the routine clinical parameter of at kVp 85 and mAs 32 by using tube output from quality control of digital mobile x-ray system. The range of ESAK corresponding to 21 exposure parameters was between 0.272 and 4.194 mGy as shown in table 4.28.

Table 4.28 The calculated ESAK of 29 cm thickness in abdomen.

kVp	mAs	Calculated ESAK
70	3.2	0.272
	6.3	0.535
	12.5	1.062
	25.0	2.124
75	3.2	0.318
	6.3	0.626
	12.5	1.241
	25.0	2.483
80	3.2	0.368
	6.3	0.724
	12.5	1.437
	25.0	2.874
85	3.2	0.419
	6.3	0.826
	12.5	1.638
	25.0	3.276
	32.0*	4.194
90	3.2	0.475
	6.3	0.934
	12.5	1.854
	25.0	3.708

*Routine clinical parameter

จุฬาลงกรณ์มหาวิทยาลัย
Chulalongkorn University

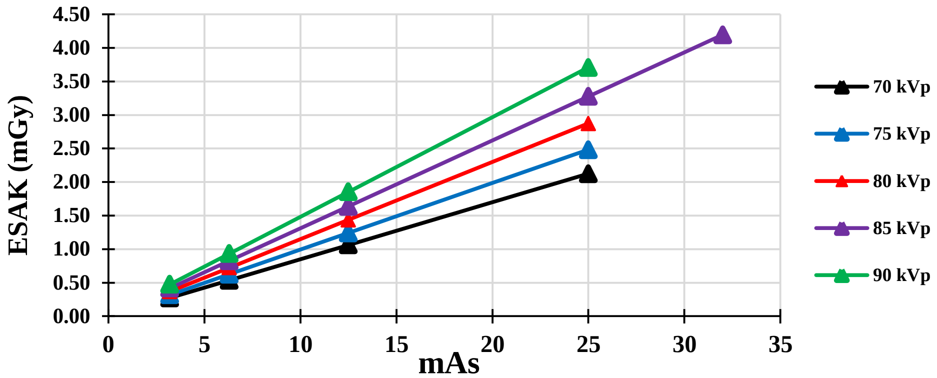

Figure 4.20 Relation between calculated ESAK and the exposure parameters in 29 cm thickness in abdomen.

4.2.3.1.3 The exposure index (EI)

The EI of the whole-body phantom with 29 cm thickness in abdomen was recorded for each parameter as shown in table 4.29.

Table 4.29 The results of EI and ESAK in each parameter in 29 cm thickness.

kVp	mAs	Calculated ESAK (mGy)	EI
70	3.2	0.272	38.98
	6.3	0.535	79.25
	12.5	1.062	151.57
	25.0	2.124	307.91
75	3.2	0.318	58.90
	6.3	0.626	120.82
	12.5	1.241	227.36
	25.0	2.483	421.37
80	3.2	0.368	84.88
	6.3	0.724	172.79
	12.5	1.437	327.40
	25.0	2.874	604.56
85	3.2	0.419	117.36
	6.3	0.826	237.32
	12.5	1.638	409.68
	25.0	3.276	825.85
	32.0*	4.194	1,036.32

*Routine clinical parameter

Table 4.29 The EI and ESAK in each parameter in 29 cm thickness in abdomen (Continued).

kVp	mAs	Calculated ESAK (mGy)	EI
90	3.2	0.475	154.60
	6.3	0.934	312.67
	12.5	1.854	539.60
	25.0	3.708	1,064.37

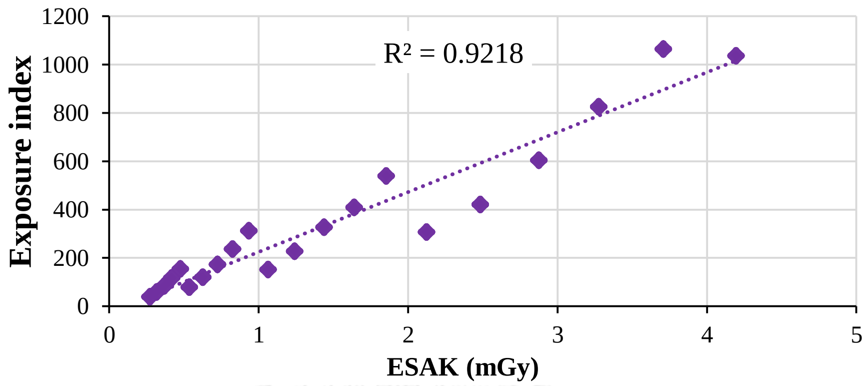

Figure 4.21 Relation between calculated ESAK and EI in 29 cm thickness in abdomen with R^2=0.9218.

For the abdomen thickness of 29 cm, there were 4 parameters that the EI closed to the target EI as shown in table 4.30.

Table 4.30 The parameters and EI phantom in 29 cm thickness of abdomen.

kVp	mAs	EI
70	25.0	307.91
80	12.5	327.40
85	12.5	409.68
90	6.3	312.67

4.2.3.2 Image quality evaluation

4.2.2.3.1 Image quality and qualitative noise analysis

The results of the image quality and qualitative noise analysis evaluated by three observers are shown in table 4.31.

Table 4.31 The image quality score abd qualitative scored by observers.

kVp	mAs	1st Observer		2nd Observer		3rd Observer	
		Image quality	Qualitative noise	Image quality	Qualitative noise	Image quality	Qualitative noise
70	3.2	3.5	2	4.5	2	3.0	3
	6.3	4.5	1	5.0	3	3.0	2
	12.5	4.0	1	6.0	1	4.5	1
	25.0	5.5	1	6.0	1	6.0	1
75	3.2	4.0	2	4.0	3	2.5	3
	6.3	4.0	1	6.5	2	5.0	1
	12.5	5.0	1	6.5	2	6.0	1
	25.0	5.5	0	6.0	1	6.0	1
80	3.2	3.0	2	4.5	1	3.0	3
	6.3	4.5	1	4.5	2	4.5	2
	12.5	5.0	1	5.0	1	5.0	1
	25.0	5.5	0	6.5	1	6.0	1
85	3.2	4.0	2	4.0	3	3.5	3
	6.3	5.0	1	4.5	2	4.5	1
	12.5	5.0	1	5.0	2	6.0	1
	25.0	6.0	0	6.5	1	6.5	0
	32.0*	6.0	0	6.5	1	6.0	1
90	3.2	3.0	1	4.5	2	3.5	2
	6.3	5.0	1	4.5	2	5.0	1
	12.5	5.5	1	6.0	2	6.0	1
	25.0	5.5	1	6.5	1	6.0	1

*Routine clinical parameter

The image quality score and qualitative noise are shown in figure 4.22 and figure 4.23.

จุฬาลงกรณ์มหาวิทยาลัย
CHULALONGKORN UNIVERSITY

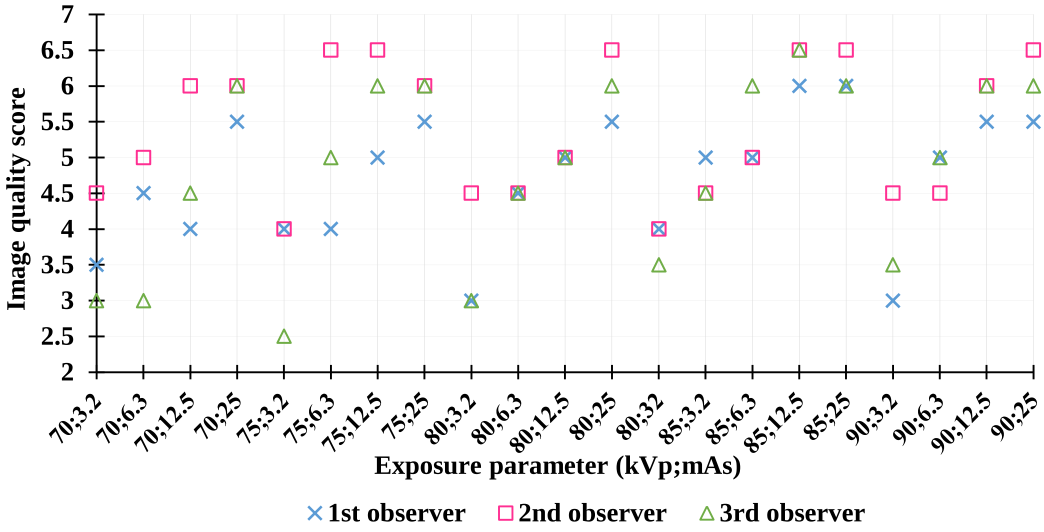

Figure 4.22 Scatter plot of image criteria score and exposure parameters by three observers.

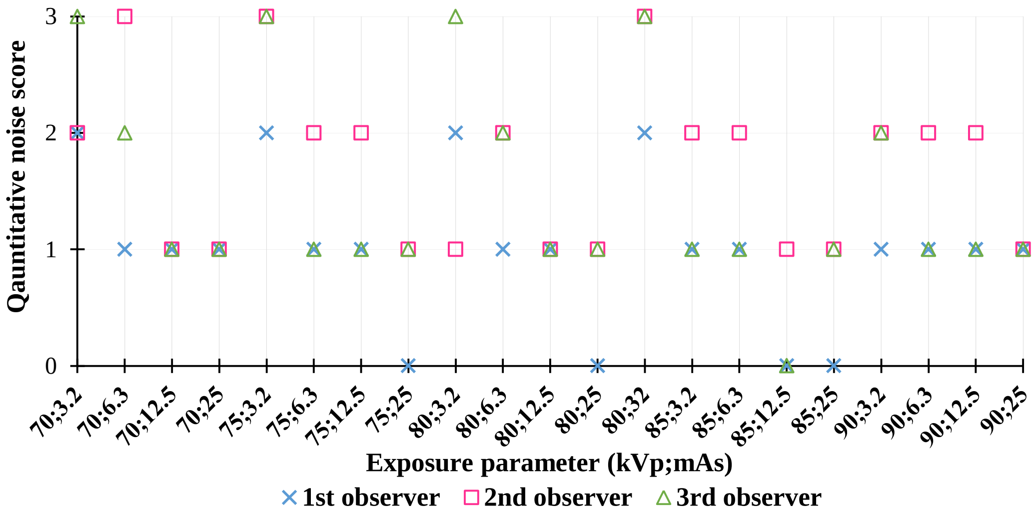

Figure 4.23 Scatter plot of qualitative noise score and exposure parameters by three observers.

The range of the image criteria and qualitative noise score were 2.5 to 6.5 and 0 to 3, respectively.

The average inter-class correlation coefficient for inter rater reliability of image quality scoring between three observers was 0.855. The strength of agreement was excellent. Therefore, the average scoring of image quality in each parameter of three observers was used for identifying the image quality score. For qualitative noise score by three observers, mode or median was used to identify the quality noise score as shown in table 4.33.

Table 4.32 The inter-item correlation matrix between observers in term of image quality scoring in 29 cm thickness in abdomen.

Observers	Inter-item correlation Value
1st observer and 2nd observer	0.631
1st observer and 3rd observer	0.850
2nd observer and 3rd observer	0.792

*The average inter-class correlation coefficient for inter rater reliability values and inter-item correlation value were calculated by using SPSS Version 22.0.

Table 4.33 The average image quality score and qualitative noise score by three observers in 29 cm thickness in abdomen.

Parameters		EI	ESAK (mGy)	Scoring	
kVp	mAs			Image quality	Qualitative noise
70	3.2	38.98	0.272	3.67	2
	6.3	79.25	0.535	4.17	2
	12.5	151.57	1.062	4.83	1
	25.0	307.91	2.124	5.83	1
75	3.2	58.90	0.318	3.50	2
	6.3	120.82	0.626	5.17	1
	12.5	227.36	1.241	5.83	1
	25.0	421.37	2.483	5.83	1
80	3.2	84.88	0.368	3.50	2
	6.3	172.79	0.724	4.50	2
	12.5	327.4	1.437	5.00	1
	25.0	604.56	2.874	6.00	1
85	3.2	117.36	0.419	3.83	3
	6.3	237.32	0.826	4.67	1
	12.5	409.68	1.638	5.33	1
	25.0	825.85	3.276	6.33	0
	32.0*	1,036.32	4.194	6.17	1
90	3.2	154.60	0.475	3.67	2
	6.3	312.67	0.934	4.83	1
	12.5	539.60	1.854	5.83	1
	25.0	1,064.37	3.708	6.00	1

*Routine clinical parameter

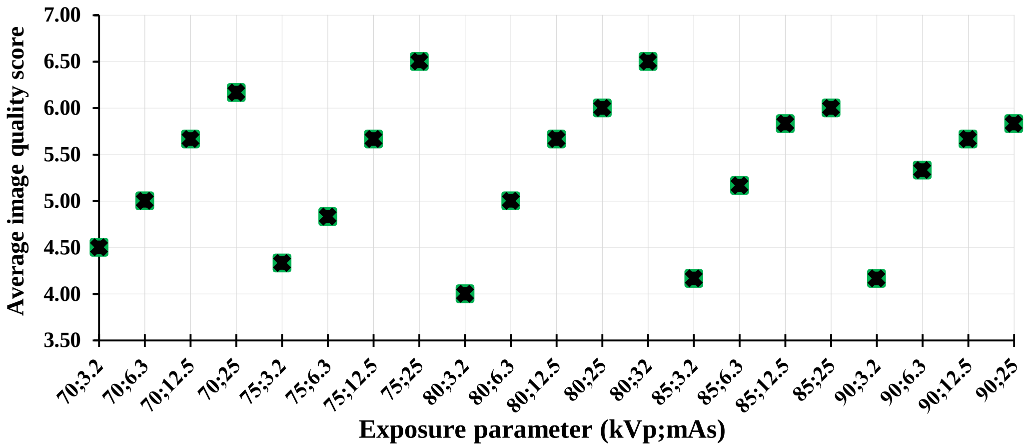

Figure 4.24 Scatter plots of mean image quality score by three observers.

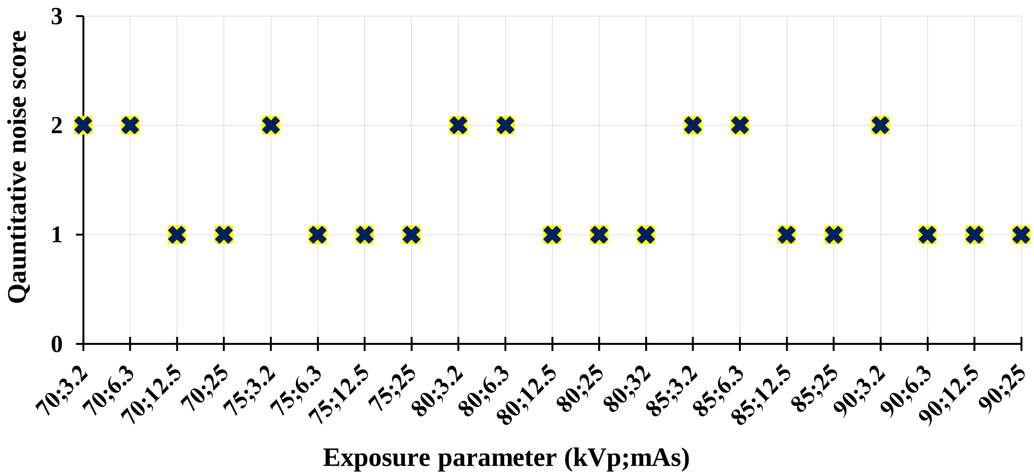

Figure 4.25 Scatter plots of qualitative noise score by three observers.

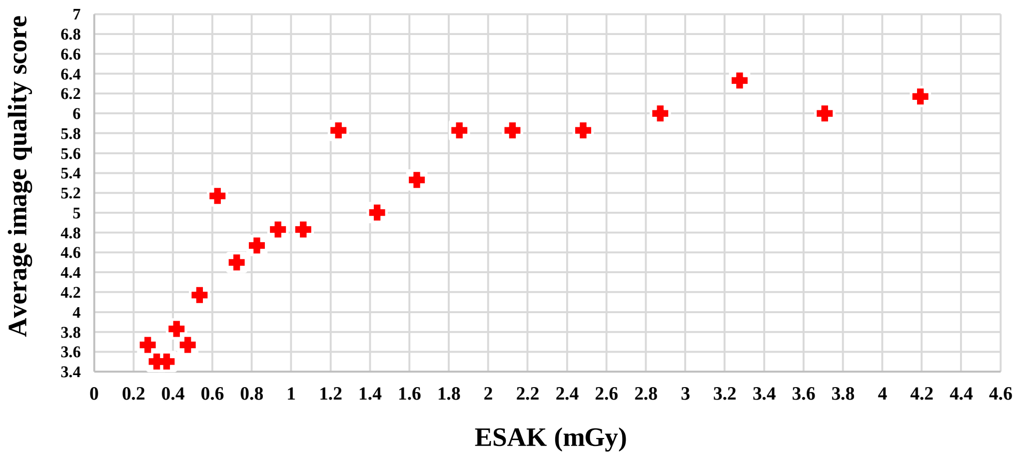

Figure 4.26 Scatter plots of the radiation dose and average image quality scoring by three observers in each parameter.

4.2.3.2.2 Quantitative image analysis

4.2.3.2.2.1 Signal-to-noise ratio (SNR)

The results of the average SNR in the 21 abdominal radiographic images are illustrated in table 4.34.

Table 4.34 The average of SNR in each parameter in the 29 cm thickness in abdominal images.

kVp	mAs	Average Signal-to-Noise Ratio (SNR)		
		1st ROI Liver	**2nd ROI 4th Lumbar**	**3rd ROI Flat bone**
70	3.2	18.04	21.56	13.45
	6.3	24.93	34.34	14.51
	12.5	28.86	48.69	14.67
	25.0	31.38	58.76	15.56
75	3.2	23.61	28.46	16.01
	6.3	27.97	46.13	16.36
	12.5	32.36	56.44	16.58
	25.0	33.33	63.26	17.27
80	3.2	27.06	37.24	17.34
	6.3	31.89	54.79	17.84
	12.5	34.42	57.65	17.87
	25.0	36.56	71.02	18.24
85	3.2	29.76	45.53	19.03
	6.3	33.22	64.37	19.16
	12.5	35.47	67.70	19.43
	25.0	37.15	72.25	19.50
	32.0*	37.43	97.65	19.68
90	3.2	32.39	53.83	19.96
	6.3	35.83	66.65	20.22
	12.5	38.51	76.37	20.36
	25.0	39.02	87.72	20.64

*Routine clinical parameter

The range of average SNR in 1st, 2nd, and 3rd ROIs were 18.04 – 39.02, 21.56 – 87.72, and 13.45-20.64, respectively.

จุฬาลงกรณ์มหาวิทยาลัย
Chulalongkorn University

4.2.2.3.2.2 Contrast-to-noise ratio (CNR)

The results of the average of CNR in the 21 abdominal radiographic images are illustrated in table 4.35.

Table 4.35 The average CNR in each parameter in the 29 cm thickness in abdominal images.

kVp	mAs	Average contrast-to-noise ratio (CNR)		
		1^{st} Area Liver Area	2^{nd} Area 4^{th} Lumbar and Left kidney	3^{rd} Area Flat bone and Right kidney
70	3.2	5.23	1.53	0.46
	6.3	5.32	2.27	0.82
	12.5	5.52	3.43	1.25
	25.0	5.66	5.43	1.32
75	3.2	5.43	1.61	0.60
	6.3	5.48	2.82	0.86
	12.5	5.57	4.47	1.36
	25.0	5.72	6.22	1.55
80	3.2	5.63	1.75	0.66
	6.3	5.78	3.09	1.27
	12.5	5.86	5.42	1.57
	25.0	5.93	6.82	1.63
85	3.2	5.87	2.35	0.75
	6.3	5.98	3.29	1.32
	12.5	6.16	5.59	1.69
	25.0	6.39	6.87	1.71
	32.0*	6.43	7.63	1.89
90	3.2	6.12	2.39	0.83
	6.3	6.24	4.55	1.39
	12.5	6.35	5.75	1.87
	25.0	6.44	7.18	1.96

*Routine clinical parameter

The ranges of average CNR in 1^{st}, 2^{nd}, and 3^{rd} areas were 5.23-6.44, 1.53-7.18, and 0.46-1.96, respectively.

CHULALONGKORN UNIVERSITY

4.2.3.3 The optimal parameter for the whole-body phantom in 29 cm thickness of abdomen

The optimal parameters from image quality with score ≥ 5 points, qualitative noise score between 1 and 2, and EI closed to target EI at 336 are shown as in table 4.37. The quantitative analysis in terms of SNR and CNR are shown in table 4.38 and table 4.39.

Finally, the optimal parameter was 85 kVp, 12.5 mAs and the ESAK was 1.638 mGy with EI at 409.68. The score on the image quality and the qualitative noise were 5.33 and 1 respectively. For the quantitative image analysis, the average SNR of the 1st, 2nd, and 3rd ROIs were 35.47, 67.70, and 19.43, respectively and the average CNR of 1st, 2nd, and 3rd areas were 5.86, 5.42, and 1.57, respectively.

Table 4.36 The ESAK, exposure index, and qualitative image analysis of the optimal and other parameters in whole-body phantom in 29 cm thickness of abdomen.

Parameters		ESAK (mGy)	EI	Scoring	
kVp	mAs			Image quality	Qualitative noise
85	12.5	1.638	409.68	5.33	1
90	6.3	1.858	539.60	5.83	1

Table 4.37 The average SNR of the optimal and other parameters in whole-body phantom in 29 cm thickness of abdomen.

Parameters		Average signal-to-noise ratio (SNR)		
kVp	mAs	1st ROI Liver	2nd ROI 4th Lumbar	3rd ROI Flat bone
85	12.5	35.47	67.70	19.43
90	12.5	38.51	76.37	20.36

Table 4.38 The CNR of the optimal and other parameters in whole-body phantom in 29 cm thickness of abdomen.

Parameters		Average contrast-to-moise ratio (CNR)		
kVp	mAs	1st Area Liver Area	2nd Area 4th Lumbar and Left kidney	3rd Area Flat bone and Right kidney
85	12.5	6.16	5.59	1.69
90	12.5	6.35	5.75	1.87

CHULALONGKORN UNIVERSITY

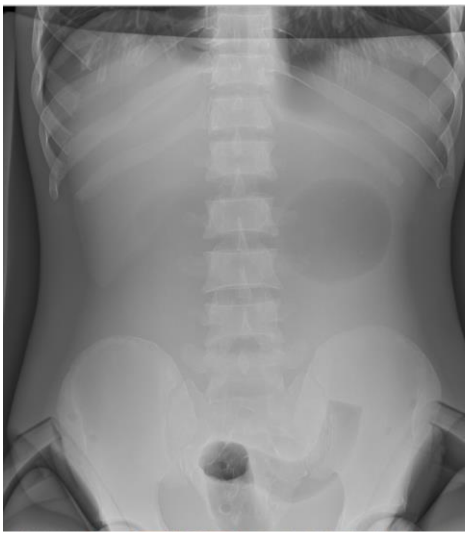

A. 85 kVp 12.5 mAs
ESAK =1.638 mGy
Image criteria = 5.33
Qualitative noise = 1

B. 90 kVp 12.5 mAs
ESAK =1.858 mGy
Image criteria = 5.83
Qualitative noise = 1

Figure 4.27 Example of phantom's radiographs from different exposure parameters for 29 cm thickness.

4.2.3.4 The comparison between routine clinical and optimal parameter for the whole-body phantom in 29 cm thickness of abdomen

The radiation dose and image quality using clinical and optimal parameter in term of ESAK, EI, image quality score, qualitative and quantitative image analysis are shown in table 4.39.

Table 4.39 The comparison between the routine clinical and optimal parameter in 29 cm thickness of abdomen.

	Routine clinical parameter	**Optimal parameter**
ESAK	4.195 mGy	1.638 mGy
EI	1036.32	409.68
Image quality score	6.17	5.33
Qualitative noise score	1	1
Quantitative image analysis		
Average SNR		
-1st ROI	37.43	35.47
-2nd ROI	97.65	67.70
-3rd ROI	19.68	19.43

Table 4.42 The comparison between the routine clinical and optimal parameter in 29 cm thickness of abdomen (Continued).

	Routine clinical parameter	Optimal parameter
Average CNR		
-1st area	6.43	6.16
-2nd area	7.63	5.59
-3rd area	1.89	1.69

By using the optimal parameter, the reduction of ESAK and EI (EI) were 61% and 60% from the routine clinical parameter respectively. The image quality score was 14% lower than the routine clinical parameter while the qualitative noise score was slightly different. For the quantitative image analysis, the average SNR of 1st, 2nd, and 3rd ROIs were decreased by 5%, 31%, and 1% from the routine clinical parameter. The average of CNR of 1st, 2nd, and 3rd areas were decreased 2%, 50%, and 26% from the routine clinical parameter, respectively as shown in figure 4.28.

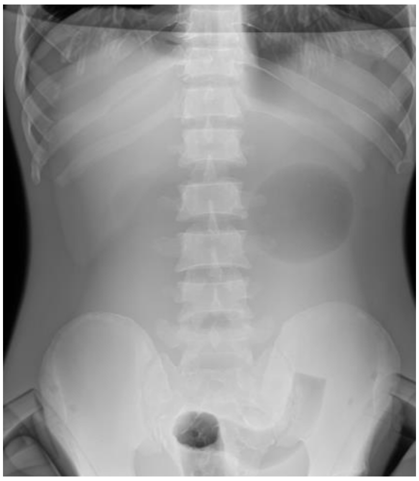

A. Clinical parameter
85 kVp 32.0 mAs
ESAK =4.195 mGy

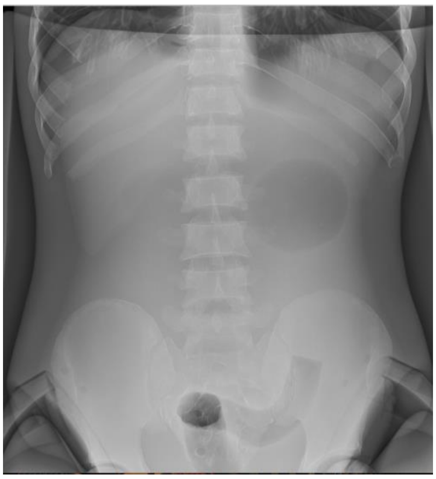

B. Optimal parameter
85 kVp 12.5 mAs
ESAK =1.638 mGy

Figure 4.28 Abdominal radiography using routine clinical and optimal parameter in 29 cm thickness of abdomen.

CHAPTER V

DISCUSSION AND CONCLUSIONS

5.1 Discussion

Currently, the technology of digital radiography could decrease the radiation dose as well as maintain the image quality for diagnosis in medical imaging field. Therefore, the radiation dose to the patient could be significantly reduced and radiation protection could be observed. The present study is revealed the investigation of the optimal parameters in abdominal radiography using digital mobile x-ray system based on the various phantom thicknesses at King Chulalongkorn Memorial Hospital.

The quality control programs in the x-ray equipment including digital mobile x-ray system, digital image receptor and display monitors play an important role to verify the accuracy and precision of the equipment for optimization. The results of quality control of x-ray tube output were used to calculate the ESAK of the anthropomorphic phantom. For digital image receptor, the detector dose indicator consistency was analyzed to verify the EI consistency and the variation of EI and radiation dose on image receptor. The quality control of display monitors was also performed before the image quality evaluation for image scoring and qualitative noise by 3 observers to ensure that the performance of the monitors was within the good condition for interpretation.

From the DRL recommended by IAEA, the ESAK in abdomen AP radiography was 10 mGy based on screen-film system. Muhogora WE, et al [18] found that the average ESAK to adult patients (70±10 kg.) of abdominal radiography in Thailand was 3.9 mGy by using film-screen system. The data were collected from 4 local hospitals. The incident air kerma for each adult patient undergoing a particular radiographic examination was determined by the product of the x-ray tube output value (derived from the output per mAs–kVp curve corrected for the inverse distance effects between the patient's distance from the x-ray focus and the distance at output measurements) and the actual tube loading (mAs) used in the radiographic examination. The ESAK value was then calculated by multiplying incident air kerma to the patient's surface by the appropriate backscatter factor (BSF) based on International Commission for Radiation Units and Measurements (ICRU). However, there was no DRL based on digital radiography from other publications.

The backscatter factor is the ratio of ESAK on the surface of the phantom to the incident air kerma. It is dependent on the tube potential, total filtration, radiation field size, material, and distant from the x-ray source. From this study, the BSF had been calculated following the equation 3.1 in 21, 25, and 29 cm thicknesses in abdomen of whole-body phantom. We have found that the BSF was changed when increasing the built-up thickness to the abdominal part of the phantom. As the x-ray photons are gradually absorbed in the thicker body, the scatter radiations reached to the ionization chamber were decreased accordingly. Therefore, the BSF from different thickness is needed to take into account for ESAK calculation as shown in table 5.1. The average percent differences of BSF from 21 cm to 25 cm thickness and 25 cm thickness to 29 cm thickness were decreased to 1.60% and 5.21%, respectively. However, for this study, we did not investigate the effect of the backscatter factor of the other filed sizes.

Table 5.1 The average BSF in different thicknesses at field size of 41x41cm^2.

kVp	Average backscatter factor		
	21 cm	**25 cm**	**29 cm**
70	1.380	1.361	1.294
75	1.394	1.373	1.302
80	1.406	1.385	1.314
85	1.417	1.393	1.320
90	1.427	1.397	1.328

The image quality criteria for determining the abdomen AP radiography in accordance with IAEA is based on 7 items. The image noise which was presented on the radiographic image was also determined in terms of qualitative noise. The criteria for determined the optimal parameter consist of image quality equal to or more than 5 points and qualitative noise between 1 and 2. We have found that the acceptable of image quality score and qualitative noise were agreed by 3 observers.

In the abdominal radiography using low exposure parameters, the low image quality score was obtained because the image was too noisy. In addition, the abdominal radiography using high exposure parameters may also receive the low image quality score because the images were loss of details at the edge of abdominal wall. The example of this explanation is illustrated as in figure 5.1.

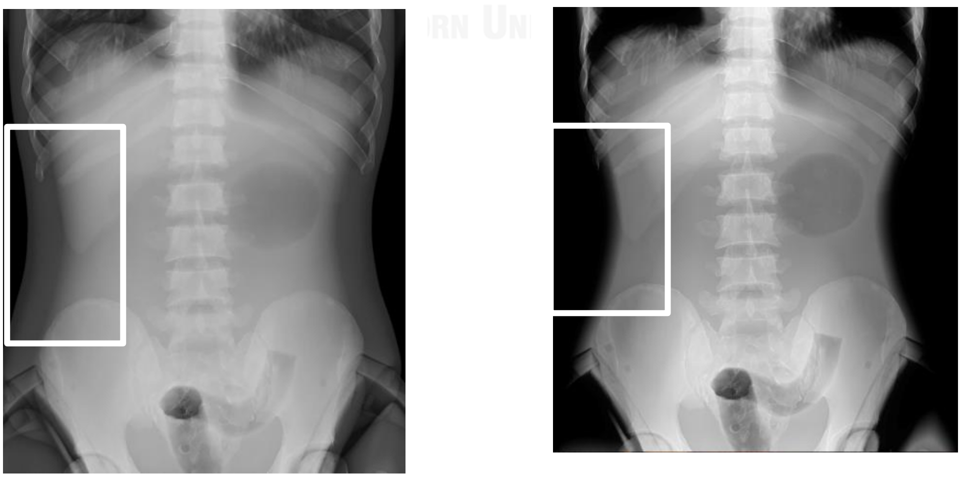

A B

Figure 5.1 The 21 cm thickness of abdominal radiography (A) 70 kVp, 3.2 mAs and (B) 90 kVp, 25 mAs. The edge of the abdominal wall of the x-ray image in the rectangular box in (B) is disappeared due to using high exposure parameter.

The exposure index (EI) is the indicator of the amount of radiation dose at the image receptor. For GE digital radiography system, the EI is directly related to radiation dose that reach to image receptor. The higher of radiation dose to image receptor, the greater of the EI. The target EI for abdominal radiography of 336 is recommended by manufacturer [23]. The comparison between EI and the image quality score in each parameter need to be considered as the EIs in some parameters were lower than the target EI. However, the obtained image quality score was still within the acceptable limit.

In the routine clinical parameter, the EI in abdominal radiography was high due to using high exposure parameter. The details of the abdominal radiography were loss because the number of signals for creating the abdominal radiography is also very high [12]. Therefore, the optimal parameter in this study would balance the factors of the image quality, radiation dose and EI recommended by manufacturer.

In different manufacturers of digital radiography system, the analysis methods to calculate the EI in each manufacturer are different as illustrated in table 2.1. The same radiation dose reached to image receptor in different manufacturer might be resulting different EI. The targets EI of different vendors were also different. Hence, the understanding of the EI in each digital radiography system is necessary for balancing between the radiation dose and image quality.

The relationship between the ESAK and EI in 21, 25, and 29 cm thicknesses of abdomen as illustrated in figure 4.2, 4.16, and 4.26 are excellent with the R^2 of 0.9038, 0.9113, and 0.9218, respectively. However, EI is the radiation dose to image receptor or exit dose and doesn’t represent the radiation dose to patient. Dose to the patient is depending on many factors, including the parts of the body being examined, presence or lack of radiation-sensitive organs being exposed to x-ray, the area of the x-ray collimation irradiating the patient, the output of the x-ray tube as a function of the kVp, tube current, exposure time and beam filtration [12]. Therefore, the calculation of radiation dose by using EI still be the question and under investigation.

For quantitative image analysis in terms of SNR and CNR, the pixel value was directly measured in the raw data radiographic images on the display monitor of the digital mobile x-ray system instead of measuring on PACS monitor. The main reason was the pixel value of the radiographic image after transferred to PACS system was fluctuated due to the image processing algorithm from manufacturer. In this study, we found that the average SNR and CNR of the abdominal image was decreased when the size of the abdominal thickness was increased as shown in table 5.2 and table 5.3.

Table 5.2 The comparison of SNR in different phantom's thickness.

Thickness (cm)	kVp	mAs	Average signal-to-noise ratio (SNR)		
			1^{st} ROI Liver	2^{nd} ROI 4^{th} Lumbar	3^{rd} ROI Flat bone
21	85	12.5	45.36	75.56	19.93
25			43.67	75.08	19.53
29			35.47	67.70	19.43

Table 5.3 The comparison of CNR in different phantom's thickness.

Thickness (cm)	kVp	mAs	Average contrast-to-noise ratio (CNR)		
			1^{st} Area Liver	2^{nd} Area 4^{th} Lumbar and Left kidney	3^{rd} Area Flat bone Right kidney
21	85	12.5	6.59	8.75	1.80
25			6.42	7.54	1.75
29			6.16	5.59	1.69

For quantitative analysis in the digital image, the consistency of ROI location should be concerned as the different site of ROI measurement can be affected the pixel value results. Hence, we have drawn the ROIs three times in each location in order to reduce the uncertainties for quantitative analysis.

5.1.1 Assessment of the optimal parameter of the whole-body phantom in 21 cm thickness of abdomen

From this study, there were 11 parameters that the average image quality score have reached the image criteria (≥ 5) and the ESAK was lower than 1.86 mGy, the reference study from Aldrich JE, et al [17] as shown in table 5.4. The parameters of 80 kVp, 3.2 mAs, 70 kVp, 6.3 mAs and 75 kVp, 6.3 mAs were the lowest ESAK at 0.318, 0.461, and 0.541 mGy, and EI of 118.82, 185.78, and 272.83 were obtained, respectively. However, those image quality scoring had range between 4.5 to 5.5, 4.5 to 6, and 4.5 to 5.5. The results showed that probably one of three observers gave image score lower than the image criteria and the EI were not closed to the target EI. Finally, the optimal parameter selected for the whole-body phantom in 21 cm thickness of abdomen was 80 kVp and 6.3 mAs with the EI of 381.53. This optimal parameter can provide the ESAK of 0.626 mGy while giving the image quality range between 5.5 and 6.

Table 5.4 The parameters using for the whole-body phantom with 21 cm thickness of abdomen for optimal parameter selection.

Parameters		ESAK (mGy)	Exposure index	Scoring	
kVp	mAs			Image quality	Qualitative noise
80	3.2	0.318	188.82	5.17	2
70	6.3	0.461	185.78	5.00	1
75	6.3	0.541	272.83	5.00	1
80	6.3	0.626	381.53	5.67	1
85	6.3	0.716	509.72	5.67	1
90	6.3	0.811	650.90	5.50	1
70	12.5	0.915	363.34	6.33	1
75	12.5	1.074	520.54	5.67	1
85	12.5	1.420	949.28	6.00	1
90	12.5	1.609	1,206.08	6.50	1
70	25.0	1.830	706.76	6.00	1

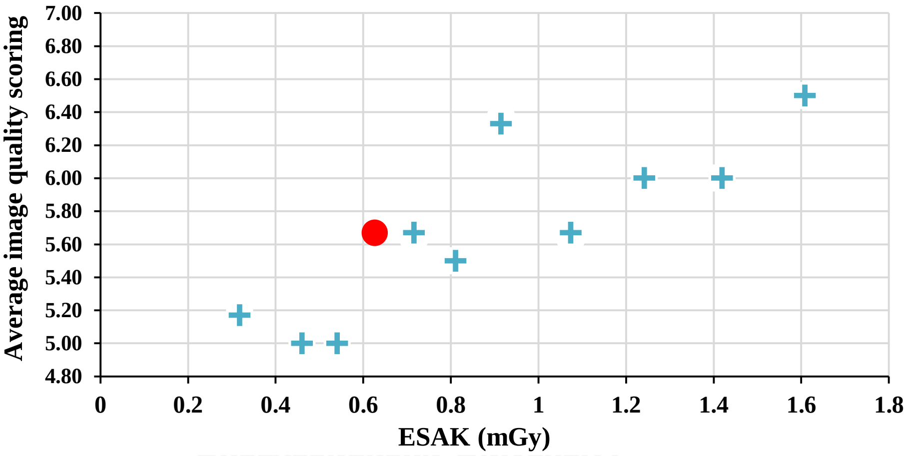

Figure 5.2 Scatter plots between the ESAK and the average image quality scoring after image analysis in 21 cm thickness of abdomen. The blue cross color represents the parameter that image scoring meets the criteria for optimal parameter selection. The red circle represents the optimal parameter selected for 21 cm thickness of abdomen.

Table 5.5 The range of optimal parameters recommened for 21 cm thickness of abdomen.

Thickness	kVp	mAs
21 cm	80-85	6.3

5.1.2 Assessment of the optimal parameter of the whole-body phantom in 25 cm thickness of abdomen

At 25 cm thickness from this study, there were 9 parameters that the average image quality score has reached the image criteria (≥ 5) and the ESAK was lower than 1.86 mGy [17] as shown in table 5.5. The parameters of 70 kVp, 6.3 mAs and 80 kVp, 6.3 mAs were the lowest ESAK at 0.505 and 0.685 mGy, and the EI of 141.18 and 293.62 were obtained, respectively. However, those image quality scoring had range between 4.5 and 5.5. The results showed that one of three observers might give image score lower than the image criteria and the EI were not closed to the target EI. However, the majority of average scoring was still higher than the acceptable limit for image quality evaluation. Finally, the optimal parameter for the whole-body phantom in 25 cm thickness of abdomen was 85 kVp and 6.3 mAs with the EI of 395.39. This optimal parameter can provide the ESAK of 0.781 mGy while giving the image quality score range between 5 and 5.5.

Table 5.6 The parameters using for the whole-body phantom with 25 cm thickness of abdomen for optimal parameter selection.

Parameters		ESAK (mGy)	Exposure index	Scoring	
kVp	mAs			Image quality	Qualitative noise
70	6.3	0.505	141.18	5.00	2
80	6.3	0.684	293.62	5.00	2
85	6.3	0.781	395.39	5.17	2
90	6.3	0.881	450.39	5.33	1
70	12.5	1.001	271.53	5.67	1
75	12.5	1.173	336.92	5.67	1
80	12.5	1.357	489.36	5.67	1
85	12.5	1.549	657.39	5.83	1
90	12.5	1.748	835.38	5.67	1

จุฬาลงกรณ์มหาวิทยาลัย
CHULALONGKORN UNIVERSITY

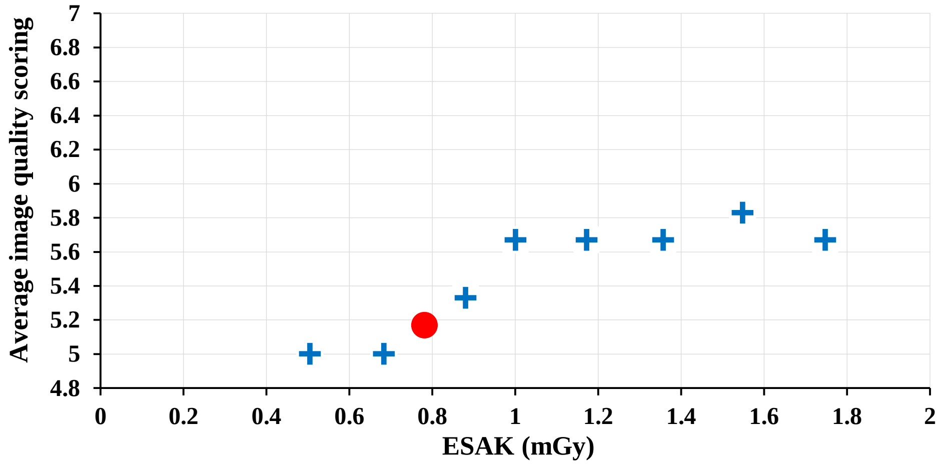

Figure 5.3 Scatter plot between the ESAK and average image quality scoring after image analysis in 25 cm thickness of abdomen. The blue cross color represents the parameter that image scoring meets the criteria for optimal parameter selection. The red circle represents the optimal parameter selected for 25 cm thickness of abdomen.

Table 5.7 The range of optimal parameters recommended for 25 cm thickness of abdomen.

Thickness	kVp	mAs
25 cm	85-90	6.3

5.1.3 Assessment of the optimal parameter of the whole-body phantom in 29 cm thickness of abdomen

From this study, there were 5 parameters that the average image quality score have met the image criteria (≥ 5) and the ESAK was lower than 1.86 mGy [17] as depicted in table 5.6. The parameter of 75 kVp 6.3 mAs was the lowest ESAK at 0.626 mGy, and the EI of 120.82 was obtained. However, the image quality scoring was range between 4 and 6. The results showed that probably the observer gave image score lower than the image criteria and the EI was not closed to the target exposure. For the parameter at 70 kVp, 12.5 mAs, the ESAK was 1.241 mGy, and the EI of 227.36 was obtained while giving the image quality scoring range between 5 and 6.5. However, the EI was not closed the target EI. For the parameter at kVp 80 mAs 12.5, the ESAK was 1.437 mGy and the EI was 327.46 with the image quality scoring of 5 from all three observers was obtained. For the parameter at 85 kVp 12.5 mAs, the ESAK was 1.638 mGy and the EI was 409.68 while giving the image quality scoring range between 5 and 6.

For the parameter at 80 kVp 12.5 mAs, the quantitative analysis in terms of SNR and CNR were evaluated. The average SNR of 1st, 2nd, and 3rd ROIs were decreased by 8%, 41%, and 9%, respectively and the average CNR of 1st, 2nd, and 3rd areas were decreased to 9%, 29%, and 17%, respectively when compared to the routine clinical parameter. For the parameter at kVp 85, mAs 12.5, the average SNR of 1st, 2nd, and 3rd ROIs were decreased 5%, 31%, and 1%, respectively and the average CNR of 1st, 2nd, and 3rd areas were decreased to 4%, 27%, and 11%, respectively when compared to the routine clinical parameter. The result showed that for parameter at 85 kVp, 12.5 mAs, the ESAK was higher than the parameter at 80 kVp, 12.5 mAs, but the average SNR and CNR were better. Finally, the parameter that was selected for the optimal parameter for the whole-body phantom in 29 cm thickness of abdomen was 85 kVp and 12.5 mAs. The ESAK was 1.638 mGy while the image quality score range between 5 and 6.

Table 5.8 The parameters using for the whole-body phantom with 29 cm thickness of abdomen for optimal parameter selection.

Parameters		ESAK (mGy)	Exposure index	Scoring	
kVp	mAs			Image quality	Qualitative noise
70	6.3	0.626	120.82	5.17	1
70	12.5	1.241	227.36	5.83	1
80	12.5	1.437	327.40	5.00	1
85	12.5	1.638	409.68	5.33	1
90	12.5	1.854	539.60	5.83	1

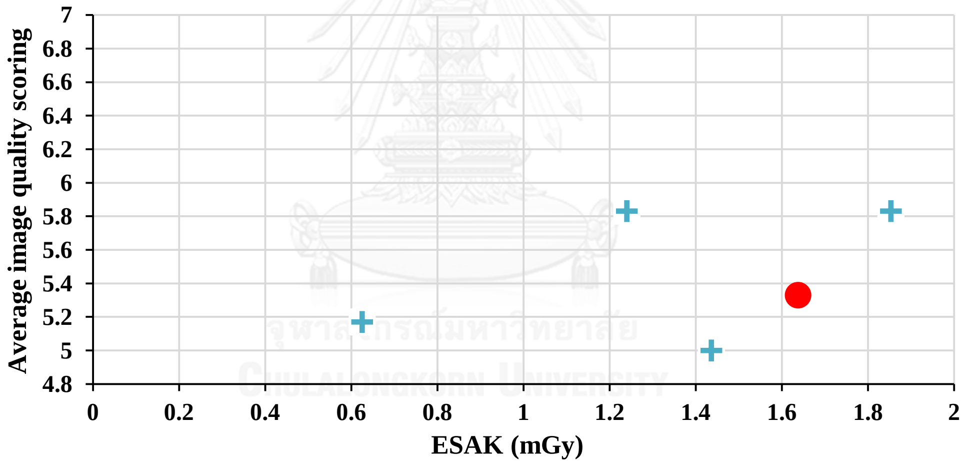

Figure 5.4 Scatter plots between the ESAK and average image quality scoring after image analysis in 29 cm thickness of abdomen. The blue cross color represents the parameter that image scoring meets the criteria for optimal parameter selection. The red circle represents the optimal parameter selected for 29 cm thickness of abdomen.

Table 5.9 The range of optimal parameters recommended for 29 cm thickness of abdomen.

Thickness	kVp	mAs
29 cm	85-90	12.5

5.1.4 The comparison of ESAK between the optimal parameters in this study and other studies

Aldrich JE, et al study [17] showed the average ESAK of the abdomen AP using digital radiography was 1.86 mGy. Asada Y, et al study [19] showed the average entrance surface dose (ESD) between computed radiography and digital radiography was 2.24 mGy (assuming that the ESAK is approximately equal to ESD). In this study, the ESAK of the optimal parameter in 21, 25, and 29 cm thickness of abdomen were 0.626, 0.781, and 1.638 mGy, respectively. Therefore, optimal parameters in this study were lower than the Aldrich JE, et al and Asada Y, et al, and can reduce the radiation dose to the patients substantially.

Table 5.10 The comparison of ESAK between the optimal parameters in this study and other studies.

This study		**Aldrich JE, et al study [17]**	**Asada Y, et al study [19]**
21 cm thickness	0.626 mGy	1.86 mGy (70 ± 10 kg, not identified the thickness of patients using digital radiogphy)	2.24 mGy (20 cm thickness of abdomen by using the average ESAK between CR and DR)
25 cm thickness	0.721 mGy		
29 cm thickness	1.638 mGy		

5.2 Conclusions

The optimal parameter to optimize the radiation dose and image quality for the abdominal radiography using digital mobile x-ray system at King Chulalongkorn Memorial Hospital in 21 cm thickness of abdomen was 80 kVp, 6.3 mAs. The range of optimal parameters was 80-85 kVp, 6.3 mAs.

For 25 cm thickness of abdomen, the optimal parameter was 85 kVp, 6.3 mAs. The ranges of optimal parameters were 85-90 kVp, 6.3 mAs.

For 29 cm thickness of abdomen, the optimal parameter was 85 kVp, 12.5 mAs. The ranges of optimal parameters were 85-90 kVp, 12.5 mAs.

As the comparison between the routine clinical and optimal parameters, the ESAK in optimal parameter of 21, 25, and 29 cm thicknesses of abdomen can reduce the entrance surface air kerma in phantom study substantially by 77%, 78%, and 61% compared to the routine clinical parameter. However, the optimal parameters still maintain the image quality for acceptable diagnosis in various abdominal thicknesses. The recommendation for the range of optimal parameter for abdominal radiography is concluded in table 5.7. This could be used as the guideline parameters for radiological technologists for abdominal radiography using portable digital detector x-ray system for the future clinical study with the patients.

Table 5.11 The range of optimal parameters recommended for abdominal radiography in various thicknesses at KCMH using digital mobile x-ray system.

Thickness (cm)	kVp	mAs
21	80-85	6.3
25	85-90	6.3
29	85-90	12.5

5.3 Recommendations

Future studies should be applied the optimal parameters with patient who is requested for abdominal radiography using digital mobile x-ray system. The optimal parameter for the other examinations with high exposure technique when using digital mobile x-ray system at King Chulalongkorn Memorial Hospital based on GE mobile system such as skull and pelvis should be further study. This will have potential to reduce the radiation dose for the patient, relatives, medical staff and technologists as well.

จุฬาลงกรณ์มหาวิทยาลัย
Chulalongkorn University

REFERENCES

1. Wikipedia. Digital radiography [Internet]. 2016 [cited 2016 Mar 26]. Available from: https://en.wikipedia.org/wiki/Digital_radiography.
2. Korner M, Weber CH, Wirth S, Pfeifer KJ, Reiser MF, Treitl M. Advances in digital radiography: physical principles and system overview. Radiographics 2007;27:675-86.
3. Sangdao P. Optimization of radiation dose and image quality in chest radiography using digital mobile x- ray system at King Chulalongkorn Memorial Hospital [Thesis]. Bangkok: Chulalongkorn University; 2014.
4. Atlantaradtech. Radiography imaging acquisition, Processing and display [Internet]. 2014 [cited 2016 Dec 21]. Available from: http://atlantaradtech.org/upload/1389630161_Radiographic%20Imaging%20Fauber%202014.pdf.
5. Radiologyinfo. X-ray (Radiography) – abdomen [Internet]. 2015 [cited 2017 Jan 5]. Available from: http://www.radiologyinfo.org/en/info.cfm?pg=abdominrad.
6. Herrmann TL, Fauber TL, Gill J, Hoffman C, Orth DK, Peterson PA, et al. Best practices in digital radiography. Central Ave. SE: The American Society of Radiologic Technologists; 2012.
7. Kotter E, Langer M. Digital radiography with large-area flat-panel detectors. Eur Radiol 2002;12:2562-70.
8. Lança L, Silva A. Digital radiography detectors: a technical overview. In: Lança L, Silva A, editors. Digital imaging systems for plain radiography. New York: Springer; 2013. p. 9-19.
9. Lança L, Silva A. Digital radiography detectors – A technical overview: Part 2. Radiography 2009;15:134-8.
10. Tabakov S, Milano F, Strand SE, Lewis C, Sprawls P. Encyclopaedia of medical physics. Boca Raton: Taylor & Francis Group; 2013.
11. Bushberg J.T., Seibert J.A., E.M. L, J.M. B. The essential physics of medical imaging. In: Bushberg J.T., Seibert J.A., E.M. L, J.M. B, editors. Radiography. 3 ed. Philadelphia: Lippincott, Williams and Wilkins; 2012. p. 207-37.
12. Seibert JA, Morin RL. The standardized exposure index for digital radiography: an opportunity for optimization of radiation dose to the pediatric population. Pediatr Radiol 2011;41:573-81.
13. Shepard SJ, Wang J, Flynn M, Gingold E, Goldman L, Krugh K, et al. An exposure indicator for digital radiography: AAPM Task Group 116 (executive summary). Med Phys 2009;36:2898-914.
14. Moore QT, Don S, Goske MJ, Strauss KJ, Cohen M, Herrmann T, et al. Image gently: using exposure indicators to improve pediatric digital radiography. Radiol Technol 2012;84:93-9.
15. Uffmann M, Schaefer-Prokop C. Digital radiography: the balance between image quality and required radiation dose. Eur J Radiol 2009;72:202-8.
16. Masoud AO, Muhogora WE, Msaki PK. Assessment of patient dose and optimization levels in chest and abdomen CR examinations at referral hospitals in Tanzania. J Appl Clin Med Phys 2015;16:5614.
17. Aldrich JE, Duran E, Dunlop P, Mayo JR. Optimization of dose and image quality for computed radiography and digital radiography. J Digit Imaging 2006;19:126-31.
18. Muhogora WE, Ahmed NA, Almosabihi A, Alsuwaidi JS, Beganovic A, Ciraj-Bjelac O, et al. Patient doses in radiographic examinations in 12 countries in Asia, Africa, and Eastern Europe: initial results from IAEA projects. AJR Am J Roentgenol 2008;190:1453-61.
19. Asada Y, Suzuki S, Minami K, Shirakawa S, Kobayashi M. Survey of patient exposure from general radiography and mammography in Japan in 2014. J Radiol Prot 2016;36:N8-N18.

20. American Association of Physicist in Medicine. Report No.74 quality control in diagnostic radiology. The American Association of Physicist in Medicine, 2002.
21. King's College Hospital. KCARE protocol for the QA of direct digital radiograph system commissioning and annual QA test. King's Center for the Assessment of Radiological Equipment, King's College Hospital, 2004.
22. Samei E, Badano A, Chakraborty D, Compton K, Cornelius C, Corrigan K, et al. Assessment of display performance for medical imaging systems: executive summary of AAPM TG18 report. Med Phys 2005;32:1205-25.
23. GE Healthcare. DEI (Detector Exposure Indicator). Optima XR200amx X-Ray System with Digital Upgrade Operator Manual 2012. p. 14-41-14-44.

จุฬาลงกรณ์มหาวิทยาลัย
Chulalongkorn University

APPENDICES

จุฬาลงกรณ์มหาวิทยาลัย
Chulalongkorn University

Appendix A: Quality control of digital radiography system

General Information

Location: **King Chulalongkorn Memorial Hospital**

Date: **8 June 2016**

Equipment number: **5 (inherent 0.9 mmAl) Addition 2 mmAl**

Manufacturer: **General Electric Company (September 2013)**

Model number: **5555000-6 (Optima XR220amx)**

Serial number: **1031653WK7**

Checklist

P	General mechanical and electrical condition
P	Tube angle indicator, tube motion and locks
P	Focus to film distance indicator (SID)
P	Field size indicator
P	Congruency of light and radiation fields
P	Crosshair centering
P	Focal spot size
N/A	Photo cell consistency
N/A	Bucky/Grid Centering
N/A	Automatic Collimation (PBL)
P	Beam Quality (Half Value Layer)
P	Consistency of exposure
P	kVp Accuracy
N/P	ESAK calculation
N/A	Timer accuracy
P	mA Linearity

P = Performed

N/P = Not Performed

N/A = Not Application

จุฬาลงกรณ์มหาวิทยาลัย
CHULALONGKORN UNIVERSITY

General Condition of Mechanical and Electrical Components

Purpose: To make sure that the equipment is mechanically stable and function as manufacture's design

N	Are there any frayed or exposed electrical wires?
N	Could electrical wires interfere with the use of the unit?
N/A	Is there play in the couch when it is locked?
N/A	Does it have the freedom of movement it was designed for?
N/A	Is the couch level in tube and perpendicular directions?
N	Is there play in the tube when it is locked?
Y	Does it have the freedom of movement it was designed to have?
Y	Does the visual, and/or, audible beam-on indicator function?
N	Is the dead man switch installed correctly?

Tube Angle Indicator Check

CW:		CCW:	
0° :	1		
45°:	47	45°:	-43
90°:	89	90°:	-91
Allowable limit = ± 5°		Pass/Fail:	**Pass**

Tube motion and lock Check

	Motion	Locks
Tube Longitudinal:	**Pass**	**Pass**
Tube Rotate:	**Pass**	**Pass**
Tube Transverse:	**Pass**	**Pass**
Tube Vertical:	**Pass**	**Pass**
Tube Angulate:	**Pass**	**Pass**
Collimator Jaws:	**Pass**	**Pass**
Collimator Rotation:	**Pass**	**Pass**

จุฬาลงกรณ์มหาวิทยาลัย
CHULALONGKORN UNIVERSITY

Target to Film Distance Indication Check (at 100 cm SID)

SID 100 cm. Allowable limit = ± 2% SID

Measured distance: 100 cm

Indicated distance: 100 cm

Radiographically (determined) distance: - cm

% Difference: 0.00 %

Passed or Failed: **Pass**

Field Size Indication

Purpose: To insure that the radiographer can set a desired field size using the light field collimator.

Requirement: ± 2% SID

SID: 100 cm

Indication Setting (cm^2)	Measured Longitudinal (cm)	Measured Transvers (cm)	% Variation	Pass/Fail
8 x 8	7.75	7.95	0.25%	**Pass**
10 x 10	9.40	10.11	0.60%	**Pass**
12 x 12	11.29	11.69	0.31%	**Pass**
14 x 14	13.46	13.70	0.54%	**Pass**
17 x 17	16.88	16.69	0.31%	**Pass**

Congruence of Light and Radiation Fields

Purpose: To determine the alignment of the light and radiation fields.

Requirement: Alignment to within ± 2% of indicated SID.

Method: Mark corners of light field and compare to radiation field.

SID: 100 cm

Field Size (cm^2)	Light Field Size (cm)		Radiation Field Size (cm)		% Variation	Pass / Fail
	Measured Longitudinal	Measured Transverse	Measured Longitudinal	Measured Transverse		
18 x 18	18.4	17.7	18	16.3	1.40%	**Pass**
25 x 25	25.4	24.2	25.6	23.2	1.00%	**Pass**
35.6 x 35.6	35.8	34.3	35.8	33.7	0.60%	**Pass**

Cross Hair Centering

Purpose: To determine if the light field cross hair indicates the central axis of the x-ray beam.

Requirement: Must be within ± 2% of indicated SID.

SID: 100 cm

Deviation between radiation and optical field centers: 1.5 cm

Pass/Fail: Pass

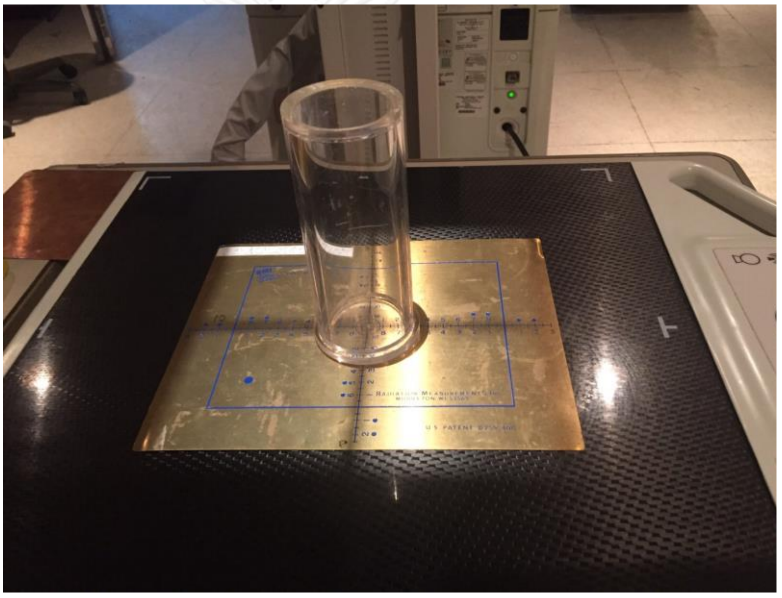

Figure 1. Set up for Cross hair centering.

Focal Spot Size

Purpose: To determine the size of the focal spot at a known technique with a view to detect degradation of the focal spot.
Method: Siemens star technique.

Set kVp 50	Set mAs: 2
Degree of Star: 2	Large or Small Focal Spot: Small
Star dimension:	
Actual: 55	Radiographic: 112.35
Blur: 23.7	Manufacturer specification: 0.6
Computed Focal Spot Size: 0.793	Meet NEMA: **Yes (Blooming 32.16 % from 50% allowed)**

Set kVp 50	Set mAs: 12.5
Degree of Star: 2	Large or Small Focal Spot: Large
Star dimension:	
Actual: 55	Radiographic: 112.35
Blur: 48.29	Manufacturer specification: 1.2
Computed Focal Spot Size: 1.626	Meet NEMA: **Yes (Blooming 35.00 % from 40% allowed)**

จุฬาลงกรณ์มหาวิทยาลัย
CHULALONGKORN UNIVERSITY

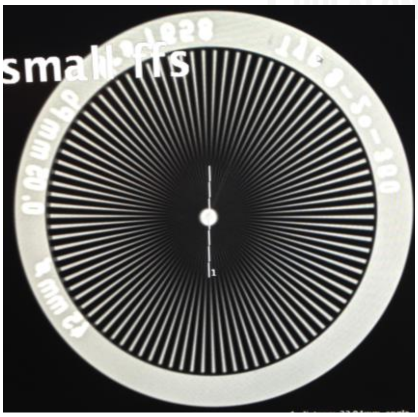

A

B

Figure 2. Show the measurement of (A) small and (B) large focal spot size.

Beam Quality (Half Value Layer)

Method: Set 80 kVp.

Requirement: - NCRP #33 recommends not less than 2.3 mmAl at 80 kVp.

- AAPM recommends not less than 2.5 mmAl at 80 kVp.

Filter (mmAl)	Instrument Reading (mGy)
Open	1.016
3.0	0.540
3.5	0.455

Calculated HVL: 3.36 mmAl

Pass/Fail: **Pass**

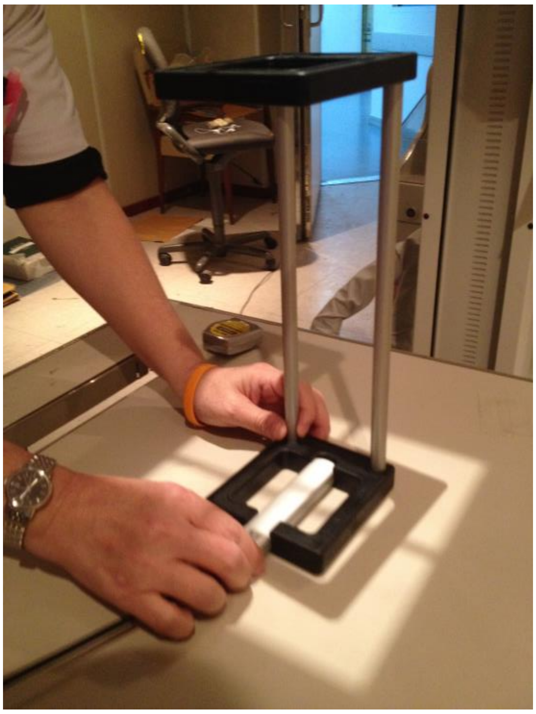

Figure 3. Set up for HVL measurement.

Exposure Consistency

Purpose: To determine if the exposure is remaining consistent.

Requirement: Coefficient of variation should be ≤ 0.05.

Set SCD: 100 cm Set kVp: 80 Field size: 10 x 10 cm^2

Set mAs: 25

	kVp	Dosimeter (mGy)
	80	1.020
	80	1.019
	80	1.020
	80	1.019
Mean		1.020
Std. Dev.		0.001
C.V.		0.001

Pass/Fail: **Pass**

จุฬาลงกรณ์มหาวิทยาลัย
Chulalongkorn University

kVp Accuracy

Method: At a mid-current station, vary the kVp from minimum to maximum in steps of 10 kVp.

Requirement: the deviation should not exceed 5 kVp or 10% of set kVp, whichever is larger.

Set SCD: 100 cm. Phase: 1 Set mAs: 25

Set kVp	Measured kVp		Air kerma (mGy)	Tube output (mGy/mAs)
	Average	% Dev.		
50	49.50	1.00%	0.33	0.0131
60	60.80	1.33%	0.53	0.0212
70	70.80	0.54%	0.76	0.0303
80	82.10	2.62%	1.02	0.0408
90	93.70	4.11%	1.31	0.0524
100	105.40	5.40%	1.63	0.0652
110	117.20	6.55%	1.98	0.0790
120	129.50	7.92%	2.35	0.0938

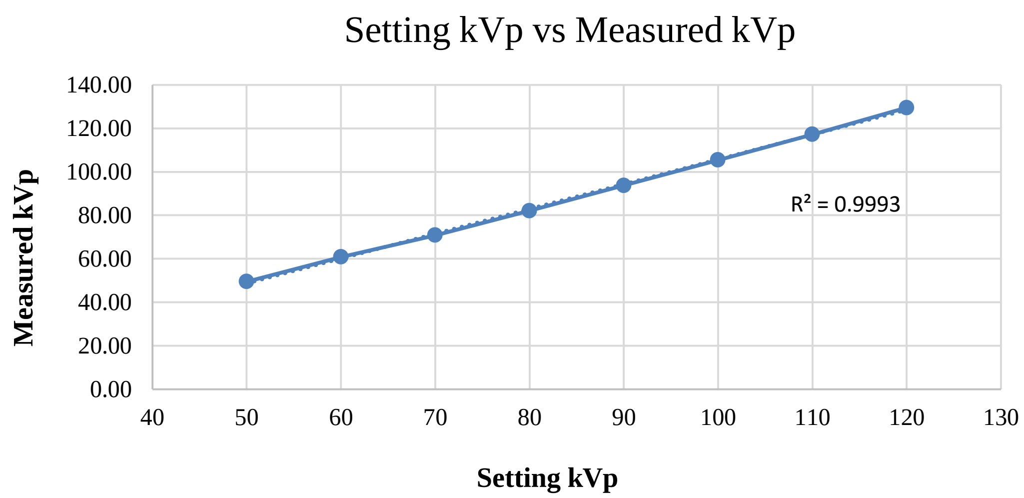

- The maximum percentage deviation of set and measured kVp is 7.92%. The relationship of set and measured kVp is good ($R^2 > 0.99$).

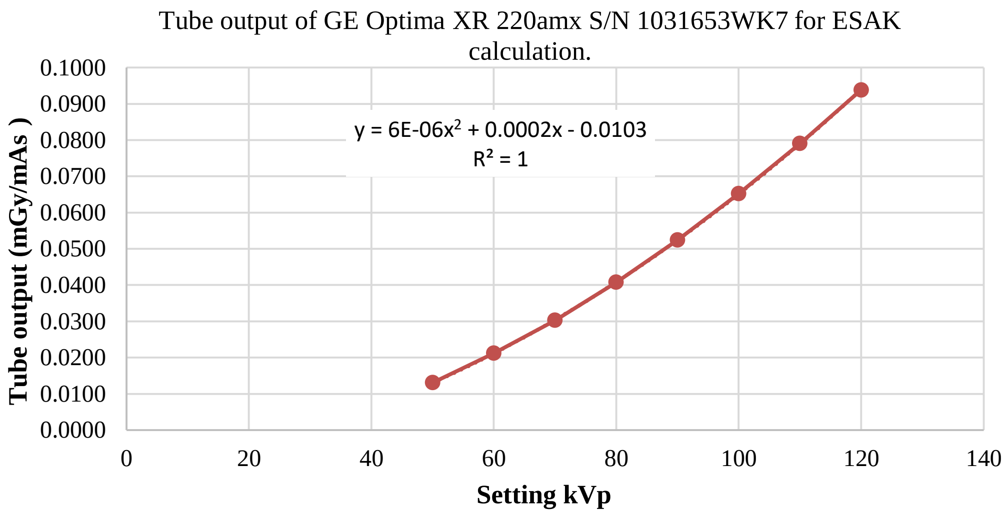

- Tube output is plotted against set kVp at 100 cm SCD and showed good correlation (R^2>0.999).

Pass/Fail: **Pass**

จุฬาลงกรณ์มหาวิทยาลัย
CHULALONGKORN UNIVERSITY

mAs Linearity

Method: Select 80 kVp vary mAs from 5 to 50 and record the exposure in mGy.

Requirement: Coefficient of variation should not exceed 0.1.

Set SCD: 100 cm Phase: 1 Set kVp: 80

Ave. kVp	mA	Time (msec)	mAs	mGy	mGy/mAs	C.V.
82.98	152.65	0.04	6.3	0.2592	0.041	-
82.51	298.47	0.04	12.5	0.5078	0.041	-0.002
82.30	301.02	0.08	25.0	1.0190	0.041	-0.033

Global Mean: 0.041

Global Std.Dev: 0.001

Global C.V: 0.027

- The mAs linearity because the global C.V. is 0.027. The maximum and minimum C.V. are -0.002 and -0.033.

Pass/Fail: **Pass**

จุฬาลงกรณ์มหาวิทยาลัย
Chulalongkorn University

Appendix B: Quality control of image receptor

General Information

Location:	**King Chulalongkorn Memorial Hospital**
Date:	**1 September 2016**
Detector Size:	**41 x 41 cm^2**
Manufacturer:	**General Electric Company (June 2013)**
Model Number:	**5340000-7 (Flat Pad)**
Serial number:	**UA45952-2**

Commission Tests

Objective

- To assess digital image receptor performance

Materials

1. Tape measurement
2. Adhesive tape
3. 1.0 mm Cu filtration
4. Dosimeter Radcal model: AGDM
5. TO20 threshold contrast test object
6. Resolution test object (Hunttner 18)
7. M1 geometry test object
8. MS1, MS3, and MS4 test object
9. Lead glass phantom (10x10)

The tests should be performed x-ray unit and workstation that machines passed QC tests. These tests require the use of the higher quality reporting workstation (3 megapixels monitor) using for clinical workstation.

Quality assurance of digital detector

1. Dosimetry

Purpose: To measure entrance receptor doses required for later test.

Method:

1. Set SID at 180 cm.
2. Set SCD at 155 cm. in front of image receptor.
3. Collimate to the dosimeter.
4. Exposed the chamber such that the inverse square law corrected dose to the chamber is approximately 10 μGy, using 70 kVp, and 1 mm Cu filtration.
5. Record the measured.
6. Under the same beam conditions determine the mAs required to deliver 1 μGy, 4 μGy, 12 μGy, and 50 μGy.

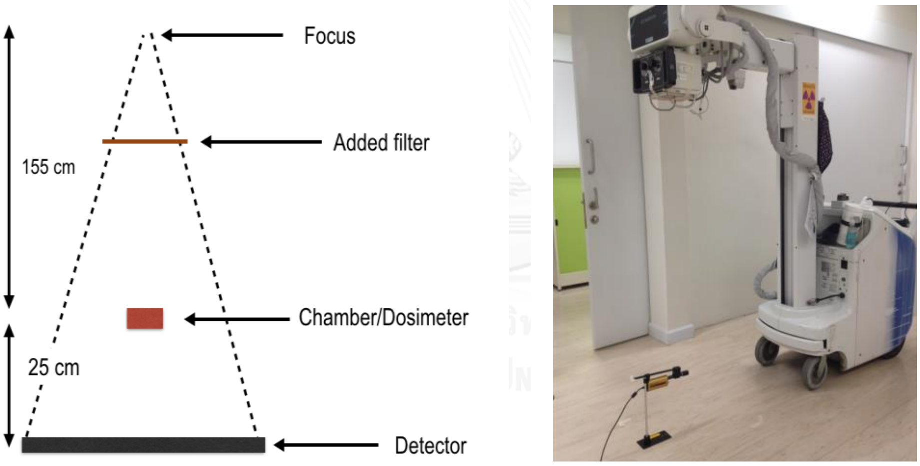

Figure 1. Set up for dosimetry.

Result

Table 1. The mAs was created receptor dose at 1 μGy, 4 μGy, 10 μGy, 12 μGy, and 50 μGy.

Radiation dose (μGy)	Field size measurement at 180 cm.	SCD (cm)	kVp	mAs	Measured dose at dosimeter (SCD) (μGy)	Calculated dose at detector (SID) (μGy)
1	41 x 41 cm^2	155	70	2.5	1.265	0.944
4	41 x 41 cm^2	155	70	10.0	5.524	4.123
10	41 x 41 cm^2	155	70	25.0	13.450	10.038
12	41 x 41 cm^2	155	70	32.0	17.170	12.814
50	41 x 41 cm^2	155	70	125.0	68.320	50.987

2. Dark Noise

Purpose: To assess the level of noise inherent in the system.

Methods:

1. Remove the grid from the system.
2. Close the collimators and cover the image receptor with a lead apron.

Figure 2. Close the collimators and cover the image receptor with a lead apron.

3. Set a low exposure at 50 kVp and 0.5 mAs.
4. Record the image receptor dose indicator value, and pixel value.

Figure 3. Dark noise images.

Result

Table 2. Show pixel value, maximum pixel value and percentage different of pixel value.

kV	mAs	Exposure index	Pixel Value	Max. Pixel Value	% different of pixel value	Artifact free? Y / N
50	0.5	0	7,745	7,751	0.0765	Y

Tolerance: This test is used to set a baseline for future QA tests.

3. Linearity and system transfer properties

Purpose: To establish the relationship between receptor dose and pixel value so that this relationship can be corrected for in image retention and uniformity tests. Also, to establish that the indicated exposure (calculated from the image receptor dose indicator responds linearly to increases in dose).

Method:

1. Remove grid from system.
2. Expose the entire area of the image receptor at 70 kVp with 1 mmCu at the tube head. Set a mAs and SID to deliver a dose of 1 μGy.
3. Record the image receptor dose indicator value.
4. Repeat for doses of order 4 μGy, 10 μGy, 12 μGy, and 50 μGy.
5. Record a pixel value from the 5 points of each image.

CHULALONGKORN UNIVERSITY

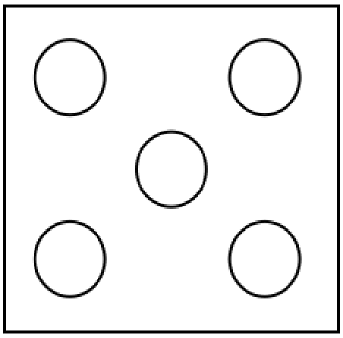

Figure 4. Position for pixel value measurement.

6. Plot a graph of pixel value versus receptor dose using a graph plotting. Obtain the equation of the trend-line for this graph (the pixel value as a function of receptor dose).

$$\text{Dose} = f\left(\text{pixel value}\right)$$

Result

Table 3. Mean pixel value and exposer index of each receptor dose.

kVp	Receptor dose (µGy)	mAs	EI	Mean pixel value
70	1	2.5	100.61	5,683.26
70	4	10	428.65	4,002.61
70	12	32	1,347.12	2,505.13
70	50	125	5,319.77	457.57

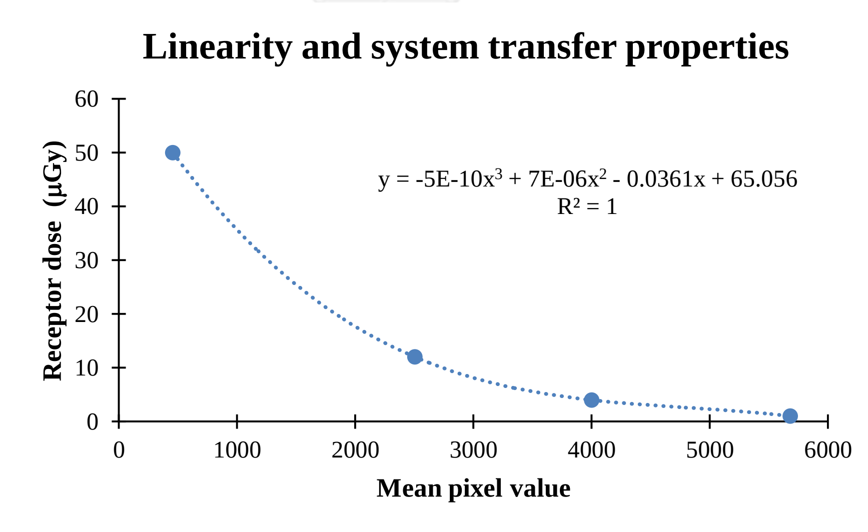

$$y = -5x10^{-10}x^3 + 7x10^{-6}x^2 - 0.0361x + 65.056 \ldots\ldots (1)$$

When y is receptor dose in µGy.

x is mean pixel value.

The relationship between receptor dose and pixel value was shown as equation (1) while the correlation of two parameters were good (R^2=1).

Tolerance:

The trend-line plotted in excel should have an R^2 fit value >0.95. (R = 0.999)

There is no tolerance for the STP equation. However, the pixel value to dose relationship should be a simple relationship.

Pass/Fail: Pass

4. Image retention

Purpose: To test any detectable residual signal (ghosting) that remains in subsequent images is minimal.

Method:

1. Remove grid from system and ensured that there is no attenuation in the beam.
2. Set the focus to detector distance (SID) to be 180 cm.
3. Close the collimators and cover the image receptor with a lead apron. Set a low exposure at 50 kVp and 0.5 mAs.
4. Open the collimators and place the attenuating Material-Lead glass 10x10 cm^2 on the image receptor. Make an exposure at 70 kVp and 10 mAs to deliver a receptor dose of 4 μGy.
5. Obtain another blank image as described in step 3. This exposure should be made 1 minute after the previous one.
6. Set a very narrow window and adjust the level. Visually inspect the image for any remnant of the previous image. If a remnant is visible, use region of interest analysis to quantify the difference in pixel value between the ghosted and unghosted areas.

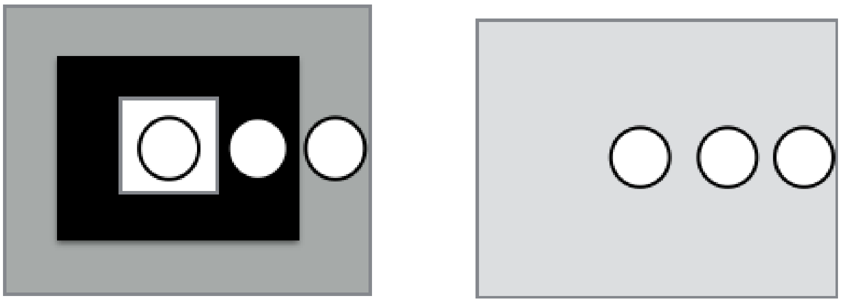

A B

Figure 5. Region of interest for image retention (A) is the position of ROI in the exposed image with lead glass at 70 kVp, 4 μGy. (B) is the position of ROI in the exposed image at 50 kVp, 0.5 mAs, closed collimation and covered image receptor by lead apron.

Result

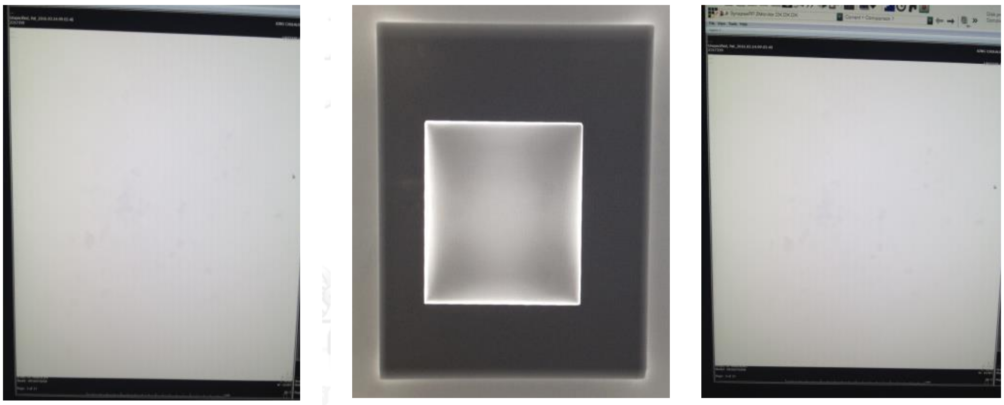

Figure 6. The images of 3 step of image retention.

Table 4. Ghosting artifact evaluation in each exposure technique using pixel value from 3 ROIs.

kVp	mAs	EI	Pb area	Area of pure radiation	Area scatter	Ghosting artifact (Y/N)
50	0.5	0	16,383	16,383	16,383	
70	10.0	0	9,066	3,840	7,398	N
50	0.5	0	16,383	16,383	16,383	

Tolerance:

If no evidence of ghosting is found from visual inspection of the images, then the test is passed and there is no need to perform ROI analysis.

Pass/Fail: **Pass**

5. Detector dose indicator consistency

Purpose: To assess the variation of EI between exposures, and set a baseline for monitoring system sensitivity for future QA testing.

Methods:

1. If possible, remove the grid from the system.
2. Set a field size to cover the entire image receptor and a SID as for the dosimetry.
3. Expose the image receptor to a known dose of 10 μGy at 70kVp with 1.0mm Cu at the tube head.
4. Record the organ program, LUT name and image receptor dose indicator, without changing the window and levelling.
5. Repeat steps 3 times
6. Also repeat for 1μGy and 12μGy (1 image for each).

Result

Table 5. Detector dose indicator consistency of image receptor.

kVp	Dose (μGy)	mAs	EI	Average EI	% different of sensitivity indices
70	10	25.0	1050.57	1050.27	0.264 %
70	10	25.0	1050.57		0.264 %
70	10	25.0	1049.68		0.057 %
70	1	2.5	101.07		
70	12	32.0	1350.22		

***LUT: Chest AP (Portable)**

- The percentage different of EI were less than 1%.

Tolerance:

The indicated sensitivity indices should not differ by greater than 20% of equivalent exposure, between exposures. The measurement should be used to set a baseline for future QA tests.

Pass/Fail: **Pass**

จุฬาลงกรณ์มหาวิทยาลัย
Chulalongkorn University

6. Uniformity

Purpose: To assess the uniformity of the recorded signal from a uniformly exposed image receptor. A non-uniform response could affect clinical image quality.

Method:

1. Remove grid from system.
2. Expose the entire area of the image receptor at 70 kVp with 1 mmCu to deliver a dose of 1μGy.
3. Also repeat for 10 μGy and 12 μGy
4. The five values obtained from ROI analysis should be used to calculate five indicated receptor dose values.

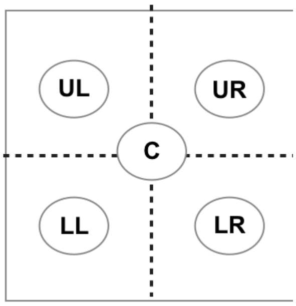

Figure 7. Position of ROI for uniformity test.

Result:

Table 6. The value obtained from ROI analysis and coefficient of variation (CV).

10 μGy	Center	UL	UR	LL	LR	Avg.	C.V.
Mean	2933.43	2796.65	2835.29	2845.12	2850.64	2852.226	0.429
Std Dev.	11.530	13.290	12.970	11.820	11.570	12.236	
10 μGy	Center	UL	UR	LL	LR	Avg.	C.V.
Mean	2935.68	2809.47	2836.12	2844.49	2854.93	2856.138	0.427
Std Dev.	11.020	13.230	13.160	12.090	11.510	12.202	
10 μGy	Center	UL	UR	LL	LR	Avg.	C.V.
Mean	2938.6	2798.67	2822.75	2836.29	2846.76	2848.614	0.433
Std Dev.	11.300	13.330	12.900	12.350	11.810	12.338	
1 μGy	Center	UL	UR	LL	LR	Avg.	C.V.
Mean	5746.7	5653.18	5653.71	5684.19	5678.15	5683.186	0.382
Std Dev.	19.620	22.800	22.350	22.330	21.500	21.720	
12 μGy	Center	UL	UR	LL	LR	Avg.	C.V.
Mean	2596.12	2444.39	2475.34	2486.02	2502.82	2500.938	0.471
Std Dev.	10.610	13.070	12.750	11.670	10.910	11.802	

- The artifact was not found and the coefficients of variation of 5 System Transfer Properties (STP) were less than 1%.

จุฬาลงกรณ์มหาวิทยาลัย
CHULALONGKORN UNIVERSITY

Tolerance:

The images should not have obvious artifacts. The ratio of the standard deviation of the 5 System Transfer Properties (STP) corrected ROI values to their mean (the coefficient of variation) should be less than 10%.

Pass/Fail: **Pass**

7. Scaling errors

Purpose: To assess the accuracy of software distance indicators and check for distortion.

Method:

1. Remove grid from system.
2. Position the M1 test object direct onto the image receptor with an SID of 180 cm.
3. Exposure the image receptor at 50 kVp 10 mAs with no attenuation in the beam.
4. Using the distance measuring software tools measure the dimensions (x and y) in both the horizontal and vertical directions. Calculate the aspect ratio x/y.

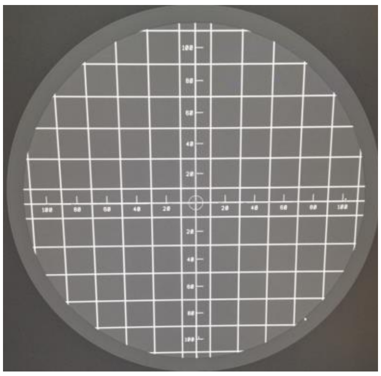

Figure 8. Scaling error test object.

Result:

M1 Object at center 200 mm.

Table 7. The distanced x, y and % different of measured to set distance.

kVp	mAs	x axis (mm)	Y axis (mm)	% different X	% different Y	x:y	1-x:y	% different of measured to set distance
50	10	200.08	200.19	0.00400	0.00095	0.99900	0.00055	0.05500

- The % different of measured to set distance of x and y axis was less than 1% (in the aspect of x and y ratio).

Tolerance:

The measured distances x and y should agree within 3% of the actual distances at the center or 5% at the corners. All calculated aspect ratios should be within 1.00 ± 0.03 at the center or 5% at the corners.

Pass/Fail: **Pass**

8. Blurring and stitching artifacts

Purpose: To test for any localized distortion or blurring and to highlight any stitching artifact if the system is formed from more than one detector element.

Method:

1. The test should be made with the grid both in and out of the image receptor. (this practicum remove grid reduce affect from grid)
2. There is no attenuation in the beam and the SID is set as 180 cm.
3. With a contact mesh on the image receptor, exposure 50 kVp 10 mAs using fine focus. MS1, MS3 and MS4 test object were used.
4. Visually inspect the image for blurring and stitching artifacts.
5. Repeat with a finer mesh.

จุฬาลงกรณ์มหาวิทยาลัย
Chulalongkorn University

MS 1 **MS 3** **MS 4**

Figure 9. MS1, MS3, and MS4 test object and exposed images.

Result:

Table 8. Blur area and stitching obtained image from MS1, MS3, and MS4.

Object	**kVp**	**mAs**	**Blur area(Y/N)**	**Stitching (Y/N)**
MS 1 without grid	50	10	N	Y
MS 3 without grid	50	10	N	Y
MS 4 without grid	50	10	N	Y
MS 1 with grid	50	10	N	Y
MS 3 with grid	50	10	N	Y
MS 4 with grid	50	10	N	Y

- There is no localized distortion or blurring and stitching artifact on the image receptor.

Tolerance:

No blurring should be present. If stitching artifacts are present, there should be no loss of information.

Pass/Fail: **Pass**

จุฬาลงกรณ์มหาวิทยาลัย
Chulalongkorn University

9. Limiting Spatial Resolution

Purpose: To test the high contrast limit of the system ability to resolve details.

Method:

1. Remove grid from system, there is no attenuation in the beam and that the SID is set as 180 cm.
2. Place the resolution test object Huttner test object onto the image receptor aligned at 45^{o} to its edges.
3. Exposure the image receptor at 50 kVp 10 mAs on fine focus.
4. Repeat the measurement with the resolution test object placed at longitudinal axis and -45^{o} to longitudinal axis.
5. Adjust the window level and magnification to optimize the resolution.

A

B

C

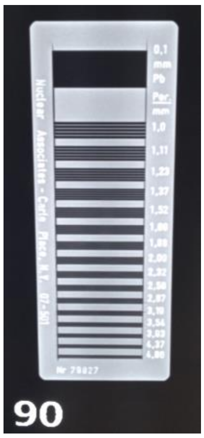

D

Figure. 10 (A) is resolution test object (Hunttner 18).
(B-D) are exposed images of resolution test object in 0°, 45°, and 90°.

Result:

Table 9 Group Line pair in 0°, 45°, and 90°.

Alignment	kVp	mAs	High Resolution monitor (lp/mm)
0°	50	10	2.58
45°	50	10	2.32
90°	50	10	2.32

Tolerance:

These measurements should be used to set a baseline for future QA tests.

10. Threshold Contrast Detail Detectability

Purpose: To monitor image quality by assessing the visibility of low contrast details.

Method:

1. Remove grid from system.
2. Set dose of 4 μGy at 70 kVp with 1 mmCu.
3. Position the TO20 test object direct on the image receptor with an SID of 180 cm and collimate down to the size of the test object.
4. Repeat this test for exposures of 1 μGy and 12 μGy.

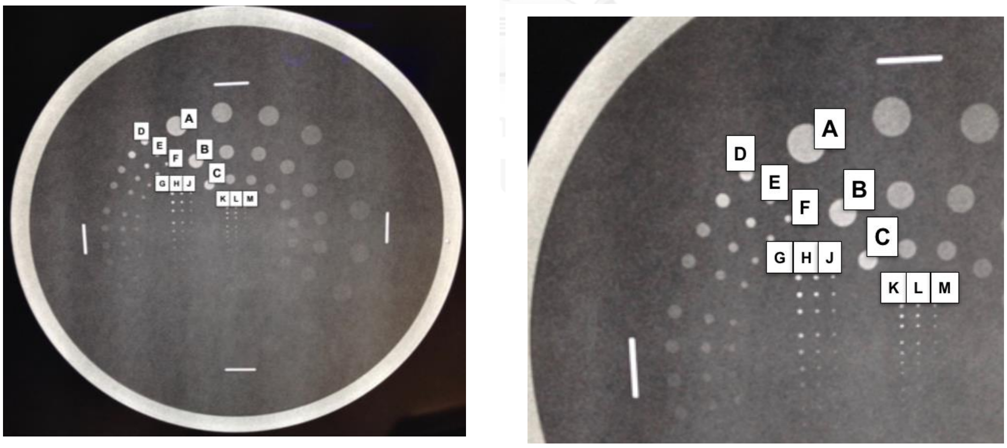

Figure 11. TO20 test object and image.

Table 10. Threshold contrast detail detectability in 1, 4, and 12 μGy.

Row	Diameter(mm)	Dose (μGy)		
		1	4	12
A	11.10	6	8	10
B	7.90	6	8	9
C	5.60	4	8	9
D	4.00	5	8	9
E	2.80	4	7	8
F	2.00	4	6	8
G	1.40	7	8	11
H	1.00	6	7	9
J	0.70	4	6	7
K	0.50	7	7	11
L	0.35	6	6	9
M	0.26	4	6	7

Tolerance:

The results of this test are used to set a baseline for future QA tests.

จุฬาลงกรณ์มหาวิทยาลัย
CHULALONGKORN UNIVERSITY

Appendix C: Quality control of display monitors

Report of display monitors (Widescreen 3 mega pixel)

General Information

Location:	**4th floor of Queen Sirikit Building**
Date:	**5 September 2016**
Manufacturer:	**Barco: Coronis**
Serial number (Left monitor):	**2059291**
Serial number (Right monitor):	**2059292**

Objective:

- To maintain consistent image appearance.
- To ensure display is good enough for required task.
- To identify problems before they become clinically significant.

Before Testing:

- Check the display devices position to minimize specular reflection from direct light sources such as ceiling lights.
- Observe the reflection of light source on the faceplate of the display.
- Check the magnetic field area.
- Warmed up for 30 minutes prior to evaluation.
- Check the monitor clean.

จุฬาลงกรณ์มหาวิทยาลัย
Chulalongkorn University

Materials

- Luminance meter (RaySafe:Unfors)
- TG18-QC
- TG18-UN10 (Black)
- TG18-UN80 (Grey)

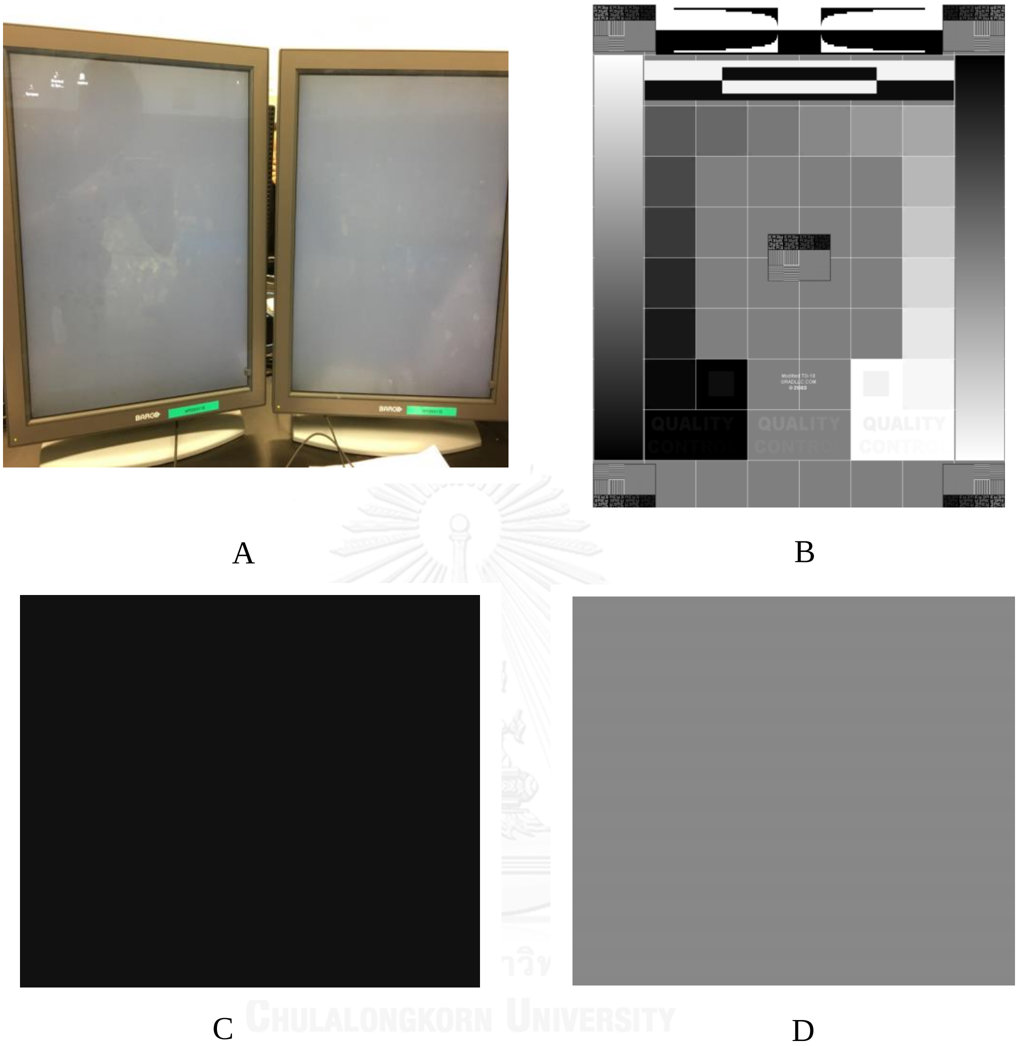

CHULALONGKORN UNIVERSITY

Figure 1. (A) Display monitor widescreen 3 mega pixel Barco: Coronis.
(B) TG18-QC (Test image).
(C) TG18-UN10 (Black).
(D) TG18-UN80 (Grey).

Quality control of display monitor

1. Display lifetime and backlight lifetime

Purpose: To check lifetime the display monitor.

Table 1. Display lifetime and backlight lifetime of right and left monitors**.**

	Right monitor (hr)	**Left monitor (hr)**
Display lifetime	22,379	22,529
Backlight lifetime	10,933	10,985

2. Visual check for fingerprints/dust and cleaning

Purpose: To check the fingerprint/dust on the monitor.

Table 2. Visual checks for fingerprints/dust and cleaning of right and left monitors.

	Right monitor (hr)	**Left monitor (hr)**
Clean	Yes	Yes

3. General image quality and artifact

Purpose: To check the display artifact and verify the ramp bars appear continuous without any contour lines.

Table 3. General image quality and artifact of right and left monitors**.**

General Image Quality	**Right monitor**	**Left monitor**
No smearing	Yes	Yes
No artifacts	Yes	Yes
Ramps continuous	Yes	Yes

CHULALONGKORN UNIVERSITY

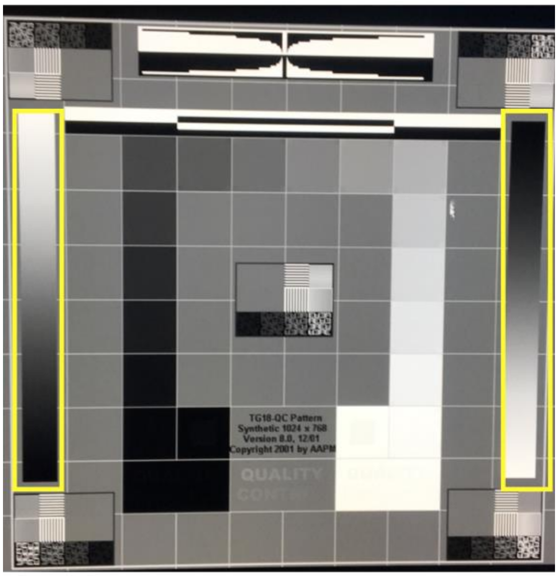

Figure 2. Ramp bar pattern.

4. Geometric distortion

Purpose: To verify that the borders and lines of the pattern are visible and straight and that the pattern appears to be centered in the active area of the display device to check distinguish the box square in greyscale patches.

Table 4. Geometric distortion of right and left monitors**.**

General distortion	Right monitor	Left monitor
Lines straight	Yes	Yes
Boxes square	Yes	Yes

A

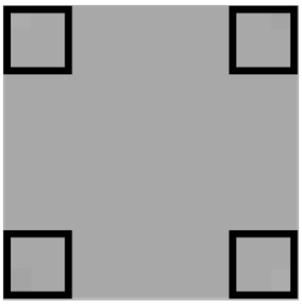

B

Figure 3. (A) Lines straight pattern.
(B) Boxes square in greyscale patches.

5. Luminance

Purpose: Verify that all 18 luminance patches are distinctly visible. Measure their luminance using a luminance meter and verify that the 5% and 95% patches are visible.

Table 5. Luminance of right and left monitors.

Luminance	Right monitor	Left monitor
Greyscale patches distinct	Yes	Yes
5% square visible in 0% background	Yes	Yes
95% square visible in 100% background	Yes	Yes

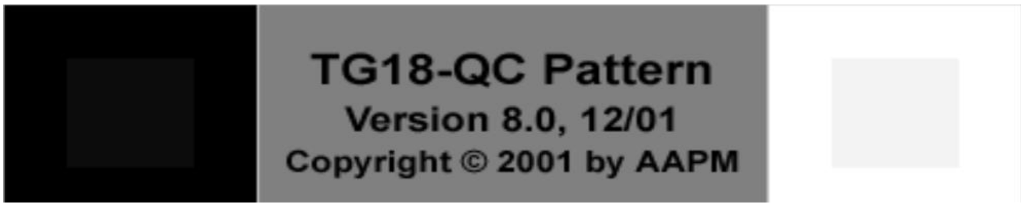

Figure 4. 5% square visible in 0% background and 95% square visible in 100% background.

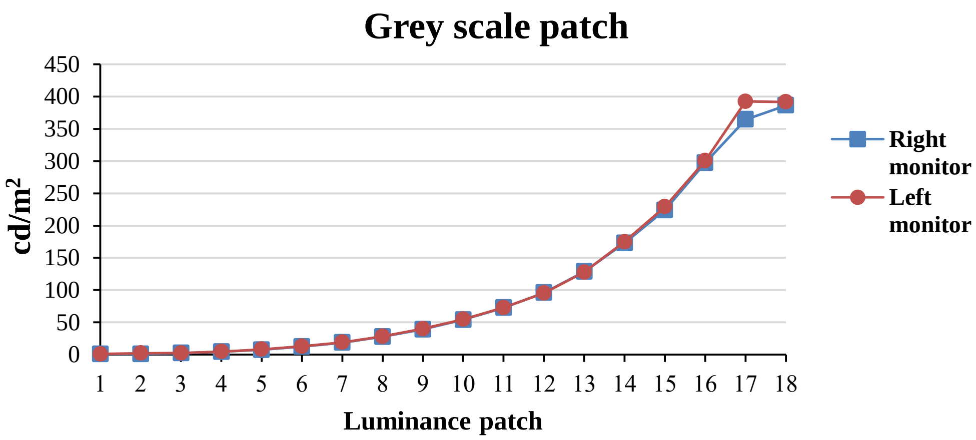

Figure 5. 5% square visible in 0% background and 95% square visible in 100% background.

6. Resolution

Purpose: to evaluate the visibility of line-pair patterns at the Nyquist frequency at the center and corners of the pattern between the vertical and horizontal high-modulation patterns.

Table 6. Resolution of right and left monitors.

Finest high contrast resolution elements visible (in all 4 corners and at center)	Right monitor	Left monitor
Horizontal line pairs	Pass	Pass
Vertical line pairs	Pass	Pass

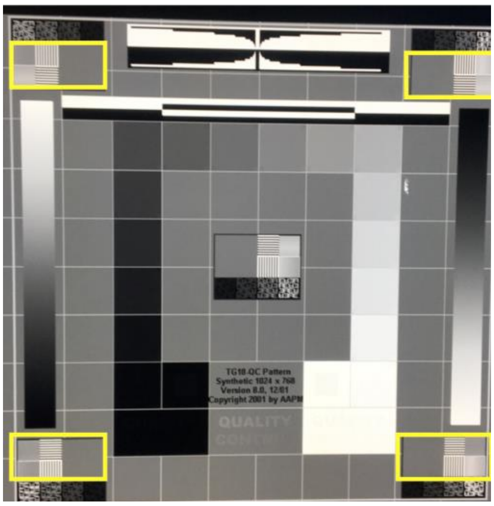

Figure 6. Line-pair patterns at the Nyquist frequency of the pattern.

จุฬาลงกรณ์มหาวิทยาลัย
Chulalongkorn University

7. Number of letters visible

Purpose: to check low contrast detectability at three luminance levels (At least 11 or “QUALITY CONT”)

Table 7. Number of letters visible of right and left monitors.

Number of letters visible	Right monitor	Left monitor
Dark	11	11
Mid-grey	13	13
Light	13	13

Figure 7. Low contrast detail words.

8. Uniformity

Purpose: To check the uniformity of the faceplate of the display device. The maximum luminance deviation (MLD) % should less than 30%.

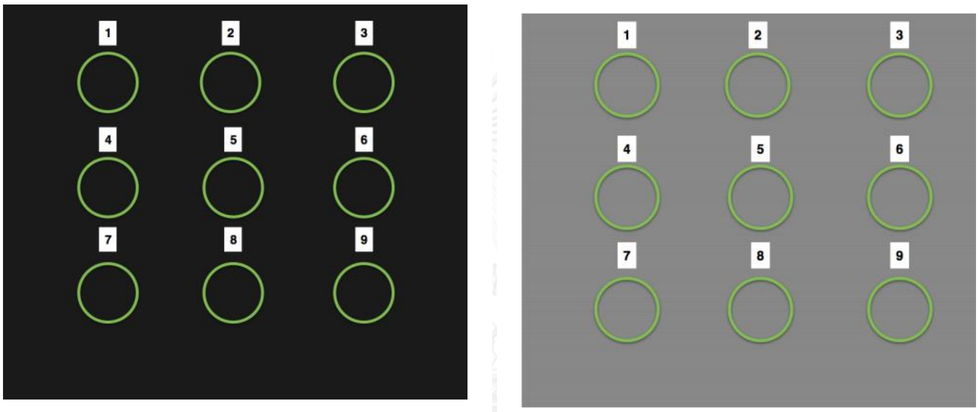

A B

Figure 8. (A) TG18-UN10 (Black) and (B) TG18-UN80 (Grey).

Table 8. Uniformity (TG18-UN10) of right and left monitors.

TG18-UN10	**(cd/m²)**	
	Right monitor	**Left monitor**
Luminance #1	2.57	2.78
Luminance #2	2.68	2.90
Luminance #3	2.41	2.60
Luminance #4	2.49	2.80
Luminance #5	2.65	2.85
Luminance #6	2.39	2.63
Luminance #7	2.40	2.65
Luminance #8	2.49	2.79
Luminance #9	2.30	2.64
Lmax	2.68	2.90
Lmin	2.30	2.60
Maximum luminance deviation (*MLD*) %	15.26 %	10.90%

The maximum luminance deviations (MLD) of right and left monitor are 15.26% and 10.90%, respectively.

Pass/Fail: **Pass**

Table 9. Uniformity (TG18-UN80) of right and left monitors.

TG18-UN80	**(cd/m^{2})**	
	Right monitor	**Left monitor**
Luminance #1	189.6	185.9
Luminance #2	196.6	193.8
Luminance #3	181.2	180.5
Luminance #4	188.7	190.4
Luminance #5	193.1	193.5
Luminance #6	182.6	179.8
Luminance #7	177.0	185.2
Luminance #8	183.0	187.8
Luminance #9	173.8	181.7
Lmax	196.6	193.8
Lmin	173.8	179.8
Maximum luminance deviation (*MLD*) %	12.31	7.49

The maximum luminance deviation (*MLD*) of right and left monitor are 12.31% and 7.49%, respectively.

Pass/Fail: **Pass**

จุฬาลงกรณ์มหาวิทยาลัย
Chulalongkorn University

Appendix D: Data record form

- **Phantom Information:**			
Model: **Whole-body Phantom PBU-60**		Thickness: ____ cm	
Exposure parameter		**Technical parameter:**	
kVp:		SID:	100 cm
mAs:		Grid:	Included

- **Radiation dose**	
Entrance Surface Air Kerma (ESAK)	**mGy**

Image quality	**Score**
A. Image criteria	
1. Sharp visualization of ribs.	
2. Visualization of lower margin of liver.	
3. Visualization of spleen.	
4. Visualization of lower margin of kidneys.	
5. Sharp Visualization of stomach & bowel loop.	
6. Visualization of ribs and transverse processes of lumbar vertebrae.	
7. Markers indicating either upright or supine position.	
Total	
Rate of image criteria score: 1 = fulfilled, 0.5 = partly fulfilled, 0 = not fulfilled	
B. Qualitative noise	
Rate of qualitative noise score: 0 = free of noise, 1 = scarce noise, 2 = significant noise, 3 = obvious noise	
Acceptance level: Image criteria score ≥ 5 point, Qualitative score 1 or 2	

Appendix E: Certificate of exemption

COE No. 013/2016

IRB No. 243/59

คณะกรรมการพิจารณาจริยธรรมการวิจัย

คณะแพทยศาสตร์ จุฬาลงกรณ์มหาวิทยาลัย

1873 ถ.พระราม 4 เขตปทุมวัน กรุงเทพฯ 10330 โทร. 662-256-4493

เอกสารรับรองการยกเว้นพิจารณาจริยธรรมโครงการวิจัย

คณะกรรมการพิจารณาจริยธรรมการวิจัย คณะแพทยศาสตร์ จุฬาลงกรณ์มหาวิทยาลัย ดำเนินการให้การรับรองการยกเว้นพิจารณาจริยธรรมโครงการวิจัยตามแนวทางหลักจริยธรรมการวิจัยในคนที่เป็นมาตรฐานสากลได้แก่ Declaration of Helsinki, The Belmont Report, CIOMS Guideline International Conference on Harmonization in Good Clinical Practice (ICH-GCP) และ 45CFR 46.101(b)

ชื่อโครงการ : การปรับค่าปริมาณรังสีและคุณภาพของภาพที่เหมาะสมในการถ่ายภาพรังสีช่องท้องด้วยเครื่องเอกซเรย์เคลื่อนที่ระบบดิจิทัล

ผู้วิจัยหลัก : นายสิรัณยาพงศ์ สุวรรณโอภาส

สังกัดหน่วยงาน : ภาควิชารังสีวิทยา คณะแพทยศาสตร์ จุฬาลงกรณ์มหาวิทยาลัย

เอกสารรับรอง :

1. โครงการวิจัย ฉบับที่ 1.0 วันที่ 3 พฤษภาคม 2559
2. โครงการวิจัยฉบับย่อ ฉบับที่ 1.0 วันที่ วันที่ 27 พฤษภาคม 2559
3. ประวัติผู้วิจัย

ลงนาม: ....

(ศาสตราจารย์กิตติคุณแพทย์หญิงธาดา สืบหลินวงศ์)

ประธาน

คณะกรรมการพิจารณาจริยธรรมการวิจัย

ลงนาม: ....

(ผู้ช่วยศาสตราจารย์ ดร.แพทย์หญิงประภาพรรณ รัชตะปีติ)

กรรมการและเลขานุการ

คณะกรรมการพิจารณาจริยธรรมการวิจัย

วันที่รับรองการยกเว้นพิจารณาจริยธรรม : 8 มิถุนายน 2559

<u>**หมายเหตุ**</u> ไม่ต้องส่งรายงานความก้าวหน้าและรายงานปิดโครงการเมื่อสิ้นสุดการศึกษา

COE No. 013/2016

IRB No. 243/59

INSTITUTIONAL REVIEW BOARD

Faculty of Medicine, Chulalongkorn University

1873 Rama IV Road, Patumwan, Bangkok 10330, Thailand, Tel 662-256-4493

Certificate of Exemption

The Institutional Review Board of the Faculty of Medicine, Chulalongkorn University, Bangkok, Thailand, has exempted the following study in compliance with the International guidelines for human research protection as Declaration of Helsinki, The Belmont Report, CIOMS Guideline, International Conference on Harmonization in Good Clinical Practice (ICH-GCP) and 45CFR 46.101(b)

Study Title : Optimization of radiation dose and image quality in abdominal radiography using digital mobile x-ray system

Principal Investigator : Mr. Siranyapong Suwan-o-pas

Study Center : Department of Radiology, Faculty of Medicine, Chulalongkorn University.

Document Approval :

1. Protocol Version 1.0 Date May 3, 2016
2. Protocol synopsis Version 1.0 Date May 27, 2016
3. Investigator's CV

Signature: Tada Sueblinvong

(Emeritus Professor Tada Sueblinvong MD)
Chairperson
The Institutional Review Board

Signature:

(Assistant Professor Prapapan Rajatapiti MD, PhD)
Member and Secretary
The Institutional Review

Date of Exemption : June 8, 2016

<u>Note</u> No continuing review report and final report when finish require

Appendix F: The calculation of entrance surface air kerma (ESAK)

Table 1. The calculation of entrance surface air kerma (ESAK) in 21 cm thickness of abdomen.

Selected kVp	Tube loading P_{It} or mAs	Tube output in specific kVp	The incident air kerma (K_i) (mGy)	Backscatter factor	ESAK (mGy)
70	3.2	0.033	0.170	1.380	0.234
	6.3	0.033	0.334	1.380	0.461
	12.5	0.033	0.663	1.380	0.915
	25.0	0.033	1.326	1.380	1.830
75	3.2	0.038	0.197	1.394	0.275
	6.3	0.038	0.388	1.394	0.541
	12.5	0.038	0.770	1.394	1.074
	25.0	0.038	1.540	1.394	2.147
	32.0	0.038	1.971	1.394	2.748
80	3.2	0.044	0.226	1.406	0.318
	6.3	0.044	0.445	1.406	0.626
	12.5	0.044	0.883	1.406	1.242
	25.0	0.044	1.767	1.383	2.443
85	3.2	0.050	0.257	1.417	0.364
	6.3	0.050	0.505	1.417	0.716
	12.5	0.050	1.002	1.417	1.420
	25.0	0.050	2.005	1.417	2.841
90	3.2	0.056	0.289	1.427	0.412
	6.3	0.056	0.568	1.427	0.811
	12.5	0.056	1.128	1.427	1.609
	25.0	0.056	2.255	1.427	3.218

จุฬาลงกรณ์มหาวิทยาลัย
Chulalongkorn University

Table 2. The calculation of entrance surface air kerma (ESAK) in 25 cm thickness of abdomen.

Selected kVp	Tube loading P_{It} or mAs	Tube output in specific kVp	The incident air kerma (K_i) (mGy)	Backscatter factor	ESAK (mGy)
70	3.2	0.033	0.188	1.361	0.256
	6.3	0.033	0.371	1.361	0.505
	12.5	0.033	0.736	1.361	1.001
	25.0	0.033	1.471	1.361	2.002
75	3.2	0.038	0.219	1.373	0.300
	6.3	0.038	0.431	1.373	0.591
	12.5	0.038	0.854	1.373	1.173
	25.0	0.038	1.709	1.373	2.346
80	3.2	0.044	0.251	1.385	0.347
	6.3	0.044	0.494	1.385	0.684
	12.5	0.044	0.980	1.385	1.357
	25.0	0.044	1.960	1.385	2.715
	32.0	0.044	2.509	1.385	3.475
85	3.2	0.050	0.285	1.393	0.397
	6.3	0.050	0.561	1.393	0.781
	12.5	0.050	1.112	1.393	1.549
	25.0	0.050	2.224	1.393	3.099
90	3.2	0.056	0.320	1.397	0.447
	6.3	0.056	0.631	1.397	0.881
	12.5	0.056	1.251	1.397	1.748
	25.0	0.056	2.502	1.397	3.496

จุฬาลงกรณ์มหาวิทยาลัย
Chulalongkorn University

Table 3. The calculation of entrance surface air kerma (ESAK) in 29 cm thickness of abdomen.

Selected kVp	Tube loading P_{It} or mAs	Tube in specific kVp	The incident air kerma (K_i) (mGy)	Backscatter factor	ESAK (mGy)
70	3.2	0.033	0.210	1.294	0.272
	6.3	0.033	0.414	1.294	0.535
	12.5	0.033	0.821	1.294	1.062
	25.0	0.033	1.642	1.294	2.124
75	3.2	0.038	0.244	1.302	0.318
	6.3	0.038	0.481	1.302	0.626
	12.5	0.038	0.953	1.302	1.241
	25.0	0.038	1.907	1.302	2.483
80	3.2	0.044	0.280	1.314	0.368
	6.3	0.044	0.551	1.314	0.724
	12.5	0.044	1.094	1.314	1.437
	25.0	0.044	2.187	1.314	2.874
85	3.2	0.050	0.318	1.320	0.419
	6.3	0.050	0.626	1.320	0.826
	12.5	0.050	1.241	1.320	1.638
	25.0	0.050	2.482	1.320	3.276
	32.0	0.050	3.177	1.320	4.194
90	3.2	0.056	0.357	1.328	0.475
	6.3	0.056	0.704	1.328	0.934
	12.5	0.056	1.396	1.328	1.854
	25.0	0.056	2.792	1.328	3.708

The tube output in specific kVp was calculated from the quality control of the x-ray system in terms of kVp accuracy as following the equation:

$$y = 6E\text{-}06x^2 + 0.0002x - 0.0103$$

where $R^2 = 0.99999$

จุฬาลงกรณ์มหาวิทยาลัย
Chulalongkorn University

VITA

Name:	Mr. Siranyapong Suwan-o-pas
Nationality:	Thai
Date of birth:	December 13, 1990
Education:	Bachelor of Science in Radiological Technology, Faculty of Medical Technology, Mahidol University, 2012
Job experience:	2013 - Present as Radiological Technologist, Department of Radiology, Faculty of Medicine, Siriraj Hospital
E-mail:	Worrawat_Terng@hotmail.com

จุฬาลงกรณ์มหาวิทยาลัย
Chulalongkorn University